Bit Error Rate Performance Evaluation of an Ultra Wide Band Communication System with Dual Carrier Modulation and Space Diversity

By

A K M Abdur Rahman Ferdous

A Thesis Submitted in Partial Fulfillment of the Requirements for
the Degree of
MASTER OF SCIENCE IN ELECTRICAL AND ELECTRONIC ENGINEERING

Department of Electrical and Electronic Engineering
BANGLADESH UNIVERSITY OF ENGINEERING AND TECHNOLOGY
August 2019

Approval Certificate

This thesis titled **"Bit Error Rate Performance Evaluation of an Ultra Wide Band Communication System with Dual Carrier Modulation and Space Diversity"** submitted by A K M Abdur Rahmn Ferdous, Roll No: 0416062300, Session: April, 2016, has been accepted as satisfactory in partial fulfillment of the requirements for the degree of Master of Science in Electrical and Electronic Engineering on 21/08/2019.

Board of Examiners

1.	Dr. Satya Prasad Majumder Professor, Department of EEE, BUET, Dhaka	Chairman (Supervisor)
2.	Dr. Md. Shafiqul Islam Professor & Head, Department of EEE, BUET, Dhaka	Member (Ex-Officio)
3.	21.8.19 Dr. Mohammed Imamul Hasan Bhuiyan Professor, Department of EEE, BUET, Dhaka	Member
4.	21.08.19 Dr. Md. Forkan Uddin Professor, Department of EEE, BUET, Dhaka	Member
5.	Dr. Md. Rubaiyat Hossain Mondal Associate Professor, IICT, BUET, Dhaka	Member (External)

DECLARATION

I, hereby declare that this thesis is based on the results found by myself. Materials of work found by other authors are mentioned as reference in bibliography. I further state that no part of my dissertation has already been or is being concurrently submitted for any degree.

Signature of the Candidate

A K M Abdur Rahman Ferdous

DEDICATION

To my dearest family

ACKNOWLEDGMENT

First and foremost praise is to ALLAH, the Almighty, the Greatest, on whom eventually we depend for sustenance and guidance. I would like to thank Almighty Allah for giving me the opportunity, determination and strength to do my research. Without His profound grace and mercy it would have been impossible to start my research.

I take the opportunity to thank my supervisor, Dr. Satya Prasad Majumder, Professor, Department of EEE, BUET, for the patient guidance, encouragement and advice that he has provided to me as his apprentice. Undoubtedly I am extremely lucky to have a supervisor like him who cared so much about my work and who responded to my queries with his knowledge and wisdom. In addition to being an admirable supervisor, he is a man of principle and has immense knowledge on modern communication technology let alone on his subject domain. I am deeply indebted to him for the selfless effort that he has extended to uphold my work.

I am grateful to my friends and colleagues who have helped a lot and provided me with adequate support for successful completion of the research. Beside all these, it is worth mentioning that none of this would have been possible without the enormous support, love and patience of my wife and kids. Hereby, I take the pleasure to express my heartfelt gratitude and profound affection to my family.

ABSTRACT

Dual carrier modulation (DCM) is taken as a global standard for ultra wide band (UWB) wireless communication system in establishing wireless personal area network (WPAN) such as wireless universal serial bus (W-USB) and wireless high definition media interface (WHDMI), where a data rate of ≥320 Mbps is desired. In practice, DCM transforms 2 Quadrature Phase Shift Keying (QPSK) symbols into two 16 Quadrature Amplitude Modulation (16 QAM) like DCM symbols using DCM matrix. Constellation rearrangement (CoRe) is an inherent part of DCM and thereby DCM achieves coding gain by constellation rearrangement (CoRe) and diversity gain by symbol repetition.

A number of research are carried out on the BER performance of a DCM MB-OFDM in an UWB wireless communication system but without space diversity. In these works, the authors claim that DCM provides a considerable amount of BER reduction in comparison to QPSK and improves the overall data handling capacity in short range wireless communication. In view of the success of space diversity in reducing BER in numerous wireless communication studies, it is envisaged that incorporation of space diversity with DCM may further reduce the BER at the receiver and thereby enhance the overall performance of a system. Hence, an analytical approach is adopted to evaluate the BER performance of DCM MB-OFDM UWB system with space diversity over a Rayleigh fading channel.

Analytical expression for BER is deduced and evaluated through numerical computation where, the graphical results are compared with the previous works to validate its effectiveness. Analyzing the results, it is found that with the increment of number of receiving antenna, receiver sensitivity increases and the overall performance improves. However, using multiple transmitting antennas without incorporating any transmission diversity coding technique causes performance deterioration. Therefore, in a DCM system, the number of transmitting antenna should not be more than that of the receiving antenna in absence of transmission diversity coding technique. The outcome of the research is expected to open a new horizon in the arena of DCM to carry out further research in quest of enhancing the performance of a DCM UWB wireless communication system in future.

CONTENTS

Chapter 2
UWB Communication System with DCM and Space Diversity

Chapter 3
Results and Discussion

Chapter 4
Conclusions and Future Work

APPENDIX

List of Tables

List of Figures

List of Abbreviation

Symbol	Meaning
ADC	Analog to digital converter
AWGN	Additive White Gaussian Noise
BER	Bit Error Rate
BG	Band Group
BPSK	Binary Phase Shift Keying
CoRe	Constellation Rearrangement
CP	Cyclic prefix
CSI	Channel State Information
DCM	Dual Carrier Modulation
DSTFC	Differential Space-Time-Frequency code
ECMA	European Computer Manufacturers Association
FCC	Federal Communications Commission
FDS	Frequency-Domain Spreading
FFI	Fixed- Frequency Interleaving
FFT	Fast Fourier Transform
Fig	Figure
GHz	Giga Hertz
i.e.	In essence
IFFT	Inverse Fast Fourier Transform
I.I.D.	Independent and Identically Distributed
IOT	Internet of Things
I-phase	In-phase
ISI	Inter Symbol Interference
ITU	International Telecommunication Union
LLR	Log Likelihood Ratio
LPF	Low Pass Filter
m	meter
M2M	Machine to Machine
MB-OFDM	Multi-band Orthogonal Frequency Division Multiplexing
Mbps	Mega bit per second

MGF	Moment Generating Function
MHz	Mega Hertz
MIMO	Multiple Input Multiple Output
MISO	Multiple Input Single Output
ML	Maximum Likelihood
MRC	Maximal Ratio Combining
NRZ	Non-return to Zero
ns	Nano Second
OFDM	Orthogonal Frequency Division Multiplexing
PAPR	Peak to Average Power Ratio
PEP	Pair wise Error Probability
pdf	Probability density function
PLL	Phase Lock Loop
ps	Pico second
PSK	Phase Shift Keying
QAM	Quadrature Amplitude Modulation
Q-phase	Quadrature phase
QPSK	Quadrature Phase Shift Keying
RF	Radio Frequency
Rx	Reception
SER	Symbol Error Rate
SIMO	Single Input Single Output
SNR	Signal to Noise Ratio
TDS	Time-Domain Spreading
TFC	Time-Frequency Code
TFI	Time-Frequency Interleaving
Tx	Transmission
UWB	Ultra Wide Band
WHDMI	Wireless High-Definition Multimedia Interface
WPAN	Wireless Personal Area Network
W-USB	Wireless USB
ZF	Zero Forcing
ZPS	Zero Padding Suffix

CHAPTER-1
INTRODUCTION

1.1 UWB Wireless Communication

The desire to have more and more bandwidth with high data transmission rate for sharing of information is endless. Besides the usual needs, due to the gradual implementation of the idea of Internet of Things (IOT) and Machine to Machine (M2M) communication, this demand is exponentially increasing. However, the hunger for more and more flawless, convenient data and information has initiated a number of advancements in the arena of communication technology let alone the sector of wireless communication. Already a quite handsome number of technologies have been developed and implemented to ease the wireless communication. But in every such case, the one shortcoming that appeared is the relative poor data throughput. It is because of the fact that in terrestrial wireless communication electromagnetic energy transmitted over the air interface is subjected to encounter different adverse environmental effects [1].

To meet the ever increasing demand of high data rate, different technologies have already been developed and among them ultra-wideband (UWB) is prominent. It provides a promising solution because of its very nature of handling wider bandwidth which is capable of supporting larger throughput [2-4]. According to the policy of International Telecommunication Union (ITU), the low power spectral density nature of UWB signal causes a low electromagnetic interference. Thus, UWB is widely implemented for indoor and outdoor wireless networking applications [5]. Generally, UWB technology is implemented for wireless transmission with high bandwidth like video, audio or real time streaming of big data between devices. But very often, it is used for short-range radio communication to rely data between devices within approximately 30 feet i.e. nearly 10 m. Generally, an orthodox UWB transmitter operates over a very wide frequency spectrum in GHz range that has either a spectrum which occupies bandwidth greater than 20% of its center frequency; or a bandwidth of minimum 500 MHz [1,6].

In February 2002, the UWB technology was proposed to be taken as standard for wireless personal area network (WPAN). Considering the potentialities, the Federal Communications Commission (FCC) of the United States allocated the spectrum of 7.5 GHz (from 3.1 to 10.6 GHz) for unlicensed use in UWB devices with the restriction on the transmit power spectral density to -41.3 dBm/MHz [6-8]. Since then, UWB communication systems have received significant attention all over the world. The main reason for the excitement about UWB is that this technology promises to deliver high data rate which scales from 110 Mbps at a distance of 10 m to 480 Mbps at a distance of 3 m in realistic multi-path environments [9].

Multiple band orthogonal frequency division multiplexing (MB-OFDM) is used as a modulation technique for UWB wireless system [9,11]. In fact, single carrier transmission can hardly exhibit desired performance in wideband wireless communication system because it requires high complexity equalizer to deal with the ISI problem of the multipath frequency selective channels. On the contrary, OFDM is a bandwidth efficient modulation technique where the parallel subcarriers generated by it are orthogonal to each other. In addition, the use of cyclic prefix with it helps the system to combat the effect of multipath fading and minimizing the effects of ISI. Moreover, it has a relatively large Peak to Average Power Ratio (PAPR) which tends to reduce the power efficiency of the RF amplifier. Altogether, OFDM appears to be a very useful modulation technique in the field of wireless communication under frequency selective channels. [10].

In case of a single carrier systems, data modulation rate is considered to be R_s. But, a multicarrier system, such as OFDM transmits data simultaneously on N_s subcarriers with a data rate of ${R_s}/{N_s}$. Though the total data rate remains same for both the cases but, OFDM along with its subcarriers expose less sensitivity to the delay spread of the channel [10].

In a system, the OFDM symbols undergo two operations. First, an inverse Fast Fourier Transformation (IFFT) is done to the symbols to shift from frequency to time domain. Then, guard interval is added to the obtained signal stream. The extension of the stream is set as such that its length is always larger than the delay spread of the channel [10].

The range and robustness of a communications system is proportional to the multi-path energy collection capability of a communication system. However, by combining OFDM with multi-banding, the strengths of the pulsed multi-band system can be retained while still addressing the issue of capturing multi-path energy. Thus, MB-OFDM, has several unique properties, including the ability to efficiently capture multi-path energy with a single RF chain, insensitivity to group delay variations, and the ability to deal with narrowband interferers at the receiver and so on. In addition, the MB-OFDM system offers simplified synthesizer architectures and relaxes the band-switching timing requirements. In a nut shell, MB-OFDM system radiates relatively low-power but provides broad-spectrum communication, enables high bandwidth data transfer [1] and helps satisfying the demand of exponentially increasing data rate in the world of communication. The use of MB-OFDMA significantly improves the performance of an UWB wireless link in terms of power requirement and data rate [1,11,12]. However, the only drawback of MB-OFDM approach is that the transmitter is more complex because of the IFFT and has slightly higher PAPR than a pulse-based multi-band system [9].

1.2 MB-OFDM UWB

MB-OFDM UWB is taken as the global UWB standard by the WiMedia Alliance and European Computer Manufacturers Association (ECMA) in 2005 and they published it as a report “ECMA-368, 2007” [13]. ECMA-368 is also chosen as physical layer of high data rate wireless specifications for high-speed Wireless USB (W-USB), Bluetooth 3.0 and Wireless High-Definition Media Interface (WHDMI) [14,15]. But due to the relative low radiation power and short-range nature of UWB, the signal integrity of a given tone/subcarrier in MB-OFDM UWB is likely to get impaired even by a nominal degree of signal fading or interference from an adjacent frequency band [1].

ECMA-368 specifies a MB-OFDM system occupying 14 bands from 3.1 to10.6 GHz in electro-magnetic spectrum as allocated by FCC. However, MB-OFDM UWB follows a unique numbering system for all channels those lie within the spectrum. Each band with a bandwidth of 528 MHz can support up to 480 Mbps. This technique helps to capture efficiently multipath energy with a single RF chain.

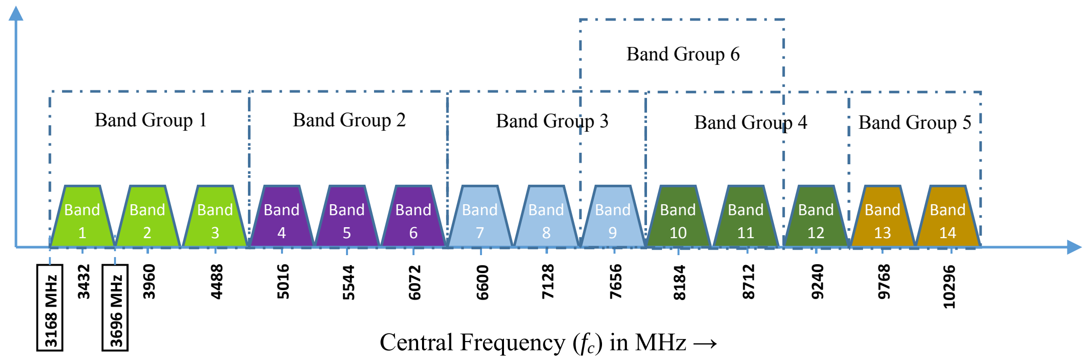

Fig. 1.1: Band Group (BG) Allocation of MB-OFDM UWB [16,17]

As shown in Fig.1.1, six Band Groups (BG) are defined for MB-OFDM UWB. The first 12 bands are grouped into a sub group of 4 bands (BG1-BG4), and the last two bands are grouped into BG5. Lastly, Band group 6 is formed comprising the bands 9, 10 and 11 from BG3 and BG4 [15,16].

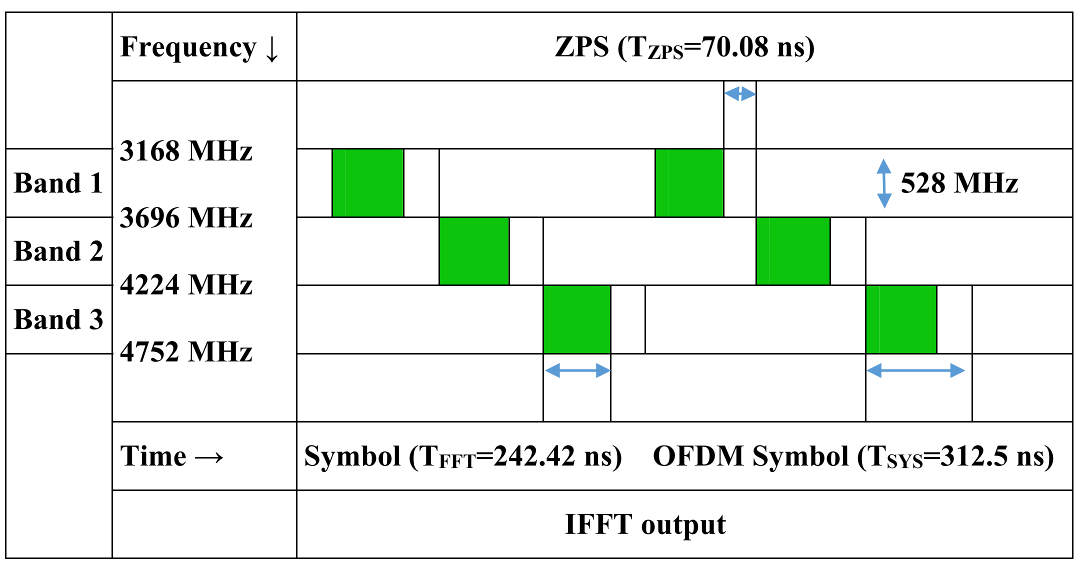

Fig. 1.2: OFDM Symbols Transmission Sequence in RF Signal [16]

Frequency hopping technique is used in ECMA-368 where the band is hopped by using a Time-Frequency Code (TFC), known to both the transmitter and receiver. The transceiver transmits a single OFDM symbol in one band, and the next OFDM symbol in the following band. There are two types of TFCs such as, Time-Frequency Interleaving (TFI) and Fixed- Frequency Interleaving (FFI). In case of TFI the coded information is interleaved over three bands as shown in Fig. 1.2. On the other hand, in case of FFI the coded information is transmitted on a single band [16].

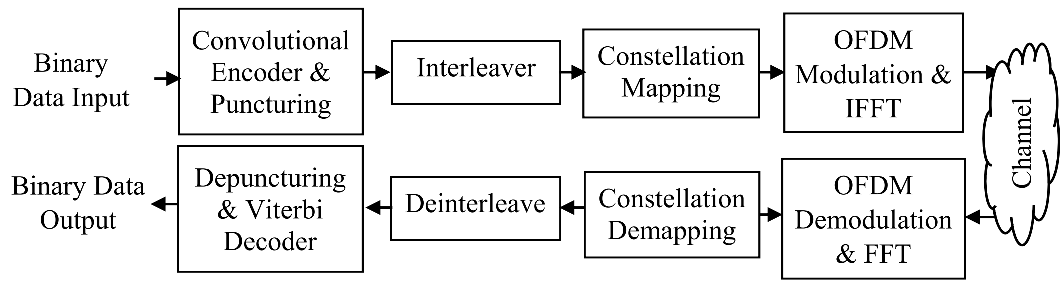

Fig. 1.3: Block Diagram of MB-OFDM UWB Transceiver

In a MB-OFDM UWB system, just before radio transmission 128 point IFFT is carried out to take the baseband signal from frequency domain to time domain. Eventually, each IFFT subcarrier comes up with a clock speed of 528 MHz [18]. According to the MB-OFDM standard, the period of one OFDM symbol is 312.5 ns between two successive transmissions and the OFDM symbol rate is RS= (1/312.5 ns) = 3.2 MHz (Fig. 1.2) [190]. A block diagram of MB-OFDM UWB transmitter and receiver system is shown in Fig. 1.3 [14,15,20].

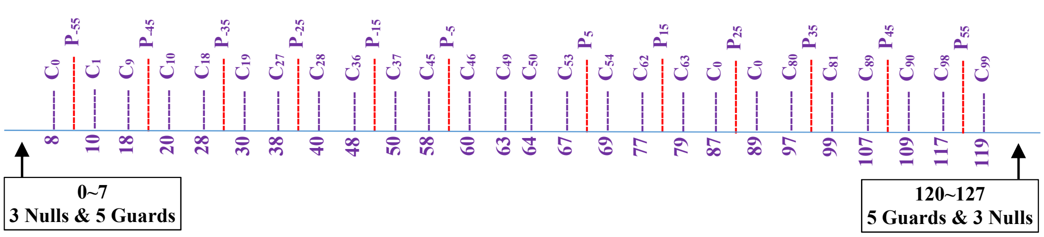

Fig. 1.4: Position of the MB-OFDM UWB Subcarriers in 128 Point IFFT [17,21]

Among the IFFT generated 128 subcarriers (as given in Fig. 1.4), 100 subcarriers (C_0 to C_{99}) are used to carry data symbols. 12 pilot subcarriers (P_s) located on P_{-55}, P_{-45}, P_{-35}, P_{-25}, P_{-15}, P_{-5}, and P_5, P_{15}, P_{25}, P_{35}, P_{45}, P_{55} are used for synchronization purpose. They carry data which is known to the receiver and is used for coherent detection. 10 subcarriers are used as guard interval (GI) to mitigate Inter Symbol Interference (ISI). GIs are located on either edge of the OFDM symbol [22]. The remaining 6 subcarriers are null. These 6 null subcarriers are kept reserve for future purpose [1,17]. However, each OFDM symbol is appended with zero-padding suffix (ZPS) to reduce multipath interference and to settle time related issues between the transmitter and receiver [15].

1.3 Modulation Technique Used in MB-OFDM UWB

In case of conventional OFDM systems, a number of data coding and redundancy techniques are utilized for error correction and data integrity purposes. These techniques improve the overall reliability of data transmissions with a tradeoff in reduction of effective data transfer rate by a significant amount [1]. Similarly, various modulation techniques are incorporated with MB-OFDM UWB such as M-PSK, M-QAM and Dual Carrier Modulation (DCM). Relevant modulation techniques are highlighted below.

1.3.1 Binary phase shift keying (BPSK)

Binary Phase Shift Keying (BPSK) is a two phase modulation scheme, where the 0's and 1's in a binary message are represented by two different phase states in the carrier signal: $\theta=0^o$ for binary 1 and $\theta=180^o$ for binary 0.

Modulation in BPSK is achieved by varying the phase of the sinusoid depending on the message bits. Therefore, within a bit duration T_b, the two different phase states of the carrier signal are represented as;

$$s_1(t) = A_c \cos(2\pi f_c t) = A_c \cos(\omega_c t), \qquad 0 \leq t \leq T_b \quad for\ binary\ 1$$

$$s_0(t) = A_c \cos(2\pi f_c t + \pi) = A_c \cos(\omega_c t + \pi), \qquad 0 \leq t \leq T_b \quad for\ binary\ 0$$

where, A_c is the amplitude of the sinusoidal signal, f_c is the carrier frequency (Hz), t being the instantaneous time in seconds, T_b is the bit period in seconds. The signal $s_1(t)$ stands for the carrier signal when information bit $a_k = 1$ is transmitted and the signal $s_0(t)$ denotes the carrier signal when information bit $a_k = 0$ is transmitted [24].

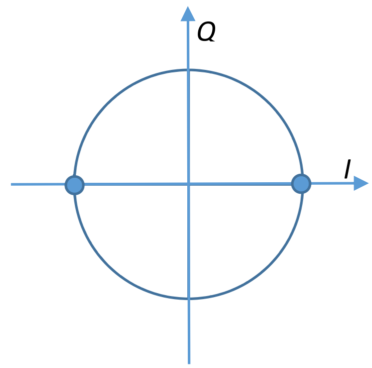

Fig. 1.5: BPSK Constellation

The constellation diagram for BPSK is shown in Fig. 1.5. It shows two constellation points on the same axis. That is, the BPSK modulated signal have only an in-phase component but no quadrature component.

1.3.1.1 BPSK transmitter

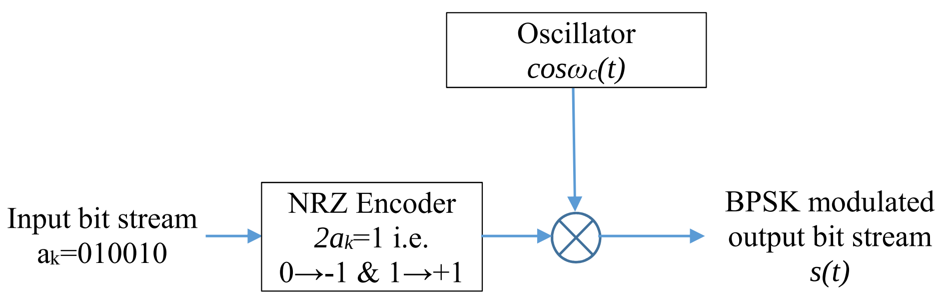

Fig. 1.6: BPSK Transmitter

A BPSK transmitter is shown in Fig. 1.6. It follows NRZ coding technique where, 1is represented by positive voltage and 0 is represented by negative voltage. The output of the coding function is in baseband and is multiplied by the carrier frequency f_c before transmission [24].

1.3.1.2 BPSK receiver

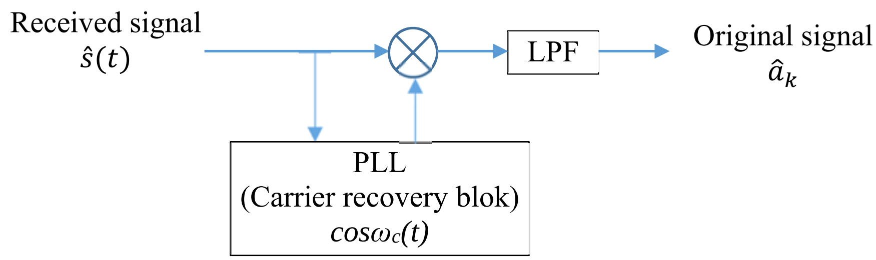

Fig. 1.7: Coherent BPSK Receiver

A coherent BPSK receiver is shown in Fig. 1.7. In coherent detection technique, the knowledge of the carrier frequency and phase is to be known to the receiver which is achieved by using a Phase Lock Loop (PLL) at the receiver. In the receiver, the signal is multiplied by a reference frequency signal f_c provided by the PLL [24].

1.3.2 Quadrature phase shift keying (QPSK)

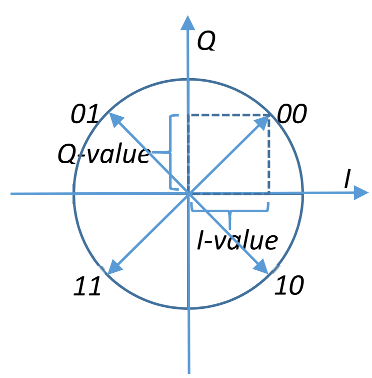

Fig. 1.8: Constellation Diagram of QPSK/4 QAM

The most commonly used modulation scheme for wireless communication systems is QPSK. It is a method for digital transmission where data bits are grouped into pairs to form symbols. However, the QPSK signal is mathematically defined as [25]:

$$x_i(t) = Acos(2\pi f_c t + \theta_i) = Acos\theta_i \cos 2\pi f_c t - Asin\theta_i \sin 2\pi f_c t \qquad \text{... (1.1)}$$

In (1.1), the carrier frequency f_c is chosen as integer multiple of the symbol rate. At any symbol interval the phase angle is either $\frac{\pi}{4}, \frac{3\pi}{4}, \frac{5\pi}{4}$ or $\frac{7\pi}{4}$. So, the constellation diagram of QPSK signal can be represented as shown in Fig. 1.8.

1.3.2.1 QPSK modulator

The QPSK modulator is a combination of two binary phase shift keying (BPSK) modulators. It modulates, two information bits simultaneously and forms a symbol in combination. As a result, the data bit rate is reduced to half i.e. $\frac{R_b}{2}$ and allows space for the other users.

The QPSK modulator uses a bit-splitter (2 bit serial to parallel converter), a local oscillator, a phase shifter, two multipliers and a summer circuit. The serial to parallel convertor is used to separate odd and even number of bits from the total information bits fed in the system. Each of the odd bits (quadrature arm) and even bits (in-phase arm) are converted to non-return to zero (NRZ) format in a parallel manner.

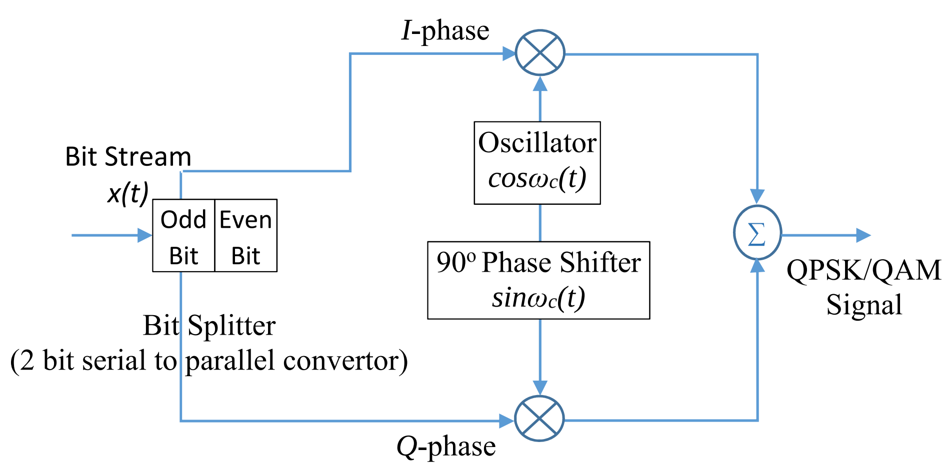

Fig. 1.9: Schematic Diagram of QPSK/QAM Modulation System

The even bit on the in-phase arm is multiplied by cosine component of the carrier generated by local oscillator and the odd bit on the quadrature arm is multiplied by the sine component. In fact the cosine component of the carrier is phase shifted by 90° to generate the sine component before modulating the signal. The diagram of QPSK modulator is given is Fig. 1.9.

In a QPSK system, let $x_1(t)$ *and* $x_2(t)$ represent the even and odd bits of the message signal respectively and ω_c be the carrier signal frequency. So, the general equation of the QPSK signal $\emptyset$ can be expressed as:

$$\emptyset = x_1(t)\cos\omega_c(t) + x_2(t)\sin\omega_c(t) \qquad \cdots\cdots\cdots (1.2)$$

1.3.2.2 QPSK demodulator

In coherent demodulation technique the information of the carrier frequency and phase must be known to the receiver. This can be achieved by using a PLL (phase lock loop) at the receiver. PLL essentially locks the incoming carrier frequency and tracks the variations in frequency and phase.

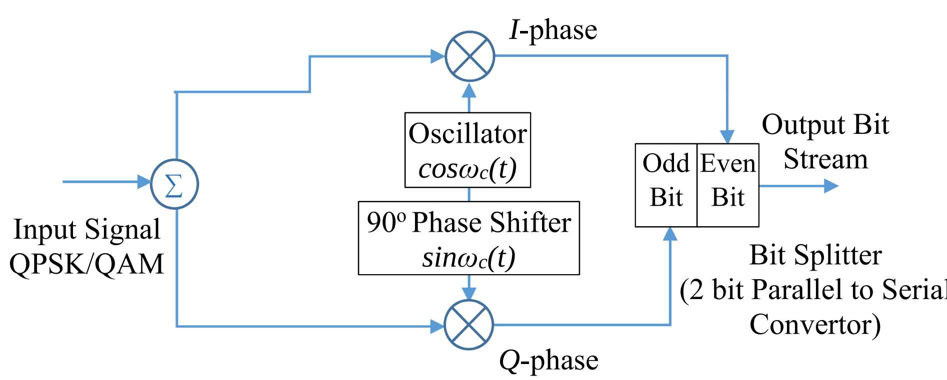

Fig. 1.10: Schematic Diagram of QPSK/QAM Demodulation System

The QPSK demodulator comprises with a local oscillator, two multipliers, two band pass filters and a 2-bit parallel to serial converters. A diagram of QPSK demodulator is given in Fig. 1.10 where, the *I*-channel and *Q*-channel signals are individually demodulated. The received signals are multiplied by a reference frequency such as $\cos\omega_c(t)$ and $\sin\omega_c(t)$ on in-phase and quadrature phase arm respectively. The demodulated outputs from each arm passes through the low pass filter (LPF) to block the higher frequency components. A threshold detector makes a decision on each integrated bit passes through it. Finally, the bits on the in-phase arm (even bits) and on the quadrature arm (odd bits) are sequentially arranged with the help of parallel to serial converter to recover the desired bit stream.

1.3.3 Quadrature amplitude modulation (QAM)

The basic idea of QAM is almost similar to that of the QPSK technique. QAM is used to transmit two bit streams signals over a single channel by shifting the phase of the carrier by 90^o and the amplitudes to a desired level. The resultant output of a QAM system consists of both amplitude and phase variations. Amongst the two modulated signals one is called "*I*" signal and the other is called "*Q*" signal which, can be mathematically represented by a cosine and a sine wave respectively. However, the schematic diagram of QAM system is similar to a QPSK system.

1.3.3.1 QAM constellation

QAM is able to carry higher data rates than ordinary amplitude modulated or phase modulated schemes. The constellation points of a QAM system are normally arranged in a square grid with equal vertical and horizontal spacing. To transmit more bits per symbol higher order modulation formats are generally used, i.e. more points exists in close proximity on the constellation. However, the higher the modulation orders the more the system is susceptible to noise and data errors. Therefore, higher order modulation schemes are considerably less resilient to adverse environmental effects and its performance is inversely proportional to the distance between the transmitter and the receiver. The most common forms of QAM are: 16 QAM, 64 QAM and 256 QAM. Among them, the lowest order is 16 QAM, because, 2 QAM is the same as BPSK and 4 QAM is the same as QPSK. However, 8 QAM is not widely used because the BER performance of 8 QAM is almost similar to that of 16 QAM - it is only about 0.5 dB better and the data rate is only three-quarters that of 16 QAM [26].

A constellation diagram shows the different position of symbols for different bit arrangement. In this regard, constellation diagrams for a variety of QAM formats are projected in Fig 1.11 below [27].

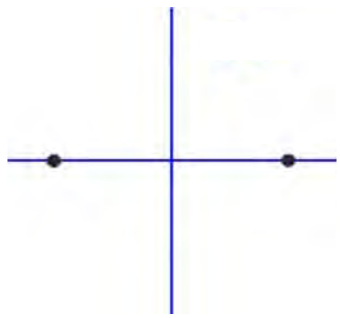

(a) BPSK/ 2 QAM

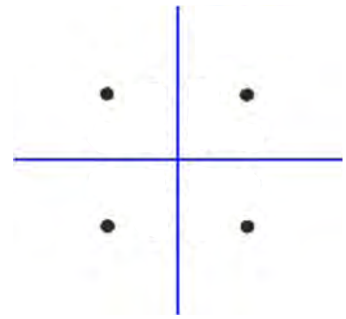

(b) QPSK/4 QAM

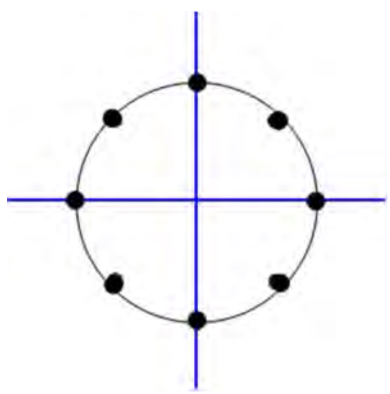

(c) 8 QAM

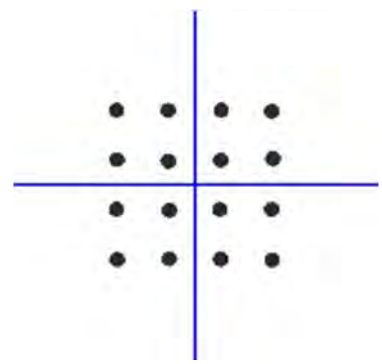

(d) 16 QAM

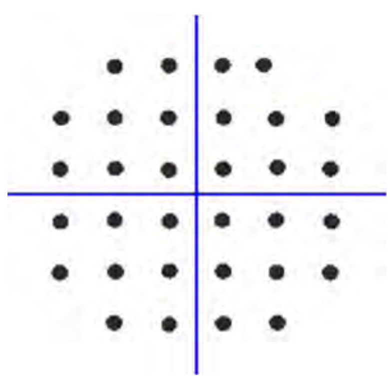

(e) 32 QAM

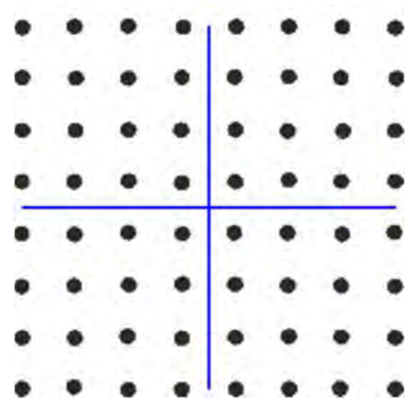

(f) 64 QAM

Fig. 1.11: Various Constellation Diagrams of QAM

The advantage of using QAM is that being a higher order form of modulation it can carry more bits of information per symbol. Table 1.1 gives a summary of the bit rates of different forms of QAM [27].

Table 1.1 Bit and Symbol Rates of Different Forms of QAM

Modulation	**Bits per Symbol**	**Symbol Rate**
BPSK/2 QAM	1	1 x bit rate
QPSK/4 QAM	2	1/2 bit rate
8 PSK/8 QAM	3	1/3 bit rate
16 QAM	4	1/4 bit rate
32 QAM	5	1/5 bit rate
64 QAM	6	1/6 bit rate

1.3.4 DCM

There was always a quest for a technique that not only provides data integrity in OFDM-based communication system but also maintains optimum data transmission rate in the field of wireless communication. This urge eventually led to invent a number of technique and DCM is one of the highly potential outcomes amongst them. In fact, DCM was introduced by Batra and Balakrishnan in 2006 [23] to be used in MB-OFDM as one of the enhancement modulation technique.

In the fading environment, information transmitted over a single path is not reliable. Diversity technique like, frequency diversity is a good option in this aspect to reduce the error rate. The probability of channel deep fading can be reduced a lot if the same information is transmitted over more than one wireless channel with a large bandwidth separation in between. However, the same is followed in DCM technique where, the same coded information is mapped onto two different subcarriers with a large bandwidth separation.
High-speed wireless communication system, with data rate of at least 480 Mbps, usually operates in frequency-selective fading channels where, different frequency components of the signal experiences uncorrelated fading. A frequency diversified scheme such as,

DCM effectively counteract against this fading effect [6]. The function of DCM associates two punctured code data elements which are transformed into a format suitable for transmission on two separate subcarriers/tones [1]. The key feature of DCM is that the two Quadrature Phase Shift Keying (QPSK) modulated symbols are multiplied by "DCM matrix" to form two 16 QAM like DCM symbols before being transmitted over two different subcarriers of OFDM systems with a large frequency separation of 50 subcarriers. Thus frequency separation between two DCM symbols is minimum of 200 MHz {(528/128) x 50} which is far greater than maximum coherent bandwidth of UWB channel (528/128) MHz [37]. Under this condition, the probability of experiencing simultaneous fading by all components of transmitted signal are very unlikely rather, individual frequency component undergoes independent fading [1,6].

Table 1.2 Band Group Allocation for UWB [21]

Band Group	Band Number (m)	Lower Frequency (MHz)	Center Frequency (MHz)	Upper Frequency (MHz)
1	1	3168	3432	3696
	2	3696	3960	4224
	3	4224	4488	4752
2	4	4752	5016	5280
	5	5280	5544	5808
	6	5808	6072	6336
3	7	6336	6600	6864
	8	6864	7128	7392
	9	7392	7656	7920
4	10	7920	8184	8448
	11	8448	8712	8976
	12	8976	9240	9504
5	13	9504	9768	10032
	14	10032	10296	10560
6	9	7392	7656	7920
	10	7920	8184	8448
	11	8448	8712	8976

In wireless transmission the adverse effect like path loss, environmental attenuation and interference effects increase proportionately with the expansion of band width. It is seen that frequency band more than 5 GHz results minor improvement in capacity at the cost of receiver complexity [28]. Due to this reason, in DCM, the first 3 bands i.e. BG-1 of UWB (Table 1.2) is considered suitable to transmit OFDM symbols [16,28]. The channelization of OFDM symbols are primarily based on a set of TFCs [29,30]. Every code specifies the center frequency of the operational band as well as operating time slot. In DCM, as shown in Fig 1.2, the 1st OFDM symbol is transmitted on band-1, 2nd symbol is on band-2, 3rd symbol is on band-3, and the fourth symbol is transmitted on band-1 again. The whole process continues in cyclic order (band 1,2,3,1,2,3,…..). This is how TFC provides frequency diversity as well as multiple accesses [18].

QPSK and DCM are currently used as the modulation schemes for MB-OFDM in the ECMA-368 defined UWB radio platform [3,13,31]. QPSK modulation is used for data rates ≤200 Mbps while, DCM is used for data rate 320 Mbps and higher [17,21].

Data rate of 480 Mbps in a normal environment is hard to be achieved due to poor radio channel condition which causes packet drop and ultimately results in a lower throughput. As a result, it demands several retransmissions of the dropped packets. However, this effect of poor radio channel can be overcome by frequency diversity technique [13] such as DCM. Therefore, DCM is often chosen as one of the most suitable method to be implemented in W-USB and Bluetooth 3.0 to support data rate ≥320 Mbps.

1.4 Literature Review

Determining BER is an important performance evaluation metrics for wireless communication systems under different channel fading scenarios. However, among the existing literatures on DCM technique it is found that Park, K. H., Sung, H. K. and Chai, K. Y. (2006) [30] carried out a thorough “BER analysis of DCM based on ML Decoding” in Rayleigh flat fading channel. The author claimed that for Additive White Gaussian Noise (AWGN) channels, the performance of DCM is the same as that of QPSK, but resulted in a considerable diversity gain for multipath fading channels.

However, author showed that the DCM with optimized constellation significantly outperforms QPSK by about 8dB and 16 QAM by 11dB at 10^{-3} BER.

Yang, R. and Sherratt, R. S. (2008) [14] in their work on "Dual Carrier Modulation Demapping Methods and Performances for Wireless USB" found that the Log-likelihood Ratio (LLR) with channel state information (CSI) is the best DCM demapping method which can achieves a distance of 3.9 m at the rate of 480 Mbps. Maximum Likelihood (ML) soft bit demapping method showed almost similar performance. On the other hand, soft bit demapping with CSI could only achieve a range of 3.4 m. The same group (2009) [15] in their work on "Fixed Point Dual Carrier Modulation Performance for Wireless USB" have presented the DCM mapping and demapping process for ECMA-368. While demapping using LLR technique augmented by CSI scheme they found that the system could achieve the same distance of 3.9 m at the rate of 480 Mbps in realistic multipath channel environment.

Tran, L. C. and Mertins, A. (2009) [32], in their research on "Differential Space-Time-Frequency Codes for MB-OFDM UWB with Dual Carrier Modulation," depicted that DSTFC MB-OFDM systems using DCM shows much better BER performance in comparison to the conventional differential MB-OFDM UWB with PSK or 4 QAM schemes with the same total transmission power.

Subsequently, Ryu, H. S., Lee, J. S. and Kang, C. G. (2010) [33], carried out "BER Analysis of Dual-Carrier Modulation (DCM) over Rayleigh Fading Channel." The author analyzed the tight upper bound BER of DCM over multipath Rayleigh fading channels and established that DCM can provide not only diversity gain by symbol repetition but also coding gain by constellation rearrangement. It further unveiled that the optimized constellation of DCM outperforms conventional QPSK, 4 QAM and 16 QAM. However, the same research team in 2011 [34] further carried out "BER Analysis of Dual-Carrier Modulation (DCM) over Nakagami-*m* Fading Channel" by using partial fraction and binomial series expansion which supported the outcome of previous research with clear indication that the performance improves as *m* (Nakagami fading parameter) increases.

However, Kondoju, S. K., Mani, V. V. and Bose, R., (2014), [18] worked on "Exact BER analysis of DCM for MB-OFDM-UWB system over uncorrelated Nakagami-*m* fading channels" and found that the MB-OFDM UWB system with DCM provides 3 dB less noise compared to the MB-OFDM system with QPSK. Again, Kondoju, S., Mani, V. V. (2017), [6] carried out "Outage and BER analysis of dual-carrier modulation over frequency-selective Nakagami-*m* fading channels" and established that the DCM is suitable for high data rate transmission and is immune to frequency-selective fading. Moreover, the outage and BER performance of DCM outstands conventional MB-OFDM transceiver.

1.5 Motivation behind the Research

Several research works are reported on the BER performance of a UWB wireless link using DCM along with MB-OFDM but without space diversity. Therefore, the scope to improve the BER performance of a DCM UWB communication system by applying space diversity still exists. At this backdrop, it appears as such that it is very much important to formulate an analytical approach to evaluate the BER performance of a DCM MB-OFDM UWB system with space diversity over fading channel.

1.6 Objectives of the Thesis

The objectives selected for this research work are;

i. To develop an analytical approach to evaluate the BER performance of an UWB communication system with DCM technique along with space diversity.

ii. To extend the analytical approach to deduce the expression of SNR for SISO, SIMO and MIMO UWB systems with the use of Maximal Ratio Combining (MRC) and Maximum-Likelihood (ML) soft bit decoding technique.

iii. To evaluate the SNR and BER performance results for different systems and channel parameters and to determine optimum system design parameters.

iv. To estimate the power penalty due to Rayleigh fading environment and the improvement in receiver sensitivity due to space diversity.

1.7 Organization of the Thesis

This thesis is structured chronologically and concisely to depict the clear picture of the research work along with the outcomes where, Chapter-1 contains the introductory parts including different related modulation-demodulation schemes, multiple channel techniques and diversity in a MB-OFDM UWB system. Chapter-2 restricts its arena on the description of the DCM transmitter, receiver, decoding technique and analytical derivation of the BER expression for MB-OFDM UWB DCM with space diversity considering Rayleigh fading environment. Subsequently, results obtained by numerical computation are presented in Chapter-3. At last, Chapter-4 portrays the conclusion and future works which is immediately followed by bibliography.

CHAPTER-2
UWB COMMUNICATION SYSTEM WITH DCM AND SPACE DIVERSITY

2.1 Block Diagram of DCM

In case of deep fade in a channel, the information on a single tone is unreliable and if the subcarrier (tone) is badly attenuated by the channel, the information is most likely to be lost. But when more than one tone of a system carrying the same information, separated by a large bandwidth, the probability of experiencing channel deep fade simultaneously by both the tones is unlikely. DCM implements exactly the same technique. In DCM two QPSK modulated symbols are mapped together using a unique DCM matrix to generate two independent 16 QAM like symbols who carry the same information. A block diagram of DCM technique is shown in Fig. 2.1 [13,24]. The resultant outputs of the system are then mounted over two individual OFDM data subcarriers who maintain a separation of 50 subcarriers in between [15]. Thus frequency separation between two DCM symbols is minimum of 200 MHz {(528/128) x 50} which is far greater than maximum coherent bandwidth of UWB channel (528/128) MHz [37].

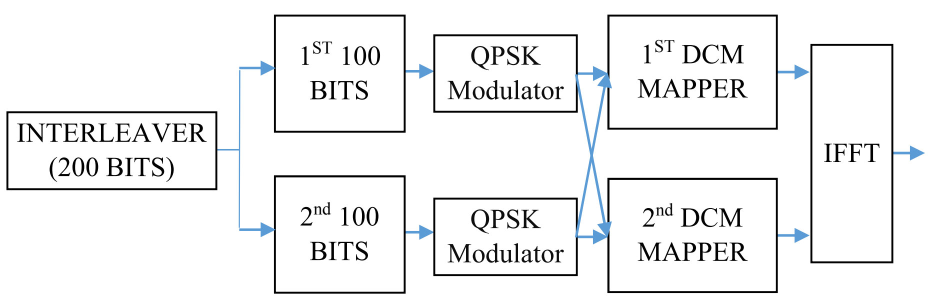

Fig. 2.1: Block Diagram of DCM Mapper

Frequency diversity is the integral part of a DCM system. By broadening the frequency domain it reduces the error probability for a high speed data rate which is generally greater than 320 Mbps, [35]. In the process of DCM, at the outset 1200 interleaved bits are divided into groups of 200 bits. These are then used to form 100 QPSK symbols. For broadening the frequency domain in the transceiver, the DCM executes mapping of the QPSK modulated symbols into 16 QAM like constellation by using DCM matrix, $W = [2 \quad 1; \quad 1 \quad -2]$. As a result, 100 QPSK symbols get transformed into 100 DCM symbols, which are then mounted onto the two independent subcarriers. The DCM repeatedly executes the mapping of the signal so that at any period of time the subcarriers y_k *and* y_{k+50} achieves a frequency separation of desired fraction of the total number of sub-carriers. Finally, these frequency spreaded symbols pass through 128-point Inverse Fast Fourier Transformer (IFFT) [32] where, each OFDM symbol occupies a duration of 312.5 ns while being transmitted over wireless channel.

In the case of a frequency-selective channel, a cyclic prefix of length T_{CP}, greater than the channel delay spread duration, is appended at the beginning of each OFDM symbol to reduce the ISI. It transforms multipath linear convolution to circular convolution and brings orthogonality among the subcarriers. Finally, a GI of length T_{GI} is added at the end of the OFDM signal to provide sufficient time to the analogue transceiver for switching between the sub-bands and to reduce the peak-to-average power ratio [8,36]. Resultant OFDM symbol is passed through a digital-to-analogue converter to get a baseband OFDM signal of duration $T_{SYM} = T_{FFT} + T_{CP} + T_{GI}$.

2.1.1 DCM mapping and transmission

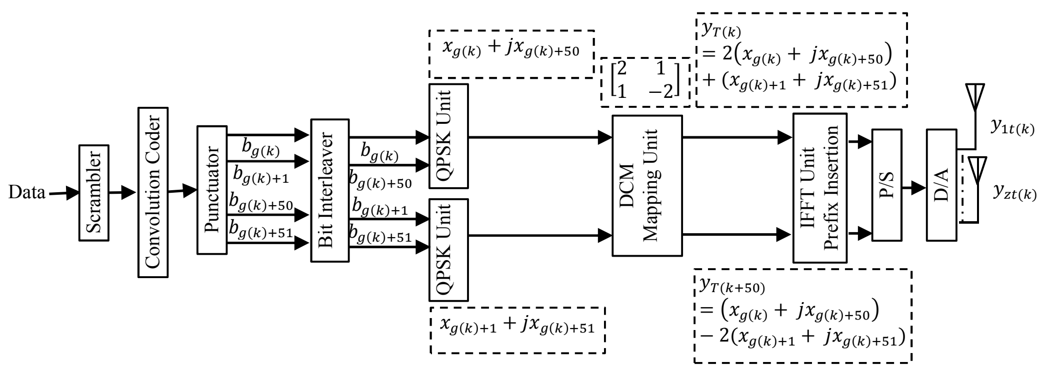

Fig. 2.2: DCM Transmission Process [14,18]

In a DCM MB-OFDM UWB system, as described in Fig. 2.2, scrambler operates on the data bits to approximate a randomization thereof and then transfer those to a convolutional coder in order to get the data output into a desired code format. The coded data is then transferred to a punctuator to reduce the coded bits [1]. These coded bits are then sent to an interleaver function. The interleaver rearranges the coded data in such a way that adjacent coded bits are not on adjacent carrier tones. Then the mapping function takes over. As described in Fig. 2.1, it converts the coded data bits to a QPSK format followed by DCM format. There after the obtained data goes through IFFT for a change over from frequency domain to time domain prior to transmission over wireless channel [1].

DCM system transforms the QPSK data into 16 QAM like format which eventually optimizes data spreading over the tones and thereby enhances the likelihood of data recovery at the receiver. It reforms the data within a single symbol s_0 by associating a given data element b_0 with another data element b_A. The combination s_0 gets separated from another data combination s_A comprising b_1 and b_B by some desired factor $\propto$. This separation factor is selected considering a number of variables of the system like, tone fading characteristics of a particular wireless system. To provide the maximum possible separation 'A' between symbol s_0 and s_A for a system with 100 carrier tone, a separation factor of 2 is desired where, the value of 'A' is determined by [1];

$$A = \frac{No. of\ tones}{\alpha} = \frac{100}{2} = 50$$

In a DCM system with 100 OFDM sub-carriers b_0 is associated with $b_A = b_{50}$ (i.e. b_{0+50}) and b_1 is associated with $b_B = b_{51}$ (i.e. b_{1+50}). These associated pairs of data elements are rendered as data symbols of column vectors $[b_0 \quad b_{50}]^T$, $[b_1 \quad b_{51}]^T$.....$[b_k \quad b_L]^T$; where each data symbol is transmitted on both the K and L=K+50 tones. This gives a clear indication that the paired sub-carriers are separated by 50 tones [1]. Further, a DCM transformation matrix W is applied to $[b_k \quad b_L]^T$, rendering a transformed symbol $[y_k \quad y_L]^T$ where, $[y_k \quad y_L]^T$ =$W \times [b_k \quad b_L]^T$. Later, $[y_k \quad y_L]$ is loaded to an IFFT system, and transmitted over wireless channel [1]. Here, the variable W is a $N \times N$ DCM transformation matrix and,

$$W = \begin{bmatrix} 2 & 1 \\ 1 & -2 \end{bmatrix} \qquad \cdots\cdots (2.1)$$

In the interleaver of DCM system, the interleaved binary data sequence is mapped onto a complex constellation. As mentioned already that the 1200 interleaved and coded bits are divided into groups of 200 bits and then further regrouped into 50 groups of 4 reordered bits in a form of DCM symbol. Each group of 4 bits is represented as a combination of $b_{g(k)}$, $b_{g(k)+1}$, $b_{g(k)+50}$, $b_{g(k)+51}$ where, k∈{0, 1, ..., 49} and,

$$g(k) = \begin{cases} 2k, & k \in \{0, 1, 2, \ldots 24\} \\ 2k + 50, & k \in \{25, 26, \ldots 49\} \end{cases}$$

However, for $g(k) = 2k$; where, $k = (0 \sim 24)$

$$so,\ if\ k = 0;\quad g(k) = 0;\quad then \begin{bmatrix} b_{g(k)} + b_{g(k)+50} \\ b_{g(k)+1} + b_{g(k)+51} \end{bmatrix} = \begin{bmatrix} b_0 + b_{50} \\ b_1 + b_{51} \end{bmatrix}$$

$$if\ k = 1;\quad g(k) = 2;\quad then \begin{bmatrix} b_{g(k)} + b_{g(k)+50} \\ b_{g(k)+1} + b_{g(k)+51} \end{bmatrix} = \begin{bmatrix} b_2 + b_{52} \\ b_3 + b_{53} \end{bmatrix}$$

$$if\ k = 24;\quad g(k) = 48;\quad then \begin{bmatrix} b_{g(k)} + b_{g(k)+50} \\ b_{g(k)+1} + b_{g(k)+51} \end{bmatrix} = \begin{bmatrix} b_{48} + b_{98} \\ b_{49} + b_{99} \end{bmatrix}$$

again, for $g(k) = 2k + 50$; where, $k = (25 \sim 49)$ then,

$$if\ k = 25;\quad g(k) = 100;\quad then \begin{bmatrix} b_{g(k)} + b_{g(k)+50} \\ b_{g(k)+1} + b_{g(k)+51} \end{bmatrix} = \begin{bmatrix} b_{100} + b_{150} \\ b_{101} + b_{151} \end{bmatrix}$$

$$if\ k = 26;\quad g(k) = 102;\ then \begin{bmatrix} b_{g(k)} + b_{g(k)+50} \\ b_{g(k)+1} + b_{g(k)+51} \end{bmatrix} = \begin{bmatrix} b_{102} + b_{152} \\ b_{103} + b_{153} \end{bmatrix}$$

$$if\ k = 49;\quad g(k) = 148;\ then \begin{bmatrix} b_{g(k)} + b_{g(k)+50} \\ b_{g(k)+1} + b_{g(k)+51} \end{bmatrix} = \begin{bmatrix} b_{148} + b_{198} \\ b_{149} + b_{199} \end{bmatrix}$$

The above development expresses that all the 200 bits of the group are well accommodated in the process. The system converts the 4 binary bits [$b_{g(k)}$, $b_{g(k)+50}$ and $b_{g(k)+1}$, $b_{g(k)+51}$] to suitable coordinates of two QPSK symbols and put them in a column matrix. In this process, each bit is multiplied by 2 and subtracted by 1 while, the second part of each row of the matrix is multiplied by j which is illustrated in equation (2.2) below [14];

$$\begin{bmatrix} b_k \\ b_L \end{bmatrix} = \begin{bmatrix} x_{g(k)} + jx_{g(k)+50} \\ x_{g(k)+1} + jx_{g(k)+51} \end{bmatrix} = \begin{bmatrix} \left(2b_{g(k)} - 1\right) + j(2b_{g(k)+50} - 1) \\ \left(2b_{g(k)+1} - 1\right) + j(2b_{g(k)+51} - 1) \end{bmatrix} \quad \cdots\cdots (2.2)$$

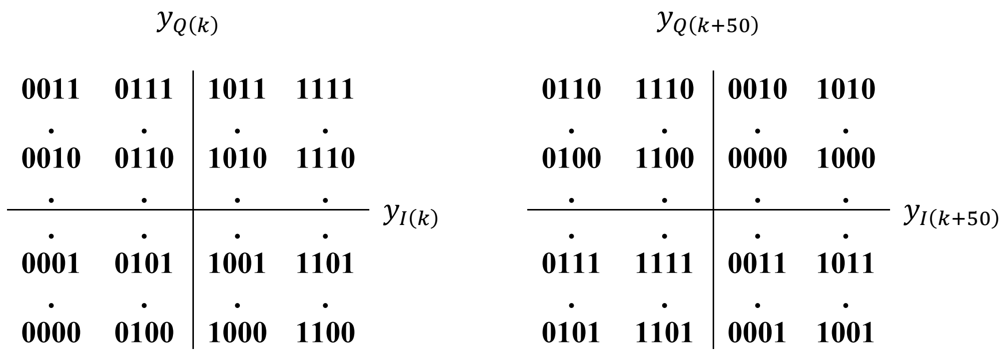

(a) Constellation for $y_{T(k)}$ **(b)** Constellation for $y_{T(k)+50}$

Fig. 2.3: Bit-to-Symbol Mappings for DCM [8,13]

The DCM mapper uses a DCM matrix W (2.4), to transform the two QPSK into two DCM symbols $\{y_{T(k)}, y_{T(k)+50};\ k = 0{\sim}49\}$ as illustrated in (2.3). The resultant bit to symbol mapping of DCM look like two 16 QAM constellations, which are shown in Fig. 2.3.

$$\begin{bmatrix} y_{T(k)} \\ y_{T(k)+50} \end{bmatrix} = W \begin{bmatrix} x_{g(k)} + jx_{g(k)+50} \\ x_{g(k)+1} + jx_{g(k)+51} \end{bmatrix} \quad \cdots\cdots (2.3)$$

$$= \begin{bmatrix} 2 & 1 \\ 1 & -2 \end{bmatrix} \begin{bmatrix} x_{g(k)} + jx_{g(k)+50} \\ x_{g(k)+1} + jx_{g(k)+51} \end{bmatrix}$$

$$= \begin{bmatrix} 2\left(x_{g(k)} + jx_{g(k)+50}\right) + \left(x_{g(k)+1} + jx_{g(k)+51}\right) \\ \left(x_{g(k)} + jx_{g(k)+50}\right) - 2\left(x_{g(k)+1} + jx_{g(k)+51}\right) \end{bmatrix} \quad \cdots\cdots (2.4)$$

Diagram of a DCM transmission process as in Fig. 2.2, depicts that the two resulting DCM symbols $\{y_{T(k)}, y_{T(k)+50}\}$ are allocated to two different OFDM data sub-carriers. In total 100 DCM symbols are given to the 128 point IFFT block for building OFDM symbols. Each OFDM sub-carrier occupies a bandwidth of around 4.125 MHz (528 MHz/128). Therefore, the bandwidth separation between the two individual OFDM data sub-carriers is at least 200 MHz (4.125 MHz x 50 sub carriers) which offers a good frequency diversity gain against channel deep fading [14].

2.1.2 DCM Receiver processing

Signal arrives from the transmitter at receiver antenna of a SIMO/MISO/MIMO DCM system via multiple paths. While travelling through the wireless media and passing through the receiver circuit the transmitted signal under goes a linear combination of numerous fading and attenuating parameters which is augmented by AWGN. For the ease of the research work it is assumed that the receiver is perfectly synchronized to carrier frequency used by the transmitter. At the receiver, the received DCM signal undergoes a number of operations, such as, cyclic prefix (CP) and guard band removal, FFT and input signal combining. This is immediately followed by DCM demapping technique. However, the chronological process carried out in the DCM receiver is depicted in Fig. 2.4.

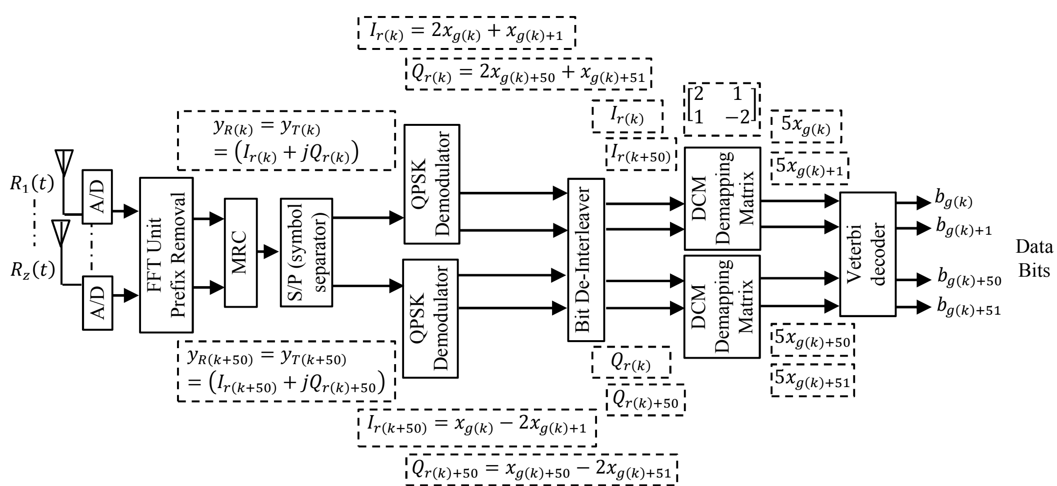

Fig. 2.4: DCM Reception and Demapping Process [35]

The DCM symbol pair upon reception can be expressed in the format of;

$$\mathrm{y}_r = \mathrm{h} \odot \mathrm{y}_t + \mathrm{n} \qquad \dots\dots (2.5)$$

where, $\odot$ represents element wise product of the matrix. In (2.15), the received symbol pair $\mathrm{y}_r = \begin{bmatrix} y_{r(k)} \\ y_{r(k+50)} \end{bmatrix}$, the corresponding channel coefficients (i.e. CSI) $h = \begin{bmatrix} h_{(k)} \\ h_{(k+50)} \end{bmatrix}$, transmitted symbol pair $\mathrm{y}_t = \begin{bmatrix} y_{t(k)} \\ y_{t(k+50)} \end{bmatrix}$ and $n = \begin{bmatrix} n_{(k)} \\ n_{(k+50)} \end{bmatrix}$ is the AWGN with zero mean and power spectral density $\frac{N_0}{2}$.

Estimating the CSI and using the process of maximum likelihood ML soft bit decoding the receiver determines the transmitted symbols. This process minimizes the Euclidean distance between the received and actual transmitted DCM symbols to optimize the symbol detection [18,30,33,38]. However, the ML soft bit decoding criterion for DCM is expressed as;

$$\min_{y_{t(k)};\, y_{t(k+50)}} \left[\left| y_{r(k)} - h_k y_{t(k)} \right|^2 + \left| y_{r(k+50)} - h_{k+50} y_{t(k+50)} \right|^2 \right] \qquad \cdots (2.6)$$

Nonetheless, the transmitted signal that we get from equation (2.3) is;

$$\begin{bmatrix} y_{T(k)} \\ y_{T(k)+50} \end{bmatrix} = W \begin{bmatrix} x_{g(k)} + jx_{g(k)+50} \\ x_{g(k)+1} + jx_{g(k)+51} \end{bmatrix} \qquad \cdots (2.7)$$

Considering the effect of CSI and noise in (2.5), the received signal $\mathrm{y}_r = [y_{R(k)} \;\; y_{R(k)+50}]^T$ can be written as:

$$\begin{bmatrix} y_{R(k)} \\ y_{R(k)+50} \end{bmatrix} = \begin{bmatrix} h_{(k)} \\ h_{(k)+50} \end{bmatrix} \begin{bmatrix} y_{T(k)} \\ y_{T(k)+50} \end{bmatrix} + \begin{bmatrix} n_{(k)} \\ n_{(k)+50} \end{bmatrix} \qquad \cdots (2.18)$$

Here, $[h_{(k)} \;\; h_{(k+50)}]^T$ is the CSI and $[n_{(k)} \;\; n_{(k+50)}]^T$ is a complex AWGN. Putting the value of (2.7) in (2.8), it becomes;

$$\begin{bmatrix} y_{R(k)} \\ y_{R(k)+50} \end{bmatrix} = \begin{bmatrix} h_{(k)} \\ h_{(k)+50} \end{bmatrix} W \begin{bmatrix} x_{g(k)} + jx_{g(k)+50} \\ x_{g(k)+1} + jx_{g(k)+51} \end{bmatrix} + \begin{bmatrix} n_{(k)} \\ n_{(k)+50} \end{bmatrix}$$

$$= \begin{bmatrix} h_{(k)} \\ h_{(k)+50} \end{bmatrix} \begin{bmatrix} 2 & 1 \\ 1 & -2 \end{bmatrix} \begin{bmatrix} x_{g(k)} + jx_{g(k)+50} \\ x_{g(k)+1} + jx_{g(k)+51} \end{bmatrix} + \begin{bmatrix} n_{(k)} \\ n_{(k)+50} \end{bmatrix} \qquad \cdots (2.9)$$

But, from Fig. 2.3 it is clear that both the received symbols are having I and Q component within it. Therefore, the received symbols $y_{R(k)}\ and\ y_{R(k)+50}$ can be expressed respectively as:

$$y_{R(k)} = I_{R(k)} + jQ_{R(k)} \qquad and \qquad y_{R(k)+50} = I_{R(k+50)} + jQ_{R(k+50)} \qquad \cdots (2.10)$$

Hence, the received symbol equation (2.9) can be expressed as;

$$\begin{bmatrix} y_{R(k)} \\ y_{R(k)+50} \end{bmatrix} = \begin{bmatrix} I_{R(k)} + jQ_{R(k)} \\ I_{R(k+50)} + jQ_{R(k+50)} \end{bmatrix}$$

$$= \begin{bmatrix} h_{(k)} \\ h_{(k)+50} \end{bmatrix} \begin{bmatrix} 2 & 1 \\ 1 & -2 \end{bmatrix} \begin{bmatrix} x_{g(k)} + jx_{g(k)+50} \\ x_{g(k)+1} + jx_{g(k)+51} \end{bmatrix} + \begin{bmatrix} n_{(k)} \\ n_{(k)+50} \end{bmatrix} \qquad \cdots (2.11)$$

2.1.3 MRC of DCM signal in MIMO system

The equation of received signal for a MIMO system with t- number of transmit and r- number of receive antennas is;

$$\begin{bmatrix} R_1(t) \\ R_2(t) \\ \vdots \\ R_r(t) \end{bmatrix} = \begin{bmatrix} x_1(t) \\ x_2(t) \\ \vdots \\ x_t(t) \end{bmatrix} \begin{bmatrix} h_{11} & h_{12} & \cdots & h_{1t} \\ h_{21} & h_{22} & \cdots & h_{2t} \\ \vdots & \vdots & \ddots & \vdots \\ h_{r1} & h_{r2} & \cdots & h_{rt} \end{bmatrix} + \begin{bmatrix} n_1 \\ n_2 \\ \vdots \\ n_r \end{bmatrix} \qquad \cdots\cdots (2.12)$$

But according to (2.3), DCM transmitted signal comprises of 2 different kinds of symbols i.e. $y_{T(k)}\ and\ y_{T(k+50)}$. They are transmitted independently over two time periods $t_1\ and\ t_2$. Therefore, for time period t_1, the DCM transmitted signal equation (2.12) can be written as;

$$\begin{bmatrix} y_{R(k)1} \\ y_{R(k)2} \\ \vdots \\ y_{R(k)r} \end{bmatrix} = \begin{bmatrix} y_{T(k)} \\ y_{T(k)} \\ \vdots \\ y_{T(k)} \end{bmatrix} \begin{bmatrix} h_{11} & h_{12} & \cdots & h_{1t} \\ h_{21} & h_{22} & \cdots & h_{2t} \\ \vdots & \vdots & \ddots & \vdots \\ h_{r1} & h_{r2} & \cdots & h_{rt} \end{bmatrix} + \begin{bmatrix} n_1 \\ n_2 \\ \vdots \\ n_r \end{bmatrix}$$

$$= y_{T(k)} \begin{bmatrix} h_{11} & h_{12} & \cdots & h_{1t} \\ h_{21} & h_{22} & \cdots & h_{2t} \\ \vdots & \vdots & \ddots & \vdots \\ h_{r1} & h_{r2} & \cdots & h_{rt} \end{bmatrix} + \begin{bmatrix} n_1 \\ n_2 \\ \vdots \\ n_r \end{bmatrix} \qquad \cdots\cdots (2.13)$$

and for time period t_2;

$$\begin{bmatrix} y_{R(k+50)1} \\ y_{R(k+50)2} \\ \vdots \\ y_{R(k+50)r} \end{bmatrix} = \begin{bmatrix} y_{T(k)+50} \\ y_{T(k)+50} \\ \vdots \\ y_{T(k)+50} \end{bmatrix} \begin{bmatrix} h_{11} & h_{12} & \cdots & h_{1t} \\ h_{21} & h_{22} & \cdots & h_{2t} \\ \vdots & \vdots & \ddots & \vdots \\ h_{r1} & h_{r2} & \cdots & h_{rt} \end{bmatrix} + \begin{bmatrix} n_1 \\ n_2 \\ \vdots \\ n_r \end{bmatrix}$$

$$= y_{T(k)+50} \begin{bmatrix} h_{11} & h_{12} & \cdots & h_{1t} \\ h_{21} & h_{22} & \cdots & h_{2t} \\ \vdots & \vdots & \ddots & \vdots \\ h_{r1} & h_{r2} & \cdots & h_{rt} \end{bmatrix} + \begin{bmatrix} n_1 \\ n_2 \\ \vdots \\ n_r \end{bmatrix} \qquad \cdots\cdots (2.14)$$

To bring simplicity in derivation and for the ease of work let's consider $y_{T(k)} = y_{T(k)+50} = y_T$. So we can write;

$$\begin{bmatrix} y_{R1} \\ y_{R2} \\ \vdots \\ y_{Rr} \end{bmatrix} = y_T \begin{bmatrix} h_{11} & h_{12} & \cdots & h_{1t} \\ h_{21} & h_{22} & \cdots & h_{2t} \\ \vdots & \vdots & \ddots & \vdots \\ h_{r1} & h_{r2} & \cdots & h_{rt} \end{bmatrix} + \begin{bmatrix} n_1 \\ n_2 \\ \vdots \\ n_r \end{bmatrix}$$

or, $$\begin{bmatrix} y_{R1} \\ y_{R2} \\ \vdots \\ y_{Rr} \end{bmatrix} = y_T \begin{bmatrix} H_1 \\ H_2 \\ \vdots \\ H_r \end{bmatrix} + N \qquad \cdots\cdots (2.15)$$

where, $$\begin{bmatrix} H_1 \\ H_2 \\ \vdots \\ H_r \end{bmatrix} = \begin{bmatrix} h_{11} & h_{12} & \cdots & h_{1t} \\ h_{21} & h_{22} & \cdots & h_{2t} \\ \vdots & \vdots & \ddots & \vdots \\ h_{r1} & h_{r2} & \cdots & h_{rt} \end{bmatrix}$$ and $$N = \begin{bmatrix} n_1 \\ n_2 \\ \vdots \\ n_r \end{bmatrix}$$

In order to combine the received signals by adopting MRC, the CSI associated with the received signal is to be nullified. The zero forcing (ZF) technique is generally used in this aspect. Here, channel estimator extracts and provides the expected CSI, H. Received signal matrix is multiplied by the pseudo inverse of H i.e. $(H^H H)^{-1} H^H$. As a result, in the output, $(H^H H)^{-1} H^H H = I$, an identity matrix remains in the form of multiplying factor with the desired signal.

In the above equation of received signal matrix (2.15), it is assumed that, $H_1 = [h_{11} \quad h_{12} \quad \cdots \quad h_{1t}]$. So,

$$H_1^H H_1 = \begin{bmatrix} h_{11} \\ h_{12} \\ \vdots \\ h_{1t} \end{bmatrix} [h_{11} \quad h_{12} \quad \cdots \quad h_{1t}] = |h_{11}|^2 + |h_{12}|^2 + \cdots + |h_{1t}|^2$$

$$= \|h\|^2 \qquad \dots \dots \dots (2.16)$$

$$\text{as,} \quad \|h\| = \sqrt{|h_a|^2 + |h_b|^2 + \cdots + |h_z|^2} = \sqrt{h_a h_a^H + h_b h_b^H + \cdots + h_z h_z^H}$$

Therefore, $(H_1^H H_1)^{-1} = \dfrac{1}{\|h_1\|^2}$ $\dots \dots \dots (2.17)$

From (2.15), the received signal of the receiver's 1st antenna can be expressed as;

$$y_{R1} = y_T H_1 + N \qquad \dots \dots \dots (2.18)$$

As per zero forcing technique, multiplying y_{R1} (2.18) with pseudo inverse of H we get;

$$\hat{y}_{R1} = y_T H_1 (H_1^H H_1)^{-1} H_1^H + N = y_T H_1^H H_1 (H_1^H H_1)^{-1} + N$$

$$= y_T \|h_1\|^2 \frac{1}{\|h_1\|^2} + N \qquad \text{putting the value of (2.16) and (2.17)}$$

$$= y_T + N \qquad \dots \dots \dots (2.19)$$

Similarly, the received signal in the receiver's r^{th} antenna can be expressed as;

$$\hat{y}_{Rr} = y_T H_r (H_r^H H_r)^{-1} H_r^H + N \qquad \text{where,} \quad \mathrm{r} \in 1\sim\mathrm{r}$$

$$= y_T H_r^H H_r (H_r^H H_r)^{-1} + N$$

$$= y_T \|h_1\|^2 \frac{1}{\|h_1\|^2} + N \qquad \text{putting the value of (2.16) and (2.17)}$$

$$= y_T + N \qquad \dots\dots (2.20)$$

Combining the outputs of all the receive antennas, the accumulated received signal can be expressed as;

$$y_R = \sum_{r=1}^{r} \hat{y}_{Rr} = r(y_T + N) = r y_T + N \qquad \dots\dots (2.21)$$

The MRC received signals in two subsequent time periods $t_1 \; and \; t_2$ passes through serial to parallel convertor, and can be written in the matrix form as;

$$\begin{bmatrix} y_{R(k)} \\ y_{R(k)+50} \end{bmatrix} = r \begin{bmatrix} y_{T(k)} \\ y_{T(k)+50} \end{bmatrix} + N \qquad \dots\dots (2.22)$$

Neglecting the multiplying factor-*r* the expression becomes;

$$\begin{bmatrix} y_{R(k)} \\ y_{R(k)+50} \end{bmatrix} = \begin{bmatrix} y_{T(k)} \\ y_{T(k)+50} \end{bmatrix} + N \qquad \dots\dots (2.23)$$

2.1.4 ML Soft Bit Demapping of DCM signal

MRC technique is used to get the best possible output from the information received through multiple channels. At the receiver, outputs of MRC are time-domain OFDM symbols. These are converted into frequency-domain symbols via FFT which is followed by DCM demapping process. There are several methods to demap the DCM symbols. For example, soft bit demapping, ML soft bit demapping and Log Likelihood

Ratio (LLR) demapping. However, here in this work the focus is narrowed down to the ML soft bit demapping method.

The DCM de-mapper uses two separate subcarriers concurrently to decode the symbol pair. If one symbol of one subcarrier is lost or degraded that can be detected or recovered by the DCM de-mapper. However, similar to the mapping unit, at the receiver the demapper repeatedly executes demapping of the two received DCM symbols to generate output groups of 200 bits. These bits from the DCM de-mapper are then sent to the Viterbi decoder which provides desired bits in output [16]. The whole process altogether performs the job of ML soft bit de-mapping.

The MRC received signal, as shown in (2.23) includes noise content in it. Through necessary filtering, the noise part can be suppressed and the output signal will be left with;

$$\begin{bmatrix} y_{R(k)} \\ y_{R(k)+50} \end{bmatrix} = \begin{bmatrix} y_{T(k)} \\ y_{T(k)+50} \end{bmatrix}$$

$$= W \begin{bmatrix} x_{g(k)} + jx_{g(k)+50} \\ x_{g(k)+1} + jx_{g(k)+51} \end{bmatrix}$$

$$= \begin{bmatrix} 2 & 1 \\ 1 & -2 \end{bmatrix} \begin{bmatrix} x_{g(k)} + jx_{g(k)+50} \\ x_{g(k)+1} + jx_{g(k)+51} \end{bmatrix} \qquad \ldots\ldots\ldots (2.24)$$

But, as per (2.11) the received signal is having both its real and imaginary part. Therefore, from (2.11) and (2.24) it can be written as:

$$\begin{bmatrix} y_{R(k)} \\ y_{R(k)+50} \end{bmatrix} = \begin{bmatrix} I_{R(k)} + jQ_{R(k)} \\ I_{R(k+50)} + jQ_{R(k+50)} \end{bmatrix} = \begin{bmatrix} 2 & 1 \\ 1 & -2 \end{bmatrix} \begin{bmatrix} x_{g(k)} + jx_{g(k)+50} \\ x_{g(k)+1} + jx_{g(k)+51} \end{bmatrix} \qquad \ldots\ldots (2.25)$$

In linear format, (2.25) can be written as;

$$y_{R(k)} = I_{R(k)} + jQ_{R(k)} = 2\left(x_{g(k)} + jx_{g(k)+50}\right) + \left(x_{g(k)+1} + jx_{g(k)+51}\right)$$

$$= \left(2x_{g(k)} + x_{g(k)+1}\right) + j\left(2x_{g(k)+50} + x_{g(k)+51}\right) \qquad and \qquad \ldots\ldots\ldots (2.26)$$

$$y_{R(k)+50} = I_{R(k+50)} + jQ_{R(k+50)} = \left(x_{g(k)} + jx_{g(k)+50}\right) - 2\left(x_{g(k)+1} + jx_{g(k)+51}\right)$$

$$= \left(x_{g(k)} - 2x_{g(k)+1}\right) + j\left(x_{g(k)+50} - 2x_{g(k)+51}\right) \quad \dots\dots\dots (2.27)$$

Segregating real and imaginary part of (2.26) and (2.27) i.e. in phase and quadrature phase component and adding the same phase components together, the reformed equations obtained are;

$$I_{R(k)} + I_{R(k+50)} = \left(2x_{g(k)} + x_{g(k)+1}\right) + \left(x_{g(k)} - 2x_{g(k)+1}\right) \quad \dots\dots\dots (2.28)$$

$$Q_{R(k)} + Q_{R(k+50)} = \left(2x_{g(k)+50} + x_{g(k)+51}\right) + \left(x_{g(k)+50} - 2x_{g(k)+51}\right) \quad \dots\dots\dots (2.29)$$

The desired symbols can be retrieved from (2.28) and (2.29). But to do so, the equations of (2.26) and (2.27) are to be multiplied by appropriate coefficients. As a result, the following will be generated [29];

$$\Re\left(2y_{R(k)} + y_{R(k)+50}\right) = 2I_{R(k)} + I_{R(k+50)} = 5x_{g(k)} \quad \dots\dots\dots (2.30)$$

$$\Re\left(y_{R(k)} - 2y_{R(k)+50}\right) = I_{R(k)} - 2I_{R(k+50)} = 5x_{g(k)+1} \quad \dots\dots\dots (2.31)$$

$$\Im\left(2y_{R(k)} + y_{R(k)+50}\right) = 2Q_{R(k)} + Q_{R(k+50)} = 5x_{g(k)+50} \quad \dots\dots\dots (2.32)$$

$$\Im\left(y_{R(k)} - 2y_{R(k)+50}\right) = Q_{R(k)} - 2Q_{R(k+50)} = 5x_{g(k)+51} \quad \dots\dots\dots (2.33)$$

While retrieving the bits [$b_{g(k)}$, $b_{g(k)+1}$, $b_{g(k)+50}$, $b_{g(k)+51}$] from the ML soft bit decoded symbols of (2.30-2.33) process reverse to (2.12) is followed. In doing so, each symbol is normalized by a factor $1/5$ and added with 1, which is further divided by 2. Therefore, the equation of generic decoded bits can be expressed as follows [17];

$$soft\left(b_{g(k)}\right) = \left\{\frac{\left(\frac{5x_{g(k)}}{5}\right) + 1}{2}\right\} = \frac{x_{g(k)} + 1}{2} \quad \dots\dots\dots (2.34)$$

$$soft\left(b_{g(k)+1}\right) = \left\{\frac{\left(\frac{5x_{g(k)+1}}{5}\right) + 1}{2}\right\} = \frac{x_{g(k)+1} + 1}{2} \qquad \dots\dots\dots (2.35)$$

$$soft\left(b_{g(k)+50}\right) = \left\{\frac{\left(\frac{5x_{g(k)+50}}{5}\right) + 1}{2}\right\} = \frac{x_{g(k)+50} + 1}{2} \qquad \dots\dots\dots (2.36)$$

$$soft\left(b_{g(k)+51}\right) = \left\{\frac{\left(\frac{5x_{g(k)+51}}{5}\right) + 1}{2}\right\} = \frac{x_{g(k)+51} + 1}{2} \qquad \dots\dots\dots (2.37)$$

2.2 BER Performance Analysis of DCM

2.2.1 Constellation rearrangement

Constellation rearrangement (CoRe) is considered as an useful means to improve the received signal quality for higher order modulations such as 16 QAM or higher and DCM [29,36,39]. Since each component bit in the DCM constellation has different decision region, its reliability varies. Again, if different constellation is employed in each retransmission, the overall error performance is improved by averaging the variation of individual reliability between different component bits [40].

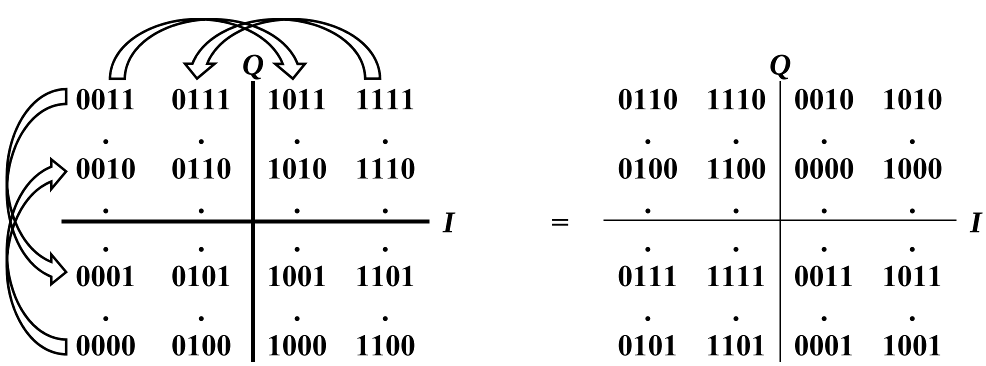

(a) (b)

Fig. 2.5: Constellation Rearrangement to Optimize DCM Coding

Generally to rearrange the constellation, the position between the outer and inner symbols is swapped with each other. The same rule is applied in DCM to optimize the technique in terms of BER reduction [42-44]. In the CoRe of DCM (Fig. 2.5), it is clear that the symbols positioned inside in the first constellation, move to the outside in the final constellation and vice versa [33].

2.2.2 Process to determine BER through PEP

$y_{R(k)}$ and $y_{R(k)+50}$ denote the two consecutive received DCM symbols through the k and $k+50$ subcarriers respectively. Therefore, inline of (2.10), this can be represented by [33]:

$$y_{R(k)} = y_{R(k)}, I + jy_{R(k)}, Q \quad and \quad y_{R(k)+50} = y_{R(k)+50}, I + jy_{R(k)+50}, Q \quad \cdots\cdots (2.38)$$

Separating the in phase and quadrature phase parts of y_1 and y_2, and putting the same phase component together they can be expressed as [33]:

$$Y_I = y_{R(k)}, I + jy_{R(k)+50}, I \qquad and \qquad Y_Q = y_{R(k)}, Q + jy_{R(k)+50}, Q \qquad \dots\dots (2.39)$$

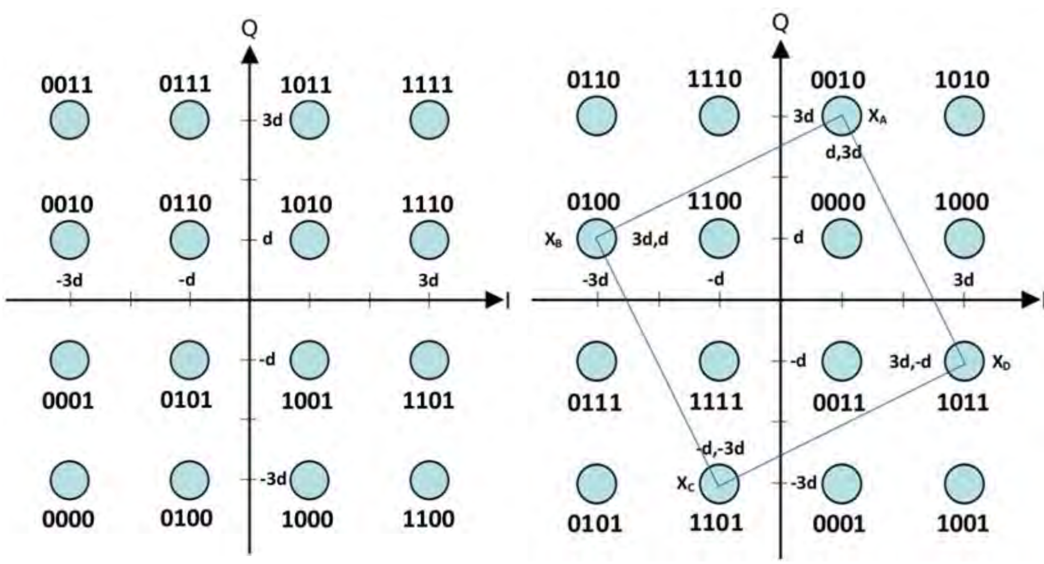

(a) **(b)**

Fig. 2.6: DCM Accumulated Constellation [18,34]

Equation (2.39) yields the DCM accumulated constellation which, represents the corresponding signal points $x_A,\ x_B,\ x_C\ and\ x_D$ in Fig. 2.6(b). For example, let 0011 of

Fig. 2.6(a), is transmitted, then according to (2.38) the two received symbols y_1 and y_2 can be well expressed consulting Fig. 2.6 as [33];

$$y_{R(k)} = y_{R(k)'}I + jy_{R(k)'}Q = -3d + j3d \qquad and \qquad \cdots\cdots\cdots (2.40)$$

$$y_{R(k)+50} = y_{R(k)+50'}I + jy_{R(k)+50'}Q = d - jd \qquad \cdots\cdots\cdots (2.41)$$

where, d depicts Euclidean distance between adjacent points in DCM constellation.

Similarly, according to (2.40) and (2.41), Y_I *and* Y_Q of (2.39) can be expressed as [33];

$$Y_I = y_{R(k)'}I + jy_{R(k)+50'}I = -3d + jd \qquad and \qquad \cdots\cdots\cdots (2.42)$$

$$Y_Q = y_{R(k)'}Q + jy_{R(k)+50'}Q = 3d - jd \qquad \cdots\cdots\cdots (2.43)$$

Thus we find that Y_I *and* Y_Q represent x_B *and* x_D respectively in Fig. 2.6(b). Similarly, for all possible bit-to-symbol mappings the respective position obtained in the constellation are depicted in the table 2.1.

Table 2.1 Symbol Position in the DCM Accumulated Constellation [21]

Serial	**Symbol**	**Fig. 2.6(a),** $y_{R(k)} = y_{R(k)'}\boldsymbol{I} + jy_{R(k)'}\boldsymbol{Q}$ **Fig. 2.6(b),** $y_{R(k)+50} = y_{R(k)+50'}\boldsymbol{I} + jy_{R(k)+50'}\boldsymbol{Q}$	$\boldsymbol{Y_I} = y_{R(k)'}\boldsymbol{I} + jy_{R(k)+50'}\boldsymbol{I}$ $\boldsymbol{Y_Q} = y_{R(k)'}\boldsymbol{Q} + jy_{R(k)+50'}\boldsymbol{Q}$	**Position in accumulated constellation Fig. 2.6(b)**
1	0000	x_1= -3d-j3d x_2= d+jd	X_1= -3d+jd X_2= -3d+jd	x_B x_B
2	0001	x_1= -3d-jd x_2= d-j3d	X_1= -3d+jd X_2= -d-j3d	x_B x_C
3	0010	x_1= -3d+jd x_2= d+j3d	X_1= -3d+jd X_2= d+j3d	x_B x_A
4	0011	x_1= -3d+j3d x_2= d-jd	X_1= -3d+jd X_2= 3d-jd	x_B x_D

Serial	Symbol	Fig. 2.6(a), $y_{R(k)} = y_{R(k)},\boldsymbol{I} + jy_{R(k)},\boldsymbol{Q}$ Fig. 2.6(b), $y_{R(k)+50} = y_{R(k)+50},\boldsymbol{I} + jy_{R(k)+50},\boldsymbol{Q}$	$\boldsymbol{Y_I} = y_{R(k)},\boldsymbol{I} + jy_{R(k)+50},\boldsymbol{I}$ $\boldsymbol{Y_Q} = y_{R(k)},\boldsymbol{Q} + jy_{R(k)+50},\boldsymbol{Q}$	Position in accumulated constellation Fig. 2.6(b)
5	0100	x_1= -d-j3d x_2= -3d+jd	X_1= -d-j3d X_2= -3d+jd	x_C x_B
6	0101	x_1= -d-jd x_2= -3d-j3d	X_1= -d-j3d X_2= -d-j3d	x_C x_C
7	0110	x_1= -d+jd x_2= -3d+j3d	X_1= -d-j3d X_2= d+j3d	x_C x_A
8	0111	x_1= -d+j3d x_2= -3d-jd	X_1= -d-j3d X_2= 3d-jd	x_C x_D
9	1000	x_1= d-j3d x_2= 3d+jd	X_1= d+j3d X_2= -3d+jd	x_A x_B
10	1001	x_1= -d-jd x_2= -3d-j3d	X_1= -d-j3d X_2= -d-j3d	x_C x_C
11	1010	x_1= d+jd x_2= 3d+j3d	X_1= d+j3d X_2= d+j3d	x_A x_A
12	1011	x_1= d+j3d x_2= 3d-jd	X_1= d+j3d X_2= 3d-jd	x_A x_D
13	1100	x_1= 3d-j3d x_2= -d+jd	X_1= 3d-jd X_2= -3d+jd	x_D x_B
14	1101	x_1= 3d-jd x_2= -d-jd	X_1= 3d-jd X_2= -d-j3d	x_D x_C
15	1110	x_1= 3d+jd x_2= -d+j3d	X_1= 3d-jd X_2= d+j3d	x_D x_A
16	1111	x_1= 3d+j3d x_2= -d-jd	X_1= 3d-jd X_2= 3d-jd	x_D x_D

Let $P_s(E)$ and $P_b(E)$ denote the Probability of average symbol error rate (SER) and BER respectively. Therefore, the relationship between BER and SER of DCM system can be approximated as [33,44];

$$P_b(E) \approx \frac{P_s(E)}{\log_2 M} \approx \frac{P_s(E)}{\log_2 4}) \approx \frac{1}{2} P_s(E) \qquad \text{for DCM,} \qquad M = 4$$

However, pair-wise error probability (PEP) is defined as the probability of decoding the matrix x_j incorrectly when x_A is transmitted. The probability of symbol error coupled with ML soft bit decoding technique for equally likely messages is approximated as the probability of error associated with an adjacent decision region having minimum Euclidian distance in the constellation. That is, likelihood of wrongly recognizing a symbol other than its nearest neighbors is negligible at high SNR. Hence, the equation of cumulative average BER for a DCM based MB-OFDM UWB system can be expressed as [33];

$$P_b(E) \approx {}^1\!/_2\, P_s(E) \leq {}^1\!/_2 \{p(x_A \to x_j)\}, \qquad j \in \{B, C, D\}$$

$$\leq {}^1\!/_2 \{p(x_A \to x_B) + p(x_A \to x_C) + p(x_A \to x_D)\} \qquad \text{......... (2.44)}$$

where, $p(x_A \to x_j), j \in \{B, C, D\}$ represents the average PEP of confusing x_A with x_j, when x_A is transmitted [34]. In a DCM constellation, lets denote the symbol and bit energy by, $\mathrm{E_s}$ and $\mathrm{E_b}$ respectively where, $\mathrm{E_s} = 2\mathrm{E_b}$ [45,46].

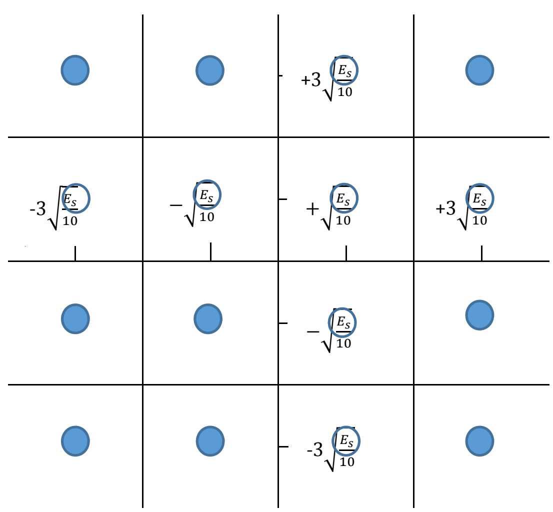

Fig. 2.7: Distance between Constellation Points of DCM/16 QAM [47]

In Fig. 2.7, $d = \sqrt{\frac{E_s}{10}}$; expresses the distance in terms of symbol energy between the adjacent points in a DCM/16 QAM like constellations [8,47]. If N_0 represents noise energy then, for a MIMO system with N_t transmit antenna and N_r receive antenna, the conditional PEP between two distinct code words can be expressed as [45,46];

$$p(x_A \rightarrow x_j | h_1, h_2 \dots h_l) = Q\left(\sqrt{\frac{\delta}{2N_t}\sum_{j=1}^{N_r}\left\|(x_A - x_j)H_j\right\|^2}\right) \quad \dots\dots (2.45)$$

where, Q denotes the Q-function
H represents the channel matrix
and the average SNR δ is expressed as,

$$\delta = \frac{E_{sig}}{N_0} = \frac{(d)^2}{N_0} \qquad but \;\; d = \sqrt{\frac{E_s}{10}}$$

$$= \frac{\left(\sqrt{\frac{E_s}{10}}\right)^2}{N_0} = \frac{E_s}{10N_0} \qquad \therefore \;\; \mathrm{E_s = 2E_b}$$

$$= \frac{2E_b}{10N_0} = \frac{E_b}{5N_0}$$

Therefore, from the above equation of SNR, the relationship between signal energy and bit energy can be expressed as;

$$E_{sig} = \frac{E_b}{5} \quad \dots\dots (2.46)$$

Basing on the DCM accumulated constellation as shown in Fig. 2.6(b), the equation of conditional PEP for a MIMO system with two symbol pair having both *I*- and *Q*- phases in each symbol, can be written in accordance with (2.45) and expressed as [8];

$$p(x_A \to x_j|h_1,h_2) = Q\left(\sqrt{\frac{\delta}{2N_t}\sum_{l=1}^{N_r}\left\{\left(x_{AI}-x_{jI}\right)^2|h_1|^2+\left(x_{AQ}-x_{jQ}\right)^2|h_2|^2\right\}}\right)$$

$$p(x_A \to x_j|h_1,h_2) = Q\left(\sqrt{\frac{E_{sig}}{2N_0N_t}\sum_{l=1}^{N_r}\left\{\left(x_{AI}-x_{jI}\right)^2|h_1|^2+\left(x_{AQ}-x_{jQ}\right)^2|h_2|^2\right\}}\right) \quad \cdots\cdots (2.47)$$

Now, if the receiving antenna $N_r = 1$, then, for such a MISO system, the conditional PEP becomes:

$$p(x_A \to x_j|h_1,h_2) = Q\left(\sqrt{\frac{E_{sig}}{2N_0N_t}\left\{\left(x_{AI}-x_{jI}\right)^2|h_1|^2+\left(x_{AQ}-x_{jQ}\right)^2|h_2|^2\right\}}\right) \quad \ldots\ (2.48)$$

2.2.2.1 Determining PEP in Rayleigh fading channel

In Rayleigh fading channel the pdf of γ_{fl} is given by [6,33];

$$f_{\gamma_{fl}}(\gamma_{fl}) = {}^{1}\!/_{\bar{\gamma}_{fl}} \exp\left(-\frac{\gamma_{fl}}{\bar{\gamma}_{fl}}\right) \quad \ldots\ldots\ (2.49)$$

where, the instantaneous SNR per bit for subcarrier l is,

$$\gamma_{fl} = |h_l|^2\frac{\mathrm{E_b}}{\mathrm{N_0}}, \qquad l \in 1,2 \qquad and \qquad \bar{\gamma}_{fl} = \mathrm{E}\left|\gamma_{fl}\right| = \mathrm{E}|h_l|^2\frac{\mathrm{E_b}}{\mathrm{N_0}} \quad \ldots\ldots\ (2.50)$$

In DCM accumulated constellation at Fig 2.6(b), let, $\mathrm{a_1}$ and $\mathrm{a_2}$ be the Euclidean symbol distance between x_A and x_j; $j \in \{B,C,D\}$ in both I- and Q- phase respectively. Therefore, the numerical value of the symbol distances corresponding to $a_1 and\ a_2$ can be measured and expressed as in Table 2.2 [6,18,33].

Table 2.2 Symbol Distance in Accumulated Constellation of DCM

Serial	**Symbol Pair**	**DCM Symbol Distance $\boldsymbol{a_1, a_2}$**	$\boldsymbol{c_{j1} = \frac{(a_1)^2}{10}, c_{j2} = \frac{(a_2)^2}{10}}$; $(\boldsymbol{j \in B, C, D})$
1	$(x_A \rightarrow x_B)$	*(4, 2)*	*(8/5, 2/5)*
2	$(x_A \rightarrow x_C)$	*(2, 6)*	*(2/5, 18/5)*
3	$(x_A \rightarrow x_D)$	*(2, 4)*	*(2/5, 8/5)*

Now, putting the value of (2.46), the conditional PEP becomes [6];

$$p(x_A \rightarrow x_j | h_1, h_2) = Q\left(\sqrt{\frac{E_{sig}}{2N_0 N_t}\left\{(x_{AI} - x_{jI})^2 |h_1|^2 + (x_{AQ} - x_{jQ})^2 |h_2|^2\right\}}\right)$$

$$= Q\sqrt{\frac{1}{N_t}\left(\frac{a_{j1}^2 |h_1|^2 + a_{j2}^2 |h_2|^2}{2}\right)\frac{E_{sig}}{N_0}}$$

$$let, (x_{AI} - x_{jI})^2 = a_{j1}^2 \ \& \ (x_{AQ} - x_{jQ})^2 = a_{j2}^2$$

$$= Q\sqrt{\frac{1}{N_t}\left(\frac{a_{j1}^2 |h_1|^2 + a_{j2}^2 |h_2|^2}{2}\right)\frac{\frac{E_b}{5}}{N_0}} \qquad \therefore \ E_{sig} = \frac{E_b}{5}$$

$$= Q\sqrt{\frac{1}{N_t}\left(\frac{a_{j1}^2 |h_1|^2 + a_{j2}^2 |h_2|^2}{10}\right)\frac{\mathrm{E_b}}{N_0}} \qquad \ldots \ldots \ldots (2.51)$$

In (2.51) let, $c_{jl} = \frac{a_{jl}^2}{10}$

But, from (2.50), the instantaneous SNR per bit for subcarrier l is;

$$\gamma_{fl} = |\mathrm{h}_l|^2 \, {}^{\mathrm{E_b}}/_{\mathrm{N_0}}, \qquad l \in 1, 2$$

Putting the above values in (2.51) i.e. the equation of conditional PEP leads to [6,33];

$$p(x_A \to x_j|\gamma_1,\gamma_2) = Q\sqrt{\frac{1}{N_t}(c_{j1}\gamma_{f1} + c_{j2}\gamma_{f2})} \qquad \ldots\ldots\ldots (2.52)$$

However, the average PEP can be obtained by integrating the conditional PEP with respect to the pdf of instantaneous SNR (γ_{fl}) having limit from 0 to ∞; i.e.

$$p(x_A \to x_j) = \int_0^\infty\int_0^\infty \underbrace{Q\left(\sqrt{{}^1/_{N_t}\,(c_{j1}\gamma_{f1} + c_{j2}\gamma_{f2})}\right)}_{conditional\ PEP} \underbrace{f_{\gamma_{f1}\gamma_{f2}}(\gamma_{f1}\gamma_{f2})}_{pdf}\, d\gamma_{f1}d\gamma_{f2} \quad \ldots (2.53)$$

However, the alternative expression of Q-function i.e. Craig's function is expressed as;

$$\mathrm{Q(z)} = \frac{1}{\pi}\int_0^{\frac{\pi}{2}} \exp(-\frac{z^2}{2\sin^2\theta})d\emptyset \qquad \ldots\ldots\ldots (2.54)$$

Using the Craig's function and considering, $z = \sqrt{{}^1/_{N_t}\,(c_{j1}\gamma_{f1} + c_{j2}\gamma_{f2})}$ in (2.54), the equation (2.63) of average PEP $p(x_A \to x_j)$ can be written as;

$$p(x_A \to x_j) = \int_0^\infty\int_0^\infty \frac{1}{\pi}\int_0^{\frac{\pi}{2}} \exp\left(-\frac{\left(\sqrt{{}^1/_{N_t}\,(c_{j1}\gamma_{f1} + c_{j2}\gamma_{f2})}\right)^2}{2sin^2\theta}\right) f_{\gamma_{f1}\gamma_{f2}}(\gamma_{f1}\gamma_{f2})\, d\gamma_{f1}d\gamma_{f2}d\theta$$

$$= \int_0^\infty\int_0^\infty \frac{1}{\pi}\int_0^{\frac{\pi}{2}} \exp\left(-\frac{\frac{c_{j1}\gamma_{f1} + c_{j2}\gamma_{f2}}{N_t}}{2sin^2\theta}\right) f_{\gamma_{f1}\gamma_{f2}}(\gamma_{f1}\gamma_{f2})\, d\gamma_{f1}d\gamma_{f2}d\theta$$

$$= \frac{1}{\pi}\int_0^{\frac{\pi}{2}}\int_0^\infty\int_0^\infty \exp\left(-\frac{c_{j1}\gamma_{f1} + c_{j2}\gamma_{f2}}{2N_t sin^2\theta}\right) f_{\gamma_{f1}\gamma_{f2}}(\gamma_{f1}\gamma_{f2})\, d\gamma_{f1}d\gamma_{f2}d\theta$$

$$= \frac{1}{\pi}\int_0^{\frac{\pi}{2}} \underbrace{\int_0^{\infty} \exp\left(-\frac{c_{j1}\gamma_{f1}}{2N_t sin^2\theta}\right) f_{\gamma_{f1}}(\gamma_{f1}) d\gamma_{f1}}_{MGF1} \underbrace{\int_0^{\infty} \exp\left(-\frac{c_{j2}\gamma_{f2}}{2N_t sin^2\theta}\right) f_{\gamma_{f2}}(\gamma_{f2}) d\gamma_{f2}}_{MGF2} d\theta \quad \ldots (2.55)$$

In the above equation (2.55), the integral part $\int_0^{\infty} \exp\left(-\frac{c_{jl}\gamma_{fl}}{2N_t sin^2\theta}\right) f_{\gamma_{fl}}(\gamma_{fl}) d\gamma_{fl}$ shows resemblance to Laplace transform of function $f_x(x)$. Hence, from the Laplace transformation the Moment Generating Function (MGF) of a random variable x can be illustrated as;

$$\mathcal{M}_x(-s) = \mathcal{L}\{f_x(x)\} = \int_0^{\infty} e^{-sx} f_x(x) dx \qquad \ldots\ldots\ldots (2.56)$$

Here, $\mathcal{L}\{.\}$ represents the Laplace transform function. The detail of Laplace transformation is given in Appendix-A. However, determination of the MGF directly by integration process is shown in Appendix-B. Now, according to Appendix-A;

$$\mathcal{M}_\gamma(s) = MGF = (1 - s\bar{\gamma})^{-1} \qquad \ldots\ldots\ldots (2.57)$$

In equation (2.55) of average PEP let's consider,

$$s = -\frac{c_{jl}}{2N_t sin^2\theta}$$

Putting the value of 's' in (2.57) we get;

$$\mathcal{M}_\gamma\left(-\frac{c_{jl}}{2N_t sin^2\theta}\right) = MGF = \left\{1 - \left(\frac{-c_{jl}}{2N_t sin^2\theta}\right)\bar{\gamma}\right\}^{-1}$$

$$= \left(1 + \frac{c_{jl}\bar{\gamma}_{fl}}{2N_t sin^2\theta}\right)^{-1}$$

$$= \left(\frac{2N_t sin^2\theta + c_{jl}\bar{\gamma}_{fl}}{2N_t sin^2\theta}\right)^{-1}$$

$$= \left(\frac{sin^2\theta + \frac{c_{jl}\bar{\gamma}_{fl}}{2\mathcal{N}_t}}{sin^2\theta}\right)^{-1} \quad \ldots\ldots\ldots (2.58)$$

To bring out the cumulative MGF for a system with $\mathcal{N}_r$ receive and $\mathcal{N}_t$ transmit antenna, the $\mathcal{N}_r$ times product of the MGF of a SIMO system is to be derived. Therefore, the MGF for a MIMO setting with $\mathcal{N}_t$ antenna transmit and $\mathcal{N}_r$ receive antenna is [8];

$$\mathcal{M}_x(s) = \prod_{L_r=1}^{\mathcal{N}_r} \left(\frac{sin^2\theta + \frac{c_{jl}\bar{\gamma}_{fl}}{2\mathcal{N}_t}}{sin^2\theta}\right)^{-1} \quad \ldots\ldots\ldots (2.59)$$

In a DCM MIMO system same signal is received through all the wireless channels. Hence, the channel wise MGF is likely to be same and the equation of cumulative MGF can be represented as;

$$\mathcal{M}_x(s) = \left(\left(\frac{sin^2\theta + \frac{c_{jl}\bar{\gamma}_{fl}}{2\mathcal{N}_t}}{sin^2\theta}\right)^{-1}\right)^{\mathcal{N}_r}$$

$$= \left(\frac{sin^2\theta + \frac{c_{jl}\bar{\gamma}_{fl}}{2\mathcal{N}_t}}{sin^2\theta}\right)^{-\mathcal{N}_r}$$

$$= \left(\frac{sin^2\theta}{sin^2\theta + \frac{c_{jl}\bar{\gamma}_{fl}}{2\mathcal{N}_t}}\right)^{\mathcal{N}_r} \quad \ldots\ldots\ldots (2.60)$$

Now, with the help of (2.60), for a MIMO setting the equation of average PEP as mentioned in (2.55) can be expressed as;

$$p\left(x_A \to x_j\right) = \frac{1}{\pi}\int_0^{\frac{\pi}{2}} \left\{ \underbrace{\frac{sin^2\theta}{sin^2\theta + \frac{c_{j1}\bar{\gamma}_{f1}}{2\mathcal{N}_t}}}_{MGF1} \underbrace{\frac{sin^2\theta}{sin^2\theta + \frac{c_{j2}\bar{\gamma}_{f2}}{2\mathcal{N}_t}}}_{MGF2} \right\}^{\mathcal{N}_r} d\theta \qquad \text{.........} (2.61)$$

In (2.61), let's consider, $\quad p_l = \dfrac{c_{jl}\bar{\gamma}_{fl}}{2\mathcal{N}_t} \qquad l\epsilon(1,2)$

So, the above equation (2.61) becomes;

$$p\left(x_A \to x_j\right) = \frac{1}{\pi}\int_0^{\frac{\pi}{2}} \left\{ \frac{sin^2\theta}{sin^2\theta + p_1} \frac{sin^2\theta}{sin^2\theta + p_2} \right\}^{\mathcal{N}_r} d\theta$$

$$= \frac{1}{\pi}\int_0^{\frac{\pi}{2}} \left\{ \frac{sin^2\theta}{1 - cos^2\theta + p_1} \frac{sin^2\theta}{1 - cos^2\theta + p_2} \right\}^{\mathcal{N}_r} d\theta \qquad \therefore \left(sin^2\theta = 1 - cos^2\theta\right)$$

$$= \frac{1}{\pi}\int_0^{\frac{\pi}{2}} \left\{ \frac{sin^2\theta}{(1+p_1)\left(\frac{1+p_1-cos^2\theta}{1+p_1}\right)} \frac{sin^2\theta}{(1+p_2)\left(\frac{1+p_2-cos^2\theta}{1+p_2}\right)} \right\}^{\mathcal{N}_r} d\theta$$

$$= \frac{1}{\pi}\int_0^{\frac{\pi}{2}} \left\{ \frac{sin^2\theta}{(1+p_1)\left(1-\frac{cos^2\theta}{1+p_1}\right)} \frac{sin^2\theta}{(1+p_2)\left(1-\frac{cos^2\theta}{1+p_2}\right)} \right\}^{\mathcal{N}_r} d\theta$$

$$= \frac{\{(1+p_1)^{-1}(1+p_2)^{-1}\}^{\mathcal{N}_r}}{\pi}\int_0^{\frac{\pi}{2}} \left\{ \frac{sin^4\theta}{\left(\left(1-\frac{cos^2\theta}{1+p_1}\right)\left(1-\frac{cos^2\theta}{1+p_2}\right)\right)} \right\}^{\mathcal{N}_r} d\theta$$

$$= \frac{(1+p_1)^{-\mathcal{N}_r}(1+p_2)^{-\mathcal{N}_r}}{\pi}\int_0^{\frac{\pi}{2}} \left\{ \frac{sin^4\theta}{\left(\left(1-\frac{cos^2\theta}{1+p_1}\right)\left(1-\frac{cos^2\theta}{1+p_2}\right)\right)} \right\}^{\mathcal{N}_r} d\theta \quad \cdots\cdots \; (2.62)$$

In (2.72), let's consider, $cos^2\theta = t$. So, the limits change to;

θ	0	$\pi/2$
t	1	0

Now, $t = cos^2\theta$

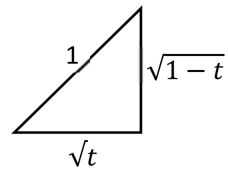

$$\therefore dt = -2sin\theta\, cos\theta\, d\theta$$

$$or, d\theta = \frac{dt}{(-2sin\theta\, cos\theta)} = \frac{-dt}{2(\sqrt{1-t})\sqrt{t}}$$

$$\left[from\ geometry,\ \ sin\theta = \sqrt{1-t}\,\right] \quad \ldots\ldots (2.63)$$

Again, $\quad sin^2\theta = 1 - cos^2\theta = (1-t)$

Putting the values from the geometry, the equation of average PEP (2.62) turns into;

$$p(x_A \to x_j) = \frac{(1+p_1)^{-\mathcal{N}_r}(1+p_2)^{-\mathcal{N}_r}}{\pi} \int_1^0 \left\{ \frac{(1-t)^2}{\left(1 - \frac{t}{1+p_1}\right)\left(1 - \frac{t}{1+p_2}\right)} \right\}^{\mathcal{N}_r} \frac{-dt}{2(\sqrt{1-t})\sqrt{t}}$$

$$= -\frac{(1+p_1)^{-\mathcal{N}_r}(1+p_2)^{-\mathcal{N}_r}}{\pi} \int_0^1 \left\{ \frac{(1-t)^2}{\left(1 - \frac{t}{1+p_1}\right)\left(1 - \frac{t}{1+p_2}\right)} \right\}^{\mathcal{N}_r} \frac{-dt}{2(\sqrt{1-t})\sqrt{t}}$$

$$[reversing\ the\ limits]$$

$$= \frac{(1+p_1)^{-\mathcal{N}_r}(1+p_2)^{-\mathcal{N}_r}}{2\pi} \int_0^1 \left\{ \left(1 - \frac{t}{1+p_1}\right)\left(1 - \frac{t}{1+p_2}\right) \right\}^{-\mathcal{N}_r} (1-t)^{2\mathcal{N}_r} \{(1-t)t\}^{-\frac{1}{2}}\, dt$$

$$= \frac{(1+p_1)^{-\mathcal{N}_r}(1+p_2)^{-\mathcal{N}_r}}{2\pi} \int_0^1 t^{-\frac{1}{2}} (1-t)^{(2\mathcal{N}_r - \frac{1}{2})} \left(1 - \frac{t}{1+p_1}\right)^{-\mathcal{N}_r} \left(1 - \frac{t}{1+p_2}\right)^{-\mathcal{N}_r} dt .. (2.64)$$

In (2.64), applying Appell hyper geometric function, i.e.

$$\frac{\Gamma(\alpha)\Gamma(\gamma-\alpha)}{\Gamma(\gamma)}F_1(\alpha;\ \beta,\beta';\ \gamma;x,y)=\int_0^1 u^{(\alpha-1)}\,(1-u)^{(\gamma-\alpha-1)}(1-ux)^{-\beta}(1-uy)^{-\beta'}\,du$$

the equation of average PEP reduces to;

$$p\left(x_A\to x_j\right)=\frac{(1+p_1)^{-\mathcal{N}_r}(1+p_2)^{-\mathcal{N}_r}}{2\pi}\times\frac{\Gamma\left({}^1\!/_2\right)\Gamma\left(2\mathcal{N}_r+\frac{1}{2}\right)}{\Gamma(2\mathcal{N}_r+1)}$$
$$\times F_1\left(\frac{1}{2};\mathcal{N}_r,\mathcal{N}_r;2\mathcal{N}_r+1;\frac{1}{1+p_1},\frac{1}{1+p_1}\right)$$

$$=\frac{(1+p_1)^{-\mathcal{N}_r}(1+p_2)^{-\mathcal{N}_r}}{2\pi}\times\frac{\sqrt{\pi}\Gamma\left(2\mathcal{N}_r+\frac{1}{2}\right)}{\Gamma(2\mathcal{N}_r+1)}$$
$$\times F_1\left(\frac{1}{2};\mathcal{N}_r,\mathcal{N}_r;2\mathcal{N}_r+1;\frac{1}{1+p_1},\frac{1}{1+p_1}\right)\qquad as\quad \Gamma\left({}^1\!/_2\right)=\sqrt{\pi}$$

$$=\frac{(1+p_1)^{-\mathcal{N}_r}(1+p_2)^{-\mathcal{N}_r}}{2\sqrt{\pi}}\times\frac{\Gamma\left(2\mathcal{N}_r+\frac{1}{2}\right)}{\Gamma(2\mathcal{N}_r+1)}$$
$$\times F_1\left(\frac{1}{2};\mathcal{N}_r,\mathcal{N}_r;2\mathcal{N}_r+1;\frac{1}{1+p_1},\frac{1}{1+p_1}\right)\qquad \ldots\ldots(2.65)$$

However, it was assumed that;

$$\left.\begin{array}{ll}\dfrac{a_{jl}^2}{10}=c_{jl} & \text{in equation (2.61) } and\\[2ex] p_l=\dfrac{c_{jl}\bar{\gamma}_{fl}}{2\mathcal{N}_t} & \text{in equation (2.71)}\end{array}\right\}\quad l\in 1,2$$

So, p_l turns into, $$p_l=\frac{c_{jl}\bar{\gamma}_{fl}}{2\mathcal{N}_t}=\frac{\frac{a_{jl}^2}{10}\bar{\gamma}_{fl}}{2\mathcal{N}_t}=\frac{a_{jl}^2\bar{\gamma}_{fl}}{20\mathcal{N}_t}\qquad l\epsilon(1,2)$$

Putting the value of p_l in (2.65), the equation of average PEP becomes;

$$p(x_A \to x_j) = \frac{\left(1+\frac{c_{j1}\bar{\gamma}_{f1}}{2\mathcal{N}_t}\right)^{-\mathcal{N}_r}\left(1+\frac{c_{j2}\bar{\gamma}_{f2}}{2\mathcal{N}_t}\right)^{-\mathcal{N}_r}}{2\sqrt{\pi}} \times \frac{\Gamma\left(2\mathcal{N}_r+\frac{1}{2}\right)}{\Gamma(2\mathcal{N}_r+1)}$$

$$\times F_1\left(\frac{1}{2};\mathcal{N}_r,\mathcal{N}_r;2\mathcal{N}_r+1;\frac{1}{1+\frac{c_{j1}\bar{\gamma}_{f1}}{2\mathcal{N}_t}},\frac{1}{1+\frac{c_{j2}\bar{\gamma}_{f2}}{2\mathcal{N}_t}}\right) \quad \cdots\cdots (2.66)$$

2.2.2.2 Determination of Cumulative Average BER

Substituting the value of (2.66) in (2.44), the simplified equation of cumulative average BER for a DCM based MB-OFDM UWB MIMO system can be illustrated as;

$$P_b(E) \le \frac{1}{2}\{p(y_A \to y_B) + p(y_A \to y_C) + p(y_A \to y_D)\}$$

$$\le \frac{1}{2}\sum_{j=B}^{D}\left\{\frac{\left(1+\frac{c_{j1}\bar{\gamma}_{f1}}{2\mathcal{N}_t}\right)^{-\mathcal{N}_r}\left(1+\frac{c_{j2}\bar{\gamma}_{f2}}{2\mathcal{N}_t}\right)^{-\mathcal{N}_r}}{2\sqrt{\pi}} \times \frac{\Gamma\left(2\mathcal{N}_r+\frac{1}{2}\right)}{\Gamma(2\mathcal{N}_r+1)}\right.$$

$$\left.\times F_1\left(\frac{1}{2};\mathcal{N}_r,\mathcal{N}_r;2\mathcal{N}_r+1;\frac{1}{1+\frac{c_{j1}\bar{\gamma}_{f1}}{2\mathcal{N}_t}},\frac{1}{1+\frac{c_{j2}\bar{\gamma}_{f2}}{2\mathcal{N}_t}}\right)\right\} \quad j \in B, C, D$$

$$\le \frac{1}{4\sqrt{\pi}} \times \frac{\Gamma\left(2\mathcal{N}_r+\frac{1}{2}\right)}{\Gamma(2\mathcal{N}_r+1)}\sum_{j=B}^{D}\left(1+\frac{c_{j1}\bar{\gamma}_{f1}}{2\mathcal{N}_t}\right)^{-\mathcal{N}_r}\left(1+\frac{c_{j2}\bar{\gamma}_{f2}}{2\mathcal{N}_t}\right)^{-\mathcal{N}_r}$$

$$\times F_1\left(\frac{1}{2};\mathcal{N}_r,\mathcal{N}_r;2\mathcal{N}_r+1;\frac{1}{1+\frac{c_{j1}\bar{\gamma}_{f1}}{2\mathcal{N}_t}},\frac{1}{1+\frac{c_{j2}\bar{\gamma}_{f2}}{2\mathcal{N}_t}}\right) \quad \ldots\ldots (2.67)$$

Putting the values of c_{jl} from Table 2.2, the equation (2.67) changes to;

$$P_b(E) \leq \frac{1}{4\sqrt{\pi}} \times \frac{\Gamma\left(2\mathcal{N}_r + \frac{1}{2}\right)}{\Gamma(2\mathcal{N}_r + 1)} \left[\left(1 + \frac{\frac{8}{5}\bar{\gamma}_{f1}}{2\mathcal{N}_t}\right)^{-\mathcal{N}_r} \left(1 + \frac{\frac{2}{5}\bar{\gamma}_{f2}}{2\mathcal{N}_t}\right)^{-\mathcal{N}_r} \right.$$

$$\times F_1\left(\frac{1}{2}; \mathcal{N}_r, \mathcal{N}_r; 2\mathcal{N}_r + 1; \frac{1}{1 + \frac{\frac{8}{5}\bar{\gamma}_{f1}}{2\mathcal{N}_t}}, \frac{1}{1 + \frac{\frac{2}{5}\bar{\gamma}_{f2}}{2\mathcal{N}_t}}\right) + \left(1 + \frac{\frac{2}{5}\bar{\gamma}_{f1}}{2\mathcal{N}_t}\right)^{-\mathcal{N}_r} \left(1 + \frac{\frac{18}{5}\bar{\gamma}_{f2}}{2\mathcal{N}_t}\right)^{-\mathcal{N}_r}$$

$$\times F_1\left(\frac{1}{2}; \mathcal{N}_r, \mathcal{N}_r; 2\mathcal{N}_r + 1; \frac{1}{1 + \frac{\frac{2}{5}\bar{\gamma}_{f1}}{2\mathcal{N}_t}}, \frac{1}{1 + \frac{\frac{18}{5}\bar{\gamma}_{f2}}{2\mathcal{N}_t}}\right) + \left(1 + \frac{\frac{2}{5}\bar{\gamma}_{f1}}{2\mathcal{N}_t}\right)^{-\mathcal{N}_r} \left(1 + \frac{\frac{8}{5}\bar{\gamma}_{f2}}{2\mathcal{N}_t}\right)^{-\mathcal{N}_r}$$

$$\left. \times F_1\left(\frac{1}{2}; \mathcal{N}_r, \mathcal{N}_r; 2\mathcal{N}_r + 1; \frac{1}{1 + \frac{\frac{2}{5}\bar{\gamma}_{f1}}{2\mathcal{N}_t}}, \frac{1}{1 + \frac{\frac{8}{5}\bar{\gamma}_{f2}}{2\mathcal{N}_t}}\right) \right]$$

or;

$$P_b(E) \leq \frac{1}{4\sqrt{\pi}} \times \frac{\Gamma\left(2\mathcal{N}_r + \frac{1}{2}\right)}{\Gamma(2\mathcal{N}_r + 1)} \left[\left(1 + \frac{8\bar{\gamma}_{f1}}{10\mathcal{N}_t}\right)^{-\mathcal{N}_r} \left(1 + \frac{2\bar{\gamma}_{f2}}{10\mathcal{N}_t}\right)^{-\mathcal{N}_r} \right.$$

$$\times F_1\left(\frac{1}{2}; \mathcal{N}_r, \mathcal{N}_r; 2\mathcal{N}_r + 1; \frac{1}{1 + \frac{8\bar{\gamma}_{f1}}{10\mathcal{N}_t}}, \frac{1}{1 + \frac{2\bar{\gamma}_{f2}}{10\mathcal{N}_t}}\right) + \left(1 + \frac{2\bar{\gamma}_{f1}}{10\mathcal{N}_t}\right)^{-\mathcal{N}_r} \left(1 + \frac{18\bar{\gamma}_{f2}}{10\mathcal{N}_t}\right)^{-\mathcal{N}_r}$$

$$\times F_1\left(\frac{1}{2}; \mathcal{N}_r, \mathcal{N}_r; 2\mathcal{N}_r + 1; \frac{1}{1 + \frac{2\bar{\gamma}_{f1}}{10\mathcal{N}_t}}, \frac{1}{1 + \frac{18\bar{\gamma}_{f2}}{10\mathcal{N}_t}}\right) + \left(1 + \frac{2\bar{\gamma}_{f1}}{10\mathcal{N}_t}\right)^{-\mathcal{N}_r} \left(1 + \frac{8\bar{\gamma}_{f2}}{10\mathcal{N}_t}\right)^{-\mathcal{N}_r}$$

$$\left. \times F_1\left(\frac{1}{2}; \mathcal{N}_r, \mathcal{N}_r; 2\mathcal{N}_r + 1; \frac{1}{1 + \frac{2\bar{\gamma}_{f1}}{10\mathcal{N}_t}}, \frac{1}{1 + \frac{8\bar{\gamma}_{f2}}{10\mathcal{N}_t}}\right) \right] \quad \ldots\ldots (2.68)$$

However, when both the channels are symmetric i.e. $\bar{\gamma}_{f1} = \bar{\gamma}_{f2} = \bar{\gamma}_f$, the equation (2.68) reduces to;

$$P_b(E) \le \frac{1}{4\sqrt{\pi}} \times \frac{\Gamma\left(2\mathcal{N}_r + \frac{1}{2}\right)}{\Gamma(2\mathcal{N}_r + 1)} \Bigg[\left(1 + \frac{8\bar{\gamma}_f}{10\mathcal{N}_t}\right)^{-\mathcal{N}_r} \left(1 + \frac{2\bar{\gamma}_f}{10\mathcal{N}_t}\right)^{-\mathcal{N}_r}$$

$$\times F_1\left(\frac{1}{2}; \mathcal{N}_r, \mathcal{N}_r; 2\mathcal{N}_r + 1; \frac{1}{1 + \frac{8\bar{\gamma}_f}{10\mathcal{N}_t}}, \frac{1}{1 + \frac{2\bar{\gamma}_f}{10\mathcal{N}_t}}\right) + \left(1 + \frac{2\bar{\gamma}_f}{10\mathcal{N}_t}\right)^{-\mathcal{N}_r} \left(1 + \frac{18\bar{\gamma}_f}{10\mathcal{N}_t}\right)^{-\mathcal{N}_r}$$

$$\times F_1\left(\frac{1}{2}; \mathcal{N}_r, \mathcal{N}_r; 2\mathcal{N}_r + 1; \frac{1}{1 + \frac{2\bar{\gamma}_f}{10\mathcal{N}_t}}, \frac{1}{1 + \frac{18\bar{\gamma}_f}{10\mathcal{N}_t}}\right) + \left(1 + \frac{2\bar{\gamma}_f}{10\mathcal{N}_t}\right)^{-\mathcal{N}_r} \left(1 + \frac{8\bar{\gamma}_f}{10\mathcal{N}_t}\right)^{-\mathcal{N}_r}$$

$$\times F_1\left(\frac{1}{2}; \mathcal{N}_r, \mathcal{N}_r; 2\mathcal{N}_r + 1; \frac{1}{1 + \frac{2\bar{\gamma}_f}{10\mathcal{N}_t}}, \frac{1}{1 + \frac{8\bar{\gamma}_f}{10\mathcal{N}_t}}\right) \Bigg] \quad \ldots\ldots (2.69)$$

But, $\Gamma z = (z-1)!$ and $\Gamma \frac{n}{2} = \frac{2^{(1-n)}(n-1)!\,\sqrt{\pi}}{\left(\frac{n-1}{2}\right)!}$

Therefore, the equation for the cumulative average BER of an UWB communication system with DCM and space diversity can be expressed as;

$$P_b(E) \le \frac{1}{4\sqrt{\pi}} \times \frac{\left(2\mathcal{N}_r - \frac{1}{2}\right)!}{(2\mathcal{N}_r)!} \Bigg[\left(1 + \frac{8\bar{\gamma}_f}{10\mathcal{N}_t}\right)^{-\mathcal{N}_r} \left(1 + \frac{2\bar{\gamma}_f}{10\mathcal{N}_t}\right)^{-\mathcal{N}_r}$$

$$\times F_1\left(\frac{1}{2}; \mathcal{N}_r, \mathcal{N}_r; 2\mathcal{N}_r + 1; \frac{1}{1 + \frac{8\bar{\gamma}_f}{10\mathcal{N}_t}}, \frac{1}{1 + \frac{2\bar{\gamma}_f}{10\mathcal{N}_t}}\right) + \left(1 + \frac{2\bar{\gamma}_f}{10\mathcal{N}_t}\right)^{-\mathcal{N}_r} \left(1 + \frac{18\bar{\gamma}_f}{10\mathcal{N}_t}\right)^{-\mathcal{N}_r}$$

$$\times F_1\left(\frac{1}{2}; \mathcal{N}_r, \mathcal{N}_r; 2\mathcal{N}_r + 1; \frac{1}{1 + \frac{2\bar{\gamma}_f}{10\mathcal{N}_t}}, \frac{1}{1 + \frac{18\bar{\gamma}_f}{10\mathcal{N}_t}}\right) + \left(1 + \frac{2\bar{\gamma}_f}{10\mathcal{N}_t}\right)^{-\mathcal{N}_r} \left(1 + \frac{8\bar{\gamma}_f}{10\mathcal{N}_t}\right)^{-\mathcal{N}_r}$$

$$\times F_1\left(\frac{1}{2}; \mathcal{N}_r, \mathcal{N}_r; 2\mathcal{N}_r + 1; \frac{1}{1 + \frac{2\bar{\gamma}_f}{10\mathcal{N}_t}}, \frac{1}{1 + \frac{8\bar{\gamma}_f}{10\mathcal{N}_t}}\right) \Bigg] \quad \ldots\ldots\ldots (2.70)$$

2.3 Summary

DCM has achieved ECMA-368 global standard for MB-OFDM UWB communication system in 2004 for establishing WPAN such as Bluetooth 3.0, W-USB and WHDMI. In operation, DCM system starts with 1200 interleaved bits and get them divided into groups of 200 bits. Each bit group generates 100 QPSK symbols where, 4 re-ordered bits passes through the system at a time. DCM module transforms these QPSK modulated symbols into DCM symbols with the help of DCM matrix, $W = [2 \quad 1; \quad 1 \quad -2]$. As a result, 100 QPSK symbols generates 100 DCM symbols which, are then mounted onto two non-adjacent subcarriers having 50 subcarrier separation in between. At the receiver, MRC, ML soft bit decoding and veterbi decoder is used to regenerate the transmitted bit stream from the received signal.

In this analytical research, PEP determination method is followed to evaluate the BER performance of an UWB communication system with DCM and space diversity considering Rayleigh fading environment. PEP is determined on the basis of pdf and output SNR where, the average PEP is obtained by integrating the conditional PEP with respect to the pdf of instantaneous SNR (γ_{fl}) having limit from 0 to ∞. Finally, expressions of cumulative average BER of a DCM system with N_t transmit and N_r receive antennas in Rayleigh fading environment is deduced by summing up the average PEPs for all the equally likely message symbols of DCM constellation.

CHAPTER-3
RESULTS AND DISCUSSION

3.1 Parameters for Computation

The BER performance of DCM with space diversity in Rayleigh fading environment is numerically analyzed using equation (2.70). Workability of the equation is validated by matching the output graph for SISO arrangement with that of the equation derived by Ryu, H. S., Lee, J. S. and Kang, C. G for SISO DCM system which is [33];

$$P_b(E) \leq \frac{1}{4}\left[3 + \frac{19}{24}\sqrt{\frac{\bar{\gamma}}{\bar{\gamma}+5}} - \frac{8}{3}\sqrt{\frac{4\bar{\gamma}}{4\bar{\gamma}+5}} - \frac{9}{8}\sqrt{\frac{9\bar{\gamma}}{9\bar{\gamma}+5}}\right] \qquad \cdots\cdots(3.1)$$

Results obtained are compared with similar type of system using QPSK modulation (detail in Appendix-C) to define its data handling proficiency. Analysis of the results are carried out to determine the optimum values for the system parameters against a particular BER. However, the parameter considered in the process of BER performance evaluation of DCM are given in Table 3.1.

Table 3.1: Parameters Used for Computation

Parameters	Value
Operating Frequency Spectrum	3.168 to 4.752 GHz
Modulation	DCM and QPSK
Channel Bandwidth	528 MHz
FFT and IFFT Points	128
Number of Transmitting and Receiving Antennas, (N_t and N_r)	1 to 4

3.2 Result Analysis

Space diversity puts a dominant effect on the overall BER performance of a wireless communication system. To evaluate its effect on DCM, a good number of graphical illustration with varying number of transmit and receive antenna combinations are studied. As sequel, SNR vs BER curve of DCM and QPSK are projected for single transmit and multiple receive antennas in Fig. 3.1. To ease the relative study, the number of receiving antenna is varied from 1 to 4, keeping the number of transmitting antenna fixed at 1. In this regard, data measured from the graph against different antenna configurations are noted in Table 3.2.

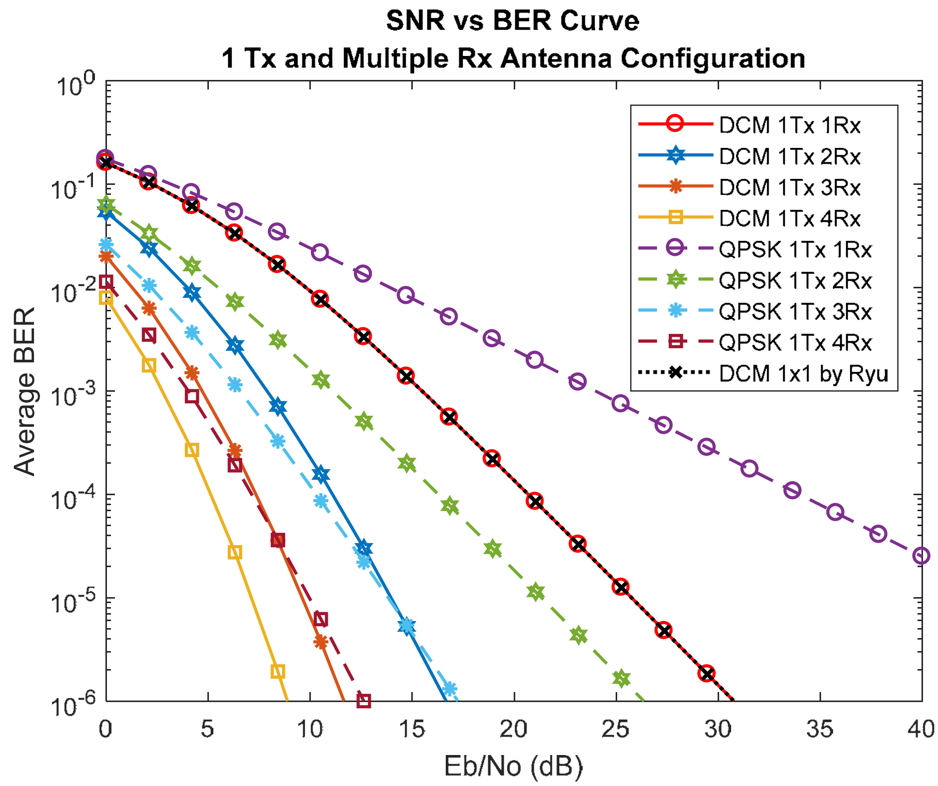

Fig. 3.1: SNR vs BER Curve for 1 Tx and Multiple Rx Antenna Setup

Table 3.2: Sensitivity (SNR in dB) of DCM and QPSK for 1Tx and Multiple Rx at BER 10^{-3} and 10^{-6} Respectively

SNR (dB) for 1 Tx	**Rx →**	**1**	**2**	**3**	**4**
at BER 10^{-3}	QPSK	24.01	11.2	6.66	4.24
	DCM	15.53	7.88	4.85	3.0
	Sensitivity Improvement in DCM	8.48	3.32	1.81	1.24
at BER 10^{-6}	QPSK	53.94	26.2	17.0	12.5
	DCM	30.65	16.55	11.68	8.9
	Sensitivity Improvement in DCM	23.29	9.65	5.32	3.6

SNR vs BER curve for DCM SISO setup using (2.70) and (3.1) superimpose on each other and thereby the workability of (2.70) for DCM with space diversity is justified. Relevant data are noted in Table 3.2 which clearly discloses that DCM out performs QPSK in every aspect. Performance of both the modulation scheme gradually improves with the increment of the number of receiving antenna against fixed number of transmitting antenna and same BER can be achieved at relatively lower SNR.

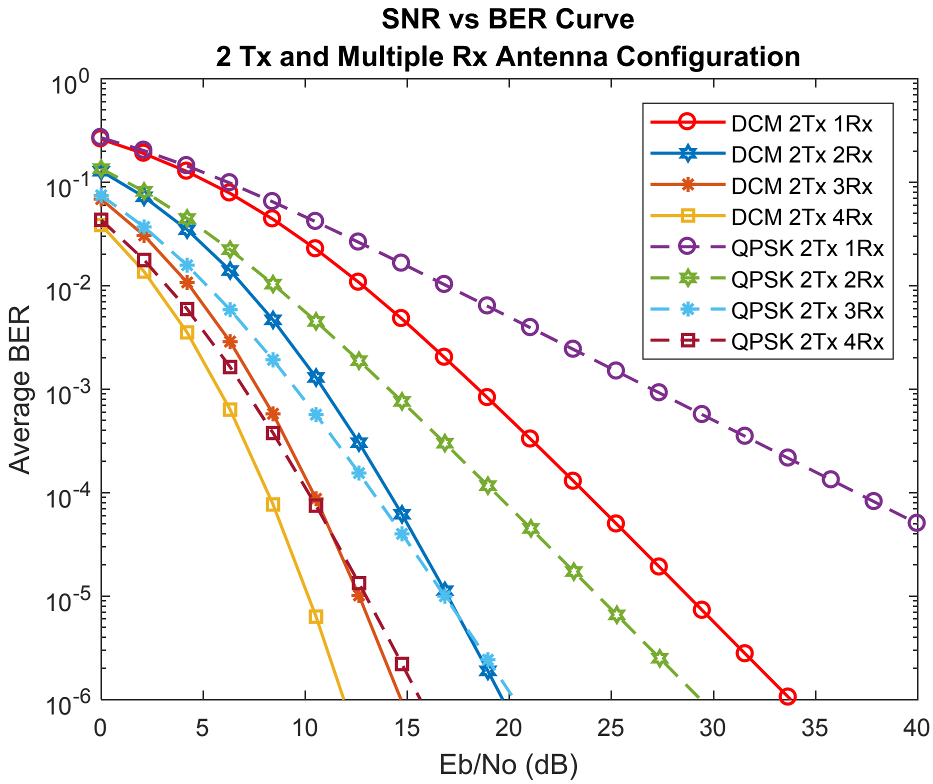

Fig. 3.2: SNR vs BER Curve for 2 Tx and Multiple Rx Antenna Setup

In Fig. 3.2, number of transmitting antenna is kept fixed at 2 while, the number of receiving antenna is increased sequentially from 1 to 4. SNR vs BER measurements are taken for different antenna configuration and noted in Table 3.3.

Table 3.3: Sensitivity (SNR in dB) of DCM and QPSK for 2Tx and Multiple Rx at BER 10^{-3} and 10^{-6} Respectively

SNR (dB) for 2 Tx \ **Rx →**		**1**	**2**	**3**	**4**
at BER 10^{-3}	QPSK	27.15	14.08	9.6	7.04
	DCM	18.44	11.0	7.7	5.8
	Sensitivity Improvement in DCM	8.71	3.08	1.9	1.24
at BER 10^{-6}	QPSK	56.98	29.5	20.3	15.6
	DCM	33.8	19.8	14.6	12.0
	Sensitivity Improvement in DCM	23.18	9.7	5.7	3.6

Data recorded in Table 3.3 indicates that increasing the number of transmitting antenna from 1 to 2 demands relatively higher SNR to achieve the same BER as that of Fig 3.1.

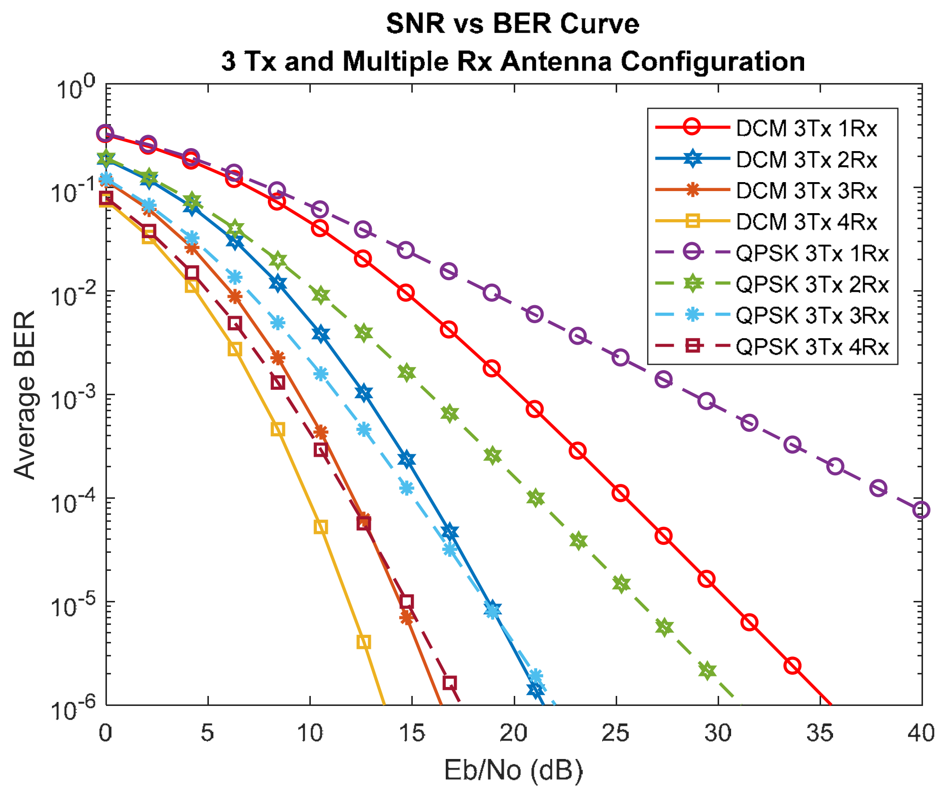

Fig. 3.3: SNR vs BER Curve for 3 Tx and Multiple Rx Antenna Setup

The number of receiving antenna is increased sequentially from 1 to 4 keeping the number of transmitting antenna fixed at 3. Outputs are graphically represented in Fig. 3.3. In this regard, relevant SNR vs BER measurements for different antenna configuration are noted in Table 3.4.

Table 3.4: Sensitivity (SNR in dB) of DCM and QPSK for 3Tx and Multiple Rx at BER 10^{-3} and 10^{-6} Respectively

SNR (dB) for 3 Tx \ **Rx →**		**1**	**2**	**3**	**4**
at BER 10^{-3}	QPSK	28.83	15.77	11.4	8.85
	DCM	20.35	12.74	9.55	7.5
	Sensitivity Improvement in DCM	8.48	3.03	1.85	1.35
at BER 10^{-6}	QPSK	58.66	31.0	21.9	17.3
	DCM	35.53	21.7	16.42	13.65
	Sensitivity Improvement in DCM	23.13	9.3	5.48	3.65

Analyzing the recorded information of Table 3.4 it becomes more clear that by increasing the number of transmit antenna to 3, it demands relatively higher SNR to achieve the same BER as depicted in Fig. 3.1 and 3.2.

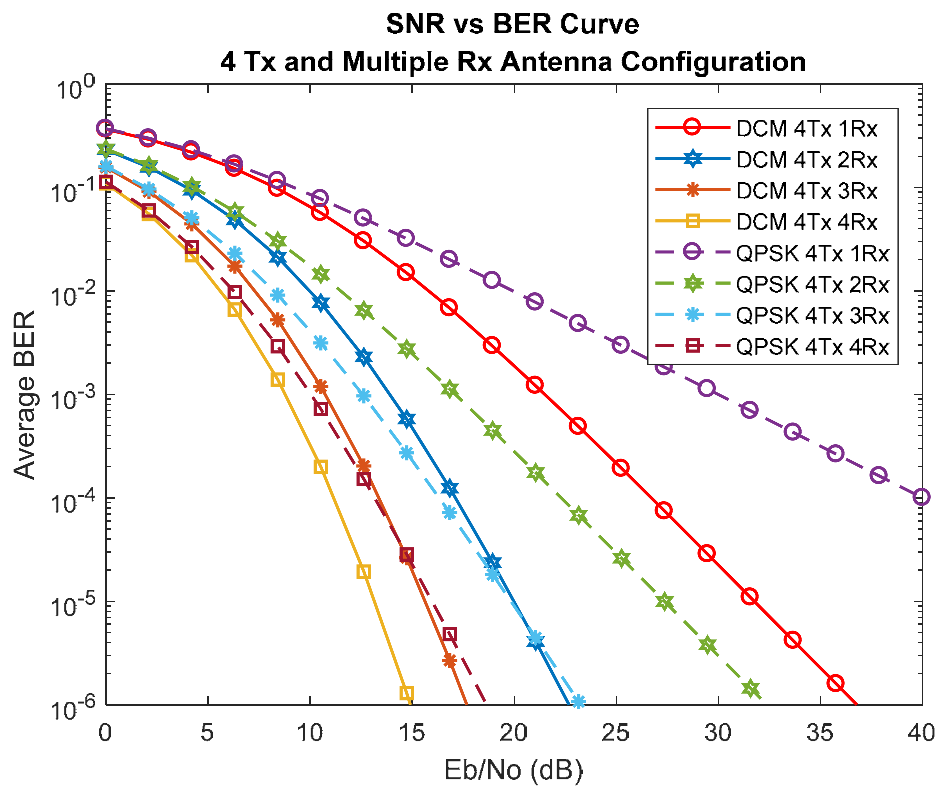

Fig. 3.4: SNR vs BER Curve for 4 Tx and Multiple Rx Antenna Setup

In Fig. 3.4, number of transmitting antenna is kept fixed at 4 while, the number of receiving antenna is increased sequentially from 1 to 4. SNR vs BER measurements are taken for different antenna configuration and noted in Table 3.5.

Table 3.5: Sensitivity (SNR in dB) of DCM and QPSK for 4Tx and Multiple Rx at BER 10^{-3} and 10^{-6} Respectively

SNR (dB) for 4 Tx / **Rx →**		**1**	**2**	**3**	**4**
at BER 10^{-3}	QPSK	30.17	17.09	12.6	10.06
	DCM	21.45	13.9	10.73	8.85
	Sensitivity Improvement in DCM	8.72	3.19	1.87	1.21
at BER 10^{-6}	QPSK	60.0	32.3	23.25	18.55
	DCM	36.65	23.0	17.6	14.9
	Sensitivity Improvement in DCM	23.35	9.3	5.65	3.65

The Table 3.5 above gives a vivid exposer that by further increasing the number of transmit antenna to 4, it demands relatively more higher SNR to achieve the same BER as depicted in Fig. 3.1, 3.2 and 3.3.

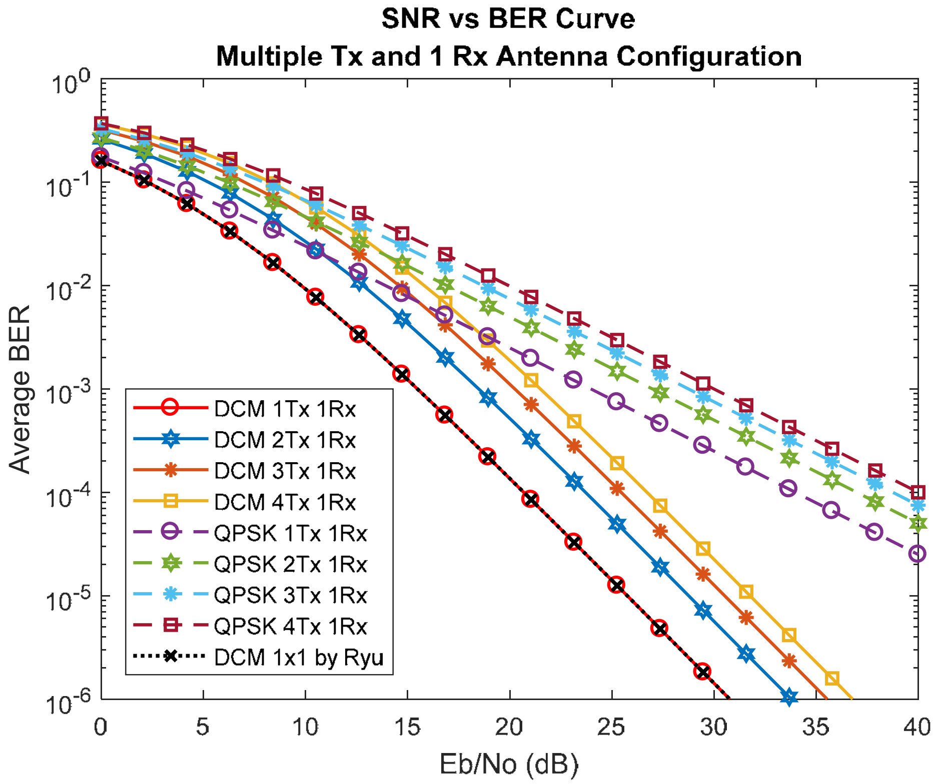

Fig. 3.5: SNR vs BER Curve for Multiple Tx and 1 Rx Antenna Setup

In line of Fig. 3.1 to 3.4, same type of information are extracted from Fig. 3.5 to 3.8. But, here the only exception is that the number of transmitting antenna is varied keeping the number of receiving antenna fixed. However, in Fig. 3.5, SNR vs BER curve for both DCM and QPSK are projected where, the number of transmitting antenna varies from 1 to 4 and the number of receiving antenna is kept fixed at 1. The data measured for different antenna configuration are noted in Table 3.6.

Table 3.6: Sensitivity (SNR in dB) of DCM and QPSK for Multiple Tx and 1 Rx at BER 10^{-3} and 10^{-6} Respectively

SNR (dB) for 1 Rx	**Tx →**	**1**	**2**	**3**	**4**
at BER 10^{-3}	QPSK	24.01	27.15	28.83	30.17
	DCM	15.53	18.44	20.35	21.45
	Sensitivity Improvement in DCM	8.48	8.71	8.48	8.72
at BER 10^{-6}	QPSK	53.94	56.98	58.66	60.0
	DCM	30.65	33.8	35.53	36.65
	Sensitivity Improvement in DCM	23.29	23.18	23.13	23.35

Information noted in Table 3.6 show that DCM attains the same BER at relatively lower SNR over QPSK. At particular BER for a fixed number of receiving antenna, the SNR value increases with the increment of number of transmitting antenna. That is, the performance deteriorates with the increment of transmitting antenna if no transmission diversity coding technique is applied.

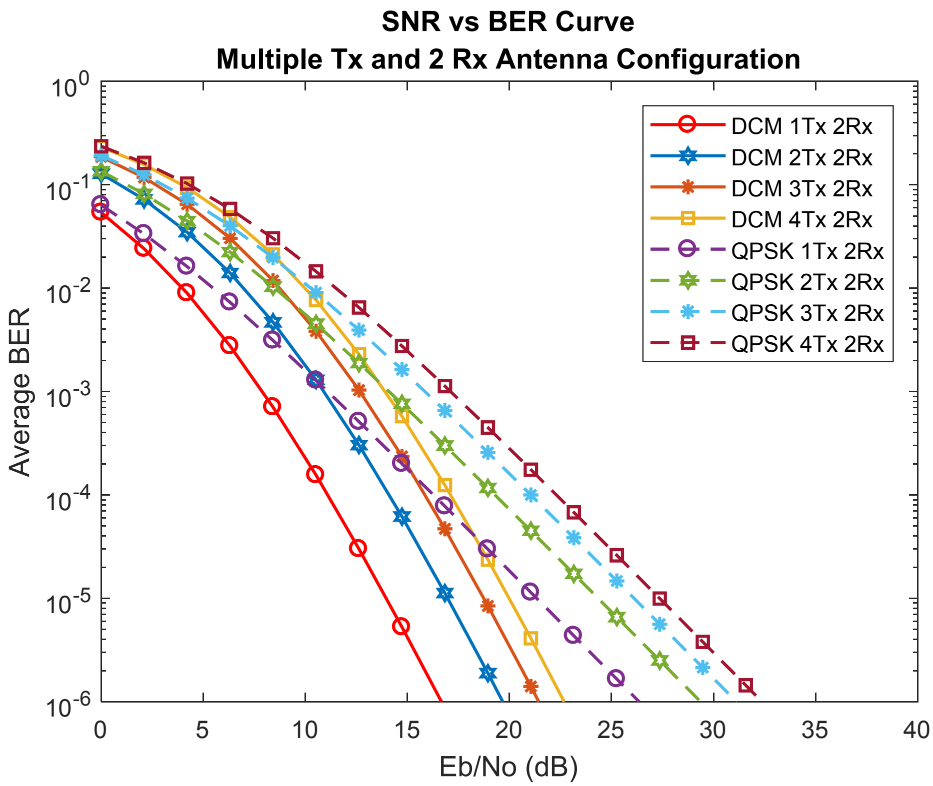

Fig. 3.6: SNR vs BER Curve for Multiple Tx and 2 Rx Antenna Setup

In Fig. 3.6, number of receiving antenna is kept fixed at 2 while, the number of transmitting antenna is increased sequentially from 1 to 4. SNR vs BER measurements are taken for different antenna configuration and noted in Table 3.7.

Table 3.7: Sensitivity (SNR in dB) of DCM and QPSK for Multiple Tx and 2 Rx at BER 10^{-3} and 10^{-6} Respectively

SNR (dB) for 2 Rx	Tx →	1	2	3	4
at BER 10^{-3}	QPSK	11.2	14.08	15.77	17.09
	DCM	7.88	11.0	12.74	13.9
	Sensitivity Improvement in DCM	3.32	3.08	3.03	3.19
at BER 10^{-6}	QPSK	26.2	29.5	31.0	32.3
	DCM	16.55	19.8	21.7	23.0
	Sensitivity Improvement in DCM	9.65	9.7	9.3	9.3

In addition to the characteristics of the system noted in Table 3.6, it is depicted in Table 3.7 that with the increment of number of transmitting antenna the sensitivity improvement of DCM gradually reduces.

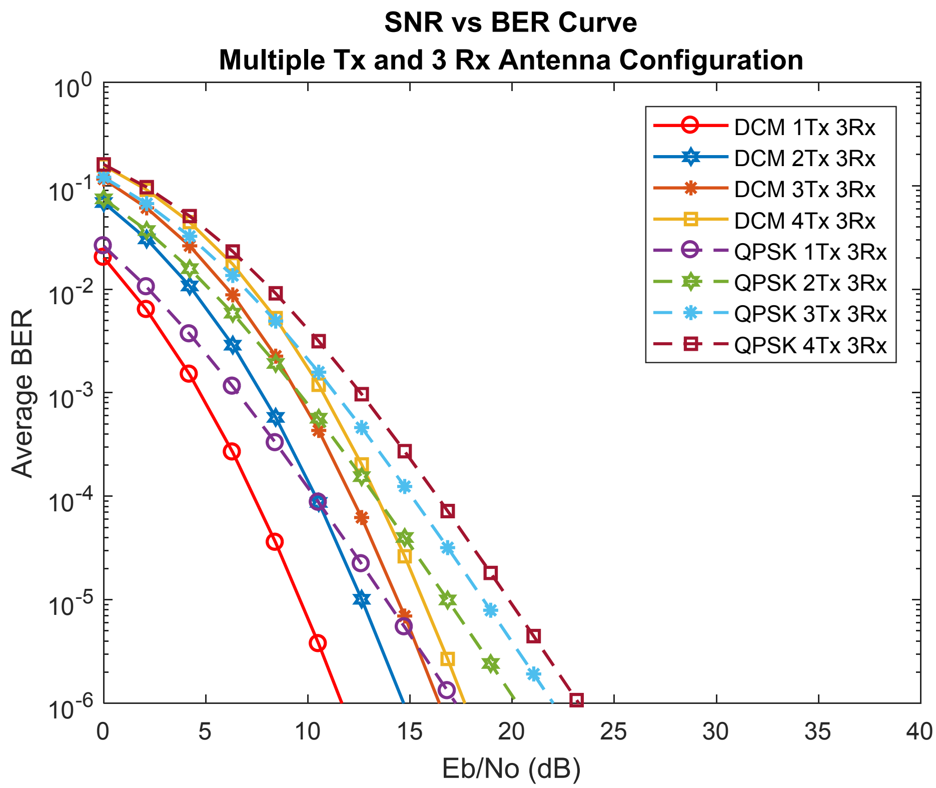

Fig. 3.7: SNR vs BER Curve for Multiple Tx and 3 Rx Antenna Setup

Keeping the number of receiving antenna fixed at 3, the number of transmitting antenna is increased from 1 to 4 sequentially and outputs are graphically represented in Fig. 3.7. SNR vs BER measurements for different antenna configuration are noted in Table 3.8.

Table 3.8: Sensitivity (SNR in dB) of DCM and QPSK for Multiple Tx and 3 Rx at BER 10^{-3} and 10^{-6} Respectively

SNR (dB) for 3 Rx / **Tx →**		**1**	**2**	**3**	**4**
at BER 10^{-3}	QPSK	6.66	9.6	11.4	12.6
	DCM	4.85	7.7	9.55	10.73
	Sensitivity Improvement in DCM	1.81	1.9	1.85	1.87
at BER 10^{-6}	QPSK	17.0	20.3	21.9	23.25
	DCM	11.68	14.6	16.42	17.6
	Sensitivity Improvement in DCM	5.32	5.7	5.48	5.65

Studying Fig. 3.7 and associated data of Table 3.8, it becomes clear that increasing the number of receiving antenna to 3, the performance of both the modulation scheme improves. However, as the number of transmitting antenna chronologically increases, the sensitivity improvement of DCM in comparison continues to decrease.

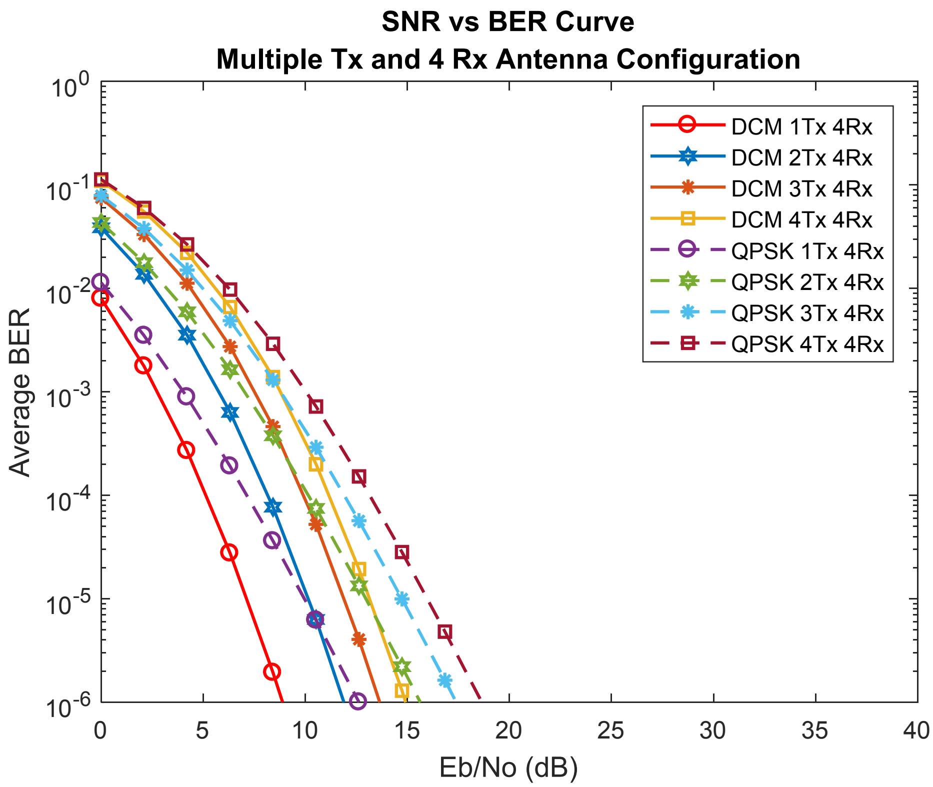

Fig. 3.8: SNR vs BER Curve for Multiple Tx and 4 Rx Antenna Setup

However, in Fig. 3.8, the number of receiving antenna is kept fixed at 4 while, the number of transmitting antenna is increased sequentially from 1 to 4. Necessary SNR vs BER measurements are noted in Table 3.9.

Table 3.9: Sensitivity (SNR in dB) of DCM and QPSK for Multiple Tx and 4 Rx at BER 10^{-3} and 10^{-6} Respectively

SNR (dB) for 4 Rx	**Tx →**	**1**	**2**	**3**	**4**
at BER 10^{-3}	QPSK	4.24	7.04	8.85	10.06
	DCM	3.0	5.8	7.5	8.85
	Sensitivity Improvement in DCM	1.24	1.24	1.35	1.21
at BER 10^{-6}	QPSK	12.5	15.6	17.3	18.55
	DCM	8.9	12.0	13.65	14.9
	Sensitivity Improvement in DCM	3.6	3.6	3.65	3.65

Table 3.9 gives a vivid exposer that the overall system performance improves if the number of receiving antenna is increased to 4 than that of using lower number of receiving antennas in comparison to the number of transmitting antennas. But the sensitivity improvement of DCM in comparison to QPSK reduces further.

The SNR vs BER Curve for different cases are shown through Fig. 3.1 to 3.8. Among these Fig. 3.1 to 3.4 illustrate how the BER changes with varying number of receiving antenna N_r against fixed number of transmit antenna N_t. While Fig. 3.5 to 3.8 demonstrate the behavior of changing the BER with varying number of N_t against fixed number of receiving antenna N_r.

Crux of the results obtained through Fig. 3.1 to 3.8 are plotted in Fig. 3.9. The graphical representation illustrates how the average BER changes with the increment of transmit and receive antennas sequentially from 1 to 4. It further exhibits that incorporation of space diversity in the system decreases the BER dramatically and improves the overall performance.

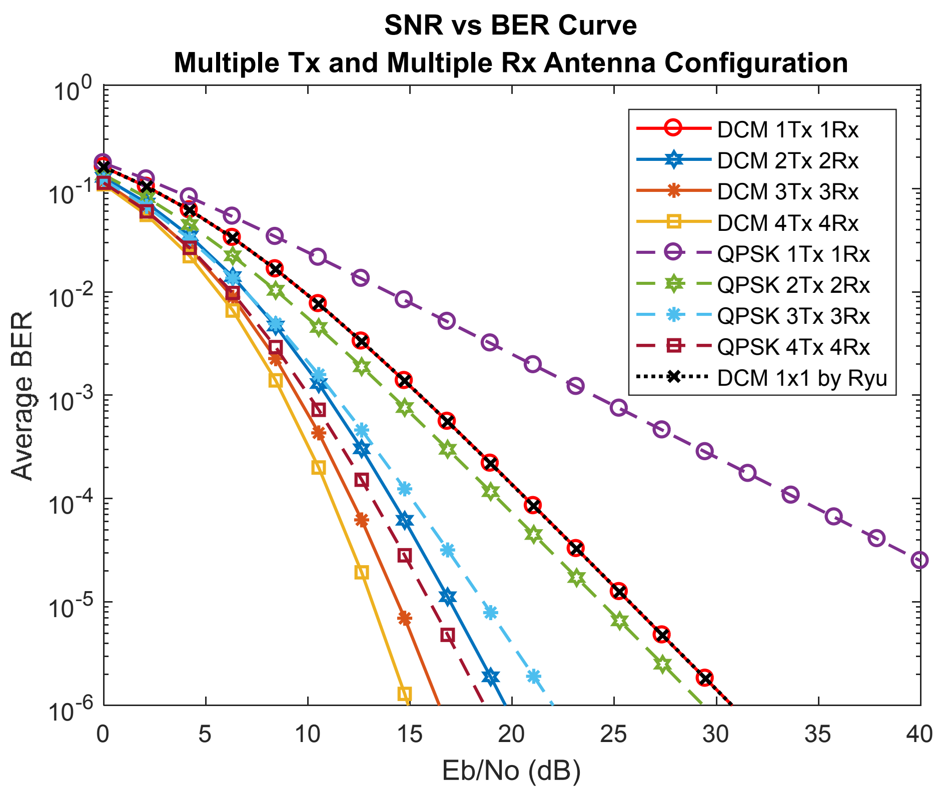

Fig. 3.9: SNR vs BER Curve of DCM and QPSK for Incremental N_t and N_r from 1 to 4

To evaluate the performance of DCM in comparison to QPSK, the SNR (dB) values obtained from Fig. 3.9 for both the modulation scheme at BER 10^{-3} and 10^{-6} against different antenna configuration such as, 1Tx 1Rx, 2Tx 2Rx, 3Tx 3Rx and 4Tx 4Rx are taken into consideration and noted in Table 3.10.

Table 3.10: Sensitivity (SNR in dB) of DCM and QPSK at BER 10^{-3} and 10^{-6} having Different Antenna Configuration

Antenna / Modulation	SNR (dB) Values for			
	1Tx, 1Rx	**2Tx, 2Rx**	**3Tx, 3Rx**	**4Tx, 4Rx**
QPSK at BER 10^{-3}	24.01	14.08	11.4	10.06
DCM at BER 10^{-3}	15.53	11.0	9.55	8.85
DCM Sensitivity Improvement Over QPSK at BER 10^{-3}	8.48	3.08	1.85	1.21
QPSK at BER 10^{-6}	53.94	29.5	21.9	18.55
DCM at BER 10^{-6}	30.65	19.8	16.42	14.9
DCM Sensitivity Improvement Over QPSK at BER 10^{-6}	23.29	9.7	5.48	3.65

The obtained results of SISO configuration as noted in Table 3.10 show that DCM significantly outperforms QPSK by about 8 dB at BER 10^{-3}. This outcome of Fig. 3.9 goes in line with the previous studies on similar type of topics carried out by Park, K. H., Sung, H. K. and Chai, K. Y. [30] as well as Ryu, H. S., Lee, J. S. and Kang, C. G. [33]. However, Table 3.10 clearly shows that to achieve BER 10^{-3} or 10^{-6} against different number of antenna combination, the SNR value decreases with the employment of higher number of antennas and more specifically due to higher number of receiving antennas.

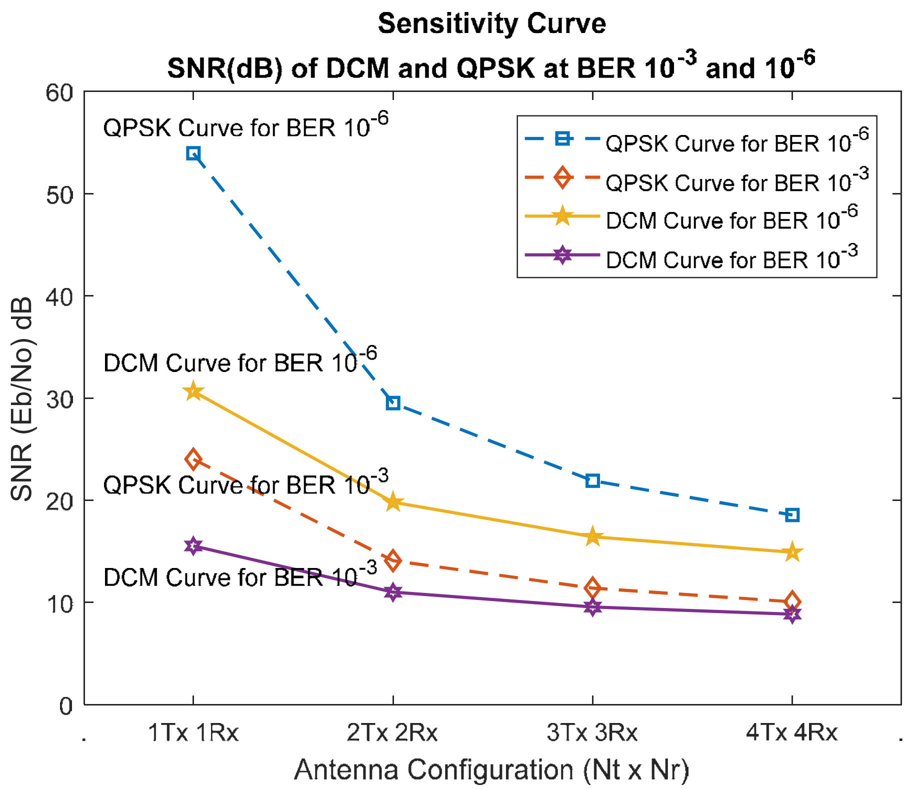

Fig. 3.10: Sensitivity of DCM and QPSK at BER 10^{-3} and 10^{-6} for Different Antenna Configuration

Fig. 3.10 is generated out of the data of Table 3.10. It shows that the benefit of employing MIMO is distinct in comparison to SISO. The sensitivity upper hand that DCM exhibits over QPSK at BER 10^{-3} with 1Tx 1Rx, 2Tx 2Rx, 3Tx 3Rx and 4Tx 4Rx antenna arrangements are 8.48, 3.08, 1.85 & 1.21 dB respectively whereas, at BER 10^{-6} they are 23.29, 9.7, 5.48 & 3.65. Though the increment of MIMO configuration (space diversity) projects improvement in sensitivity but the rate of improvement does not follow the same curve. With the increment of space diversity, the rate of relative sensitivity improvement reduces and become insignificant in comparison to the system complexity which is in fact the basic characteristic of MIMO technique.

From the obtained figures, data on the change of sensitivity (dB) in DCM and QPSK system for different antenna configuration in comparison to the system with SISO QPSK at BER 10^{-3} and BER 10^{-6} are extracted and noted in Table 3.11 and Table 3.12 respectively. The SNR measured for both DCM and QPSK system against the fixed BER 10^{-3} or 10^{-6} show that gradual increment of the number of receiving antenna provides improvement in sensitivity than the previous. It is just the echo of the fact that for any fixed number of transmit antenna (N_t), the same BER can be achieved at relatively lower SNR by increasing the number of receiving antenna (N_r). However, for any fixed number of receiving antenna, if the number of transmit antenna is increased, the sensitivity improvement (in terms of SNR in dB) of DCM in comparison to SISO QPSK decreases. This comparative performance analysis becomes more vivid when it is projected graphical through Fig. 3.11 and 3.12.

Table 3.11 Improvement of Sensitivity (dB) in DCM and QPSK System for Different Antenna Configuration in Comparison to the SISO QPSK System at BER 10^{-3}

	Rx \ Tx	1	2	3	4
QPSK at BER 10^{-3}	**1**	0	-3.14	-4.82	-6.16
	2	12.81	9.93	8.24	6.92
	3	17.35	14.41	12.61	11.41
	4	19.77	16.97	15.16	13.95
DCM at BER 10^{-3}	**1**	8.48	5.57	3.66	2.56
	2	16.13	13.01	11.27	10.11
	3	19.16	16.31	14.46	13.28
	4	21.01	18.21	16.51	15.16

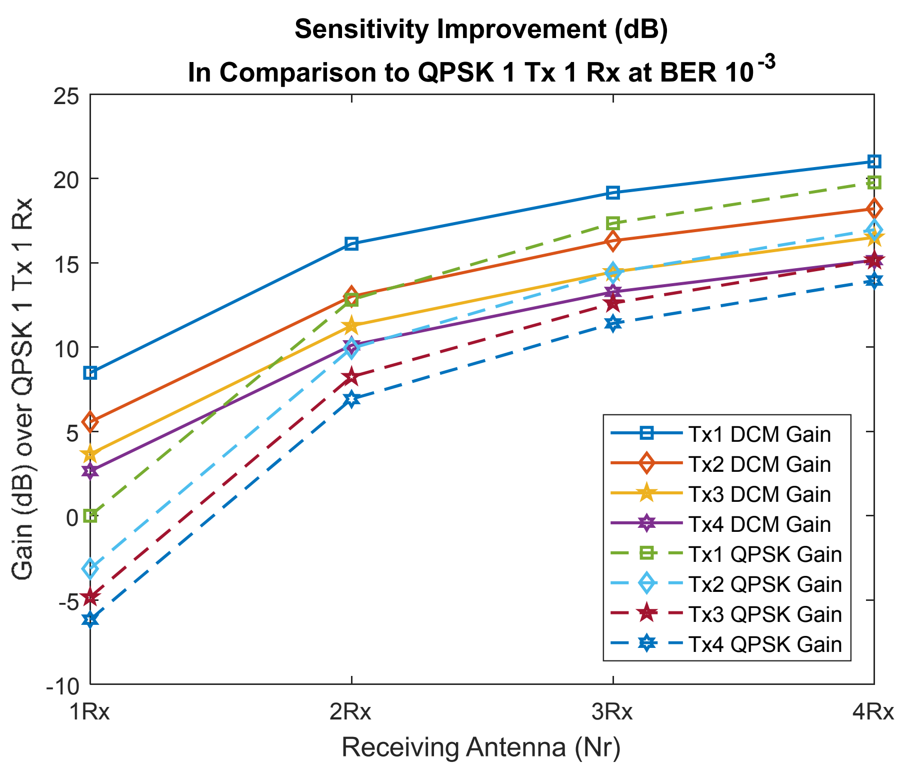

Fig. 3.11: Sensitivity Improvement (dB) of QPSK and DCM in Comparison to SISO QPSK at BER 10^{-3}

Table 3.12 Improvement of Sensitivity (dB) in QPSK and DCM System for Different Antenna Configuration in Comparison to the SISO QPSK System at BER 10^{-6}

	Rx \ Tx	1	2	3	4
QPSK at BER 10^{-6}	**1**	0	-3.04	-4.72	-6.06
	2	27.74	24.44	22.94	21.64
	3	36.94	33.64	32.04	30.69
	4	41.44	38.34	36.64	35.39
DCM at BER 10^{-6}	**1**	23.29	20.14	18.41	17.29
	2	37.39	34.14	32.24	30.94
	3	42.26	39.34	37.52	36.34
	4	45.04	41.94	40.29	39.04

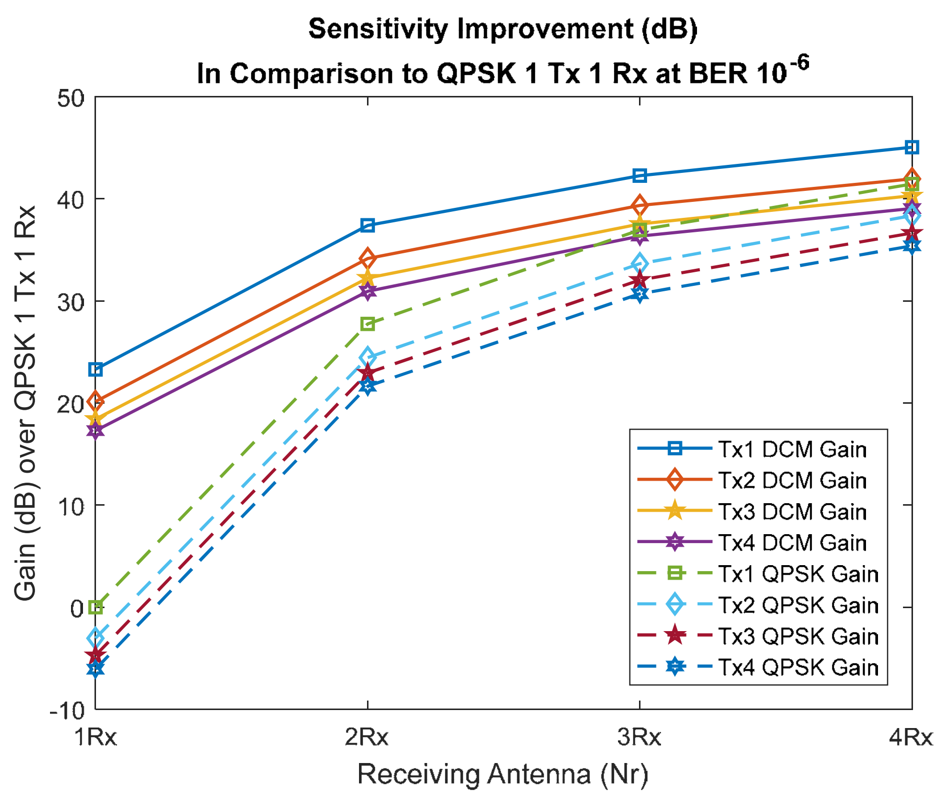

Fig. 3.12: Sensitivity Improvement (dB) of DCM and QPSK in Comparison to SISO QPSK at BER 10^{-6}

However, study on Fig. 3.11 and 3.12 aided to reach at the following deduction:

i. The BER performance of DCM is better than that of QPSK for any similar type of SISO, SIMO, MISO or MIMO arrangement.

ii. Comparing the curves, corresponding to the BER performance improvement in case of DCM MB-OFDM UWB communication system with space diversity, it is found that deploying multiple antennas at receiving end remarkably improve the BER performance. However, use of multiple antennas at transmitting end causes relative performance deterioration.

iii. Keeping the number of transmitting antenna (Nt) fixed at either 1, 2, 3 or 4, and increasing the number of receiving antenna (Nr) from 1 to 4, gradually decreases the system BER. In Fig. 3.2, for DCM with transmitting antenna Nt=2, against varying number of receiving antenna, Nr=1, 2, 3, 4, at SNR 10 dB, the BER changes from 2.636×10^{-2}, 1.753×10^{-3}, 1.362×10^{-4} and 1.141×10^{-5} respectively. Similar type of behaviour is observed in case of QPSK modulated system too (i.e. BER 4.578×10^{-2}, 5.461×10^{-3}, 7.498×10^{-4} and 1.085×10^{-4}). The reason for this phenomenon is that in case of such a system, the channel diversity remains fixed at the transmitting end, but at the receiving end the diversity and array gain increases with the increase of number of receiving antenna, Nr.

3.3 Summary

Results obtained through numerical computation show that DCM SISO configuration significantly outperforms QPSK by about 8 dB at BER 10^{-3} which goes in line with the research carried out by K. H. Park, H. K. Sung and Chai, K. Y. [30] as well as Ryu, H. S., Lee, J. S. and Kang, C. G. [33]. Analyzing the results, it is found that MIMO technique works fine with DCM technique. Use of multiple antennas with the receiver significantly improves the BER performance. On the other hand, using multiple antennas with the transmitter without incorporating any transmission diversity coding technique causes relative performance deterioration.

CHAPTER-4
CONCLUSIONS AND FUTURE WORK

4.1 Conclusions

BER analysis of an UWB communication system with DCM and space diversity is carried out through analytical development of the expression of SNR and PEP. SISO, SIMO, MISO and MIMO arrangement are taken into consideration to satisfy the requirement of space diversity. In the process, formula of pdf for the output SNR of such a system is derived considering Rayleigh fading environment. Average BER expression through PEP is determined on the basis of pdf and output SNR for the DCM system. This has ultimately helped estimating the cumulative average BER. Alternative expression of Q-function (Craig's function) has generated the desired MGF to ease up the analytical process of BER determination. In fact, the BER expression is deduced from the summation of the conditional PEPs between pair of distinct codes for a MB-OFDM UWB system with N_t transmit and N_r receive antennas. In doing so, the Euclidian distance between the related pair of coordinates of a DCM system is measured from the accumulated constellation which has eventually aided ascertaining the cumulative average BER.

In this research, performance of the DCM system is analyzed through multiple combination of transmit and receive antennas which has generated different multipath fading channels such as SISO, MISO, SIMO and MIMO. For better assimilation regarding performance enhancement of such MB-OFDM UWB DCM system with space diversity, number of SNR verses BER curves are projected through numerical computation. The SNR measured for both DCM and QPSK system against the fixed BER 10^{-3} or 10^{-6} shows that gradual increment of the number of receiving antenna provides improvement in sensitivity. In fact, it echoes the teaching that for any fixed number of transmit antenna N_t, the same BER can be attained at relatively lower SNR by increasing the number of receiving antenna N_r. The reason for this phenomenon is that for such a system, the channel diversity remains fixed from transmission side, but at the receiver end the diversity and array gain increases with the increment of number of receiving antenna N_r. However, use of multiple antennas at transmitting end without incorporating any transmission diversity coding technique in the system causes relative performance deterioration.

Numerical computation based on the analytically developed equation shows that the BER performance of DCM communication system is distinctly better than that of QPSK for any similar type of SISO, SIMO, MISO or MIMO arrangement. But, while deploying multiple antennas, the most important point that is to be kept in mind that the number of receiving antennas should be at least equal or more than that of the number of transmitting antennas. However, in order to get further enhancement in BER performance of a DCM UWB communication system with space diversity, transmitter diversity is to be exploited simultaneously along with receiver diversity.

4.2 Scope of Future Work

MIMO is an emerging technology that can effectively improve the performance of a wireless system in fading environment. Multiple antenna of a MIMO system increases the throughput without involving any extra bandwidth or extra power. To exploit the maximum out of a MIMO diversified wireless communication system it is essential to incorporate some transmission diversity coding technique, such as STC. However, in a DCM UWB communication system, OFDM converts the frequency selective fading channels into a set of flat fading channels. Therefore, STC can very well be implemented with a DCM system operating with space diversity.

In 1998, Alamouti proposed STBC technique which guarantees a full space diversity and full rate transmission with 2x2 MIMO system. Later on, Tarok provided almost the same for a 4x4 MIMO system. However, Alamuti STBC has the advantages of a lower computational complexity and a high data rate which is two times than that of the MB-OFDM system. Therefore, in quest of much better performance out of a DCM MB-OFDM UWB communication system with space diversity further research may be carried out incorporating Alamouti STBC technique.

BIBLIOGRAPHY

[1] Balakrishnan et al., “Versatile System for Dual Carrier Transformation in Orthogonal Frequency Division Multiplexing,” United States Patent. Patent No.: US 7,889,635 B2. 15Feb 2011.

[2] Fisher, R. et al., “DS-UWB Physical Layer Submission to 802.15,” Task Group 3a, IEEE 802.15-04/137r3, Jul, 2004.

[3] Mehbodniya, A. and Aissa, S., “Ultra wideband technologies coexistence in Nakagami-m fading channels,” IET Communications, vol. 3, no. 7, Pp. 1081-1088, 2009.

[4] Ghildiyal, A., Godara, B. et al., “UWB for low power, short range, in-body medical implants,” in Proceedings of the IEEE International Conference on Wireless Information Technology and Systems (ICWITS’10), Pp. 1-4, IEEE, Honolulu, Hawaii, USA, Sep 2010.

[5] Yang, L., and Giannakis, G., “Ultra-wideband communications: an idea whose time has come”, IEEE on Signal Processing Magazine, Vol. 21, Pp. 26-54, 2004.

[6] Kondoju, S., Mani, V. V., “Outage and BER analysis of dual-carrier modulation over frequency-selective Nakagami-m fading channels,” COMPEL - The international journal for computation and mathematics in electrical and electronic engineering. Vol. 36, Pp. 90-107. 2017.

[7] Rahayu, Y., Rahman, T., et al., “Ultra wideband technology and its applications,” WOCN 08 5th IFIP International Conference on Wireless and Optical Communications Networks, Surabaya, Pp. 1-5. 2008.

[8] Siriwongpairat, W. P., Su, W., et al., “Multiband-OFDM MIMO Coding Framework for UWB Communication Systems,” IEEE Transactions on Signal Processing, vol. 54, p 214-224, Jan 2006.

[9] Batra, A., Balakrishnan, J., and Dabak, A., “MULTI-BAND OFDM: A NEW APPROACH FOR UWB,” IEEE International Symposium on Circuits and Systems, Vancouver, BC, Canada, May 2004.

[10] Delestre, F., “Channel Estimation and Performance Analysis of MIMO-OFDM Communications using Space-Time and Space-Frequency Coding Schemes”.

Science and Technology Research Institute (STRI), University of Hertfordshire, United Kingdom, Jun 2011.

[11] Ouyang, C. Y., Lin, W. P. and Liu, C. C., "Performance Analysis of the Multiband Orthogonal Frequency Division Multiplexing Ultra-Wideband Systems for Multipath Fading and Multiuser Interference Channels," Hindawi Publishing Corporation, Mathematical Problems in Engineering, Article ID 190809, 2015.

[12] Dawar, A. S., Choubey, A., "Multiband-OFDM Based Ultra-Wideband Communication System," International Journal on Emerging Technologies. Vol. 3, No. 1, Pp. 141-148. 2012.

[13] Cho, S. and Park, S. K. "PAPR Performance of Dual Carrier Modulation using Improved Data Allocation Scheme," Published 2011 in 13th International Conference on Advanced Communication Technology (ICACT 2011).

[14] Yang, R. and Sherratt, R. S., "Dual Carrier Modulation Demapping Methods and Performances for Wireless USB," 9th Annual Postgraduate Symposium: Convergence of Telecommunications, Networking and Broadcasting, Liverpool, UK, Jun 2008.

[15] Yang, R. and Sherratt, R. S., "Fixed point dual carrier modulation performance for wireless USB," ISCE 09 IEEE 13th International Symposium on Consumer Electronics, Vancouver, Pp. 325-328, 2009.

[16] Yang, R., and Sherratt, R. S., "Multiband OFDM modulation and demodulation for ultra-wideband communications," Novel Applications of the UWB Technologies. Intech Open Publishing, Pp. 3-30. ISBN 9789533073248, 2011.

[17] Nguyen, T. H., Hieu, N. T. et al., "A Scheme of Dual Carrier Modulation with Soft-Decoding for MB-OFDM MIMO Systems," International Conference on Advanced Technologies for Communications, ATC, 2011.

[18] Kondoju, S. K., Mani, V. V. and Bose, R., "Exact BER analysis of DCM for Multiband OFDM-UWB System over uncorrelated Nakagami-m fading channels," IEEE International Conference on Ultra-WideBand (ICUWB) 2014.

[19] Sharon et al. "Dual Carrier Modulator for a Multiband OFDM UWB Transceiver," Patent No: US 7,512,185 B2, Date of Patent: Mar. 31, 2009.

[20] Tran, L. C., Mertins, A. and Wysocki, T. A., "Unitary differential space-time-frequency codes for MB-OFDM UWB wireless communications," IEEE Transactions on Wireless Communications, vol. 12, No. 2, Pp. 862-876, 2013.

[21] ECMA, "Standard ECMA-368: High data rate ultra wideband PHY and MAC standard," 3rd Edition, Dec 2008.

[22] Yang, R., and Sherratt, R. S., "A dual QPSK soft-demapper for multiband OFDM exploiting time-domain spreading and guard interval diversity," IEEE Transactions on Consumer Electronics, vol. 53, no.1, Pp. 46-49, Feb 2007.

[23] Batra, A. and Balakrishnan, J., "Improvements to the Multi-band OFDM Physical Layer," 3rd IEEE Consumer Communications and Networking Conference, Volume 2, 8-10, Pp. 701-705, Jan 2006.

[24] Mathuranathan, "Binary Phase Shift Keying (BPSK)–modulation and Demodulation," https://www.gaussianwaves.com/2010/04/bpsk-modulation-and -demodulation-2/ [Online, accessed on: 20 Dec 2018].

[25] Tayab, D. M. and Walliullah, G. et al., "Quadrature Phase Shift Keying Modulator & Demodulator for Wireless Modem," Mehran University of Engineering and Technology (MUST), Pakistan, Conference Paper, Mar 2009.

[26] https://www. Radio -electronics.com/ info /rf-technology-design/ quadrature-amplitude-modulation-qam/what-is-qam-tutorial.php [Online, accessed on: 21 Jul 2018].

[27] https://www.radio-electronics.com/info/rf-technology-design/quadrature-amplitude-modulation-qam/8qam-16qam-32qam-64qam-128qam-256qam.php [Online, accessed on: 21 Jul 2018].

[28] Mandke, Ketan et al., "The evolution of UWB and IEEE 802.15. 3a for very high data rate WPAN," EE381K-11 Wireless Communications UWB Group, the University of Texas at Austin, 2003.

[29] Lin, J. C, Chen, R. J. et al., "Enhanced HARQ Technique using Constellation Rearrangement," IEEE 802.16m-07/292r1, Nov. 2007.

[30] Park, K. H., Sung, H. K. and Chai, K. Y., "BER Analysis of Dual Carrier Modulation Based on ML Decoding," Communications, 2006. APCC'06. Asia-Pacific Conference on, Pp. 1-4, Aug 2006.

[31] Yang, R., Bian, J. and Zhu, C., “Fixed Point Dual Circular 32-QAM Performance for High Speed Wireless USB,” CISME Vol.1, No.6, 2011 Pp.1-8, www.jcisme.org, World Academic Publishing.

[32] Tran, L. C. and Mertins, A., “Differential Space-Time-Frequency Codes for MB-OFDM UWB with Dual Carrier Modulation,” IEEE Communications Society subject matter experts for publication in the IEEE ICC 2009.

[33] Ryu, H. S., Lee, J. S. and Kang, C. G., “BER Analysis of Dual-Carrier Modulation (DCM) over Rayleigh Fading Channel,” Ultra-Modern Telecommunications and Control Systems and Workshops (ICUMT), Pp. 717-720, Oct 2010.

[34] Ryu, H. S., Lee, J. S. and Kang, C. G., “BER Analysis of Dual-Carrier Modulation (DCM) over Nakagami-m Fading Channel,” IEICE TRANS. COMMUN., Vol. E94-B, 7 July 2011.

[35] Kim, Young, Y. et al., “Dual carrier modulation (DCM) demapping method and demapper,” European Patent Application, 07105726.9, 05 Apr 2007.

[36] Kimura, R., Wengerter, C. et al., “Enhanced HARQ Scheme with Signal Constellation Rearrangement,” IEEE 802.16m-08/771r1, Jul 2008.

[37] Park, J., Kim, K. et al., “High Diversity Achievement Algorithm for Dual Carrier Modulation in MBOFDM UWB Systems” Ultra-Wideband (ICUWB), 2012 IEEE Interna- tional Conference on, Pp. 217-221, Sep 2012.

[38] David, T., Viswanath, P., “Fundamentals of Wireless Communication,” Cambridge University Press, 2005.

[39] Wengerter, C., Elbwart, A. G. E. V. et al., “Advanced Hybrid ARQ Technique employing a Signal Constellation Rearrangement,” in proc. IEEE VTC 2002 fall, Pp. 2002-2006, Sep 2002.

[40] Ryu, H. S., Lee, J. S. and Kang, C. G., “BER Analysis of Constellation Rearrangement for Cooperative Relaying Networks over Nakagami-m Fading Channel,” 978-1-61284-233/2/11 IEEE, 2011.

[41] Khormuji, M. N. and Larsson, E. G., “Improving Collaborative Transmit Diversity by Using Constellation Rearrangement,” in Proc. IEEE WCNC 2007, Pp. 803-807, Mar 2007.

[42] Khormuji, M. N. and Larsson, E. G., “Rate-Optimized Constellation Rearrangement for the Relay Channel,” IEEE Commun. Letters, vol. 12, Sep 2008.

[43] Kim, J. W., Lee, H. S. et al,. ”Design of Signal Constellation Rearrangement (CoRe) for Multiple Relay Links,” in proc. IEEE GLOBECOM 2009, Pp. 1-6, Nov 2009.

[44] Goldsmith, A. J., “Wireless Communications,” Cambridge University Press, 2005.

[45] Desta, Y. T., Tao, J. and Massinanke, S., “Performance Analysis of MIMO Multi Band OFDM System for UWB Communication,” International Journal of Future Generation Communication and Networking Vol. 6, 4 Aug 2013.

[46] Proakis, J. G., “Digital-Communications,” 5th-Edition, McGraw Hill Higher Education, 2005.

[47] Krishna, S., “Symbol Error Rate (SER) for 16-QAM,” http://www.dsplog.com/2008/03/29/comparing-16psk-vs-16qam-for-symbol-error-rate/ [Online,accessed on: 21 Dec 2018].

[48] Barry, J. R., Lee,E. A., and Messerschmitt, D. G., “Digital Communications,” 3rd Edition. New York: Springer, 2004.

APPENDIX-A

DETERMINING MGF BY LAPLACE TRANSFORMATION

According to (2.55), the equation of average PEP is,

$$p(x_A \to x_j) = \frac{1}{\pi}\int_0^{\frac{\pi}{2}} \underbrace{\int_0^{\infty} \exp\left(-\frac{c_{j1}\gamma_{f1}}{2N_t sin^2\theta}\right) f_{\gamma_{f1}}(\gamma_{f1}) d\gamma_{f1}}_{MGF1} \underbrace{\int_0^{\infty} \exp\left(-\frac{c_{j2}\gamma_{f2}}{2N_t sin^2\theta}\right) f_{\gamma_{f2}}(\gamma_{f2}) d\gamma_{f2}}_{MGF2} d\theta$$

$$let, s = -\frac{c_{jl}}{2N_t sin^2\theta}$$

So, $p(x_A \to x_j) = \frac{1}{\pi}\int_0^{\frac{\pi}{2}} \underbrace{\int_0^{\infty} \exp(s) f_{\gamma_{f1}}(\gamma_{f1}) d\gamma_{f1}}_{MGF1} \underbrace{\int_0^{\infty} \exp(s) f_{\gamma_{f2}}(\gamma_{f2}) d\gamma_{f2}}_{MGF2} d\theta \quad \ldots\ldots\ldots (A1)$

Now, to integrate the above equation (A1) by parts and to determine the MGF, let's assume:

$$\mathcal{M}_\gamma(s) = MGF = \int_0^{\infty} \exp(s) f_{\gamma_{f1}}\left(\gamma_{f1}\right) d\gamma_{f1} \qquad \ldots\ldots\ldots (A2)$$

However, the formula of Laplace Transformation is;

$$\mathrm{t^n e^{-at} u(t)} \xleftrightarrow{\mathcal{L}} \frac{\mathrm{n!}}{\mathrm{(a+s)^{n+1}}} \qquad \ldots\ldots\ldots (A3)$$

and PDF of Rayleigh fading channel is;

$$f_\gamma(\gamma) = {}^{1}/_{\Gamma} \exp(-{}^{\gamma}/_{\Gamma}) \qquad \ldots\ldots\ldots (A4)$$

If $\Gamma = \bar{\gamma}$ and $\gamma = x$ then,

$$f_\gamma(x) = {}^{1}/_{\bar{\gamma}} \exp\left(-{}^{x}/_{\bar{\gamma}}\right) = k\exp\left(-{}^{x}/_{\bar{\gamma}}\right) \qquad \ldots\ldots\ldots (A5)$$

$k\ is\ a\ constant, where, k = {}^{1}/_{\bar{\gamma}}$

Analogies between (A3) and (A5) are; $n = 0, \quad a = {}^{1}/_{\bar{\gamma}} \quad and \quad t = x$

So, the Laplace transformation of (A5) is,

$$G(s) = k\frac{\mathrm{n!}}{(\mathrm{a}+\mathrm{s})^{\mathrm{n}+1}} = {}^{1}/_{\bar{\gamma}}\frac{0!}{\left(s + {}^{1}/_{\bar{\gamma}}\right)} = {}^{1}/_{\bar{\gamma}}\left(\frac{1}{s + {}^{1}/_{\bar{\gamma}}}\right) \qquad \dots\dots\dots(A6)$$

To determine FFT from Laplace transformation, a (-) sign is to be used in front of the value of 's'. Hence, from (A6) the FFT result is;

$$\mathcal{M}_{\gamma}(s) = MGF = {}^{1}/_{\bar{\gamma}}\left(\frac{1}{\frac{1}{\bar{\gamma}} - s}\right)$$

$$= {}^{1}/_{\bar{\gamma}}\left(\frac{1}{\frac{1}{\bar{\gamma}}(1 - s\bar{\gamma})}\right) = \frac{1}{1 - s\bar{\gamma}} = (1 - s\bar{\gamma})^{-1} \qquad \dots\dots\dots(A7)$$

Now, in (A7), let's put the assumed value

$$s = -\frac{c_{jl}}{2N_t sin^2\theta}$$

So, the equation of MGF for Rayleigh fading channel (A7) becomes;

$$\mathcal{M}_{\gamma}\left(-\frac{c_{jl}}{2N_t sin^2\theta}\right) = \left\{1 - \left(\frac{-c_{jl}}{2N_t sin^2\theta}\right)\bar{\gamma}\right\}^{-1} = \left(1 + \frac{c_{jl}\bar{\gamma}_{fl}}{2N_t sin^2\theta}\right)^{-1}$$

$$= \left(\frac{2N_t sin^2\theta + c_{jl}\bar{\gamma}_{fl}}{2N_t sin^2\theta}\right)^{-1} = \left(\frac{sin^2\theta + \frac{c_{jl}\bar{\gamma}_{fl}}{2\mathcal{N}_t}}{sin^2\theta}\right)^{-1} \qquad \dots\dots\dots(A8)$$

APPENDIX-B

DETERMINING MGF DIRECTLY BY INTEGRATION

According to (2.55), the equation of average PEP is,

$$p(x_A \to x_j) = \frac{1}{\pi}\int_0^{\frac{\pi}{2}} \underbrace{\int_0^{\infty} \exp\left(-\frac{c_{j1}\gamma_{f1}}{2N_t sin^2\theta}\right) f_{\gamma_{f1}}(\gamma_{f1}) d\gamma_{f1}}_{MGF1} \underbrace{\int_0^{\infty} \exp\left(-\frac{c_{j2}\gamma_{f2}}{2N_t sin^2\theta}\right) f_{\gamma_{f2}}(\gamma_{f2}) d\gamma_{f2}}_{MGF2} d\theta$$

$$let, s = -\frac{c_{jl}}{2N_t sin^2\theta}$$

So, $p(x_A \to x_j) = \frac{1}{\pi}\int_0^{\frac{\pi}{2}} \underbrace{\int_0^{\infty} \exp(s) f_{\gamma_{f1}}(\gamma_{f1}) d\gamma_{f1}}_{MGF1} \underbrace{\int_0^{\infty} \exp(s) f_{\gamma_{f2}}(\gamma_{f2}) d\gamma_{f2}}_{MGF2} d\theta \qquad \ldots\ldots\ldots (B1)$

Now, to integrate the above equation by parts and to determine the MGF, let's assume:

$$\mathcal{M}_\gamma(s) = MGF = \int_0^{\infty} \exp(s) f_{\gamma_{f1}}(\gamma_{f1})\, d\gamma_{f1} \qquad \ldots\ldots\ldots (B2)$$

But, pdf of Rayleigh fading channel is;

$$f_{\gamma_{fl}}(\gamma_{fl}) = {}^{1}\!/_{\overline{\gamma}_{fl}} \exp\left(-{}^{\gamma_{fl}}\!/_{\overline{\gamma}_{fl}}\right) \qquad \ldots\ldots\ldots (B3)$$

Putting the value of (B3) in (B2), the MGF for Rayleigh fading channel is obtained as;

$$\mathcal{M}_\gamma(s) = MGF = \int_0^{\infty} {}^{1}\!/_{\overline{\gamma}_{fl}} \exp\left(-{}^{\gamma_{fl}}\!/_{\overline{\gamma}_{fl}}\right) \exp(s)\, d\gamma_{fl}$$

$$= \frac{1}{\overline{\gamma}_{fl}}\int_0^{\infty} e^{-\frac{\gamma_{fl}}{\overline{\gamma}_{fl}}} e^{s}\, d\gamma_{fl} = \frac{1}{\overline{\gamma}_{fl}}\int_0^{\infty} e^{-\gamma_{fl}\left(\frac{1}{\overline{\gamma}_{fl}} - s\right)}\, d\gamma_{fl}$$

$$= \frac{1}{\bar{\gamma}_{fl}}\left(\frac{1}{\bar{\gamma}_{fl}} - s\right)^{-1} \quad = \frac{1}{\bar{\gamma}_{fl}} \times \frac{1}{\left(\frac{1}{\bar{\gamma}_{fl}} - s\right)}$$

$$= \frac{1}{\bar{\gamma}_{fl}} \times \frac{1}{\frac{1}{\bar{\gamma}_{fl}}\left(1 - s\bar{\gamma}_{fl}\right)} = \left(1 - s\bar{\gamma}_{fl}\right)^{-1} \qquad \ldots\ldots\ldots (B4)$$

Now, in (B4), let's put the assumed value

$$s = -\frac{c_{jl}}{2N_t sin^2\theta}$$

So, the equation of MGF for Rayleigh fading channel (B4) becomes;

$$\mathcal{M}_{\gamma}\left(-\frac{c_{jl}}{2N_t sin^2\theta}\right) = \left\{1 - \left(\frac{-c_{jl}}{2N_t sin^2\theta}\right)\bar{\gamma}\right\}^{-1}$$

$$= \left(1 + \frac{c_{jl}\bar{\gamma}_{fl}}{2N_t sin^2\theta}\right)^{-1}$$

$$= \left(\frac{2N_t sin^2\theta + c_{jl}\bar{\gamma}_{fl}}{2N_t sin^2\theta}\right)^{-1}$$

$$= \left(\frac{sin^2\theta + \frac{c_{jl}\bar{\gamma}_{fl}}{2\mathcal{N}_t}}{sin^2\theta}\right)^{-1} \qquad \ldots\ldots\ldots (B5)$$

APPENDIX-C

DETERMINING BER OF QPSK THROUGH PEP METHOD

Let $P_s(E)$ and $P_b(E)$ denote the average Symbol Error Rate (SER) and Bit Error Rate (BER) respectively where, $P_b(E) \approx {}^1/_2\, P_s(E)$. In case of QPSK transmission, assuming that each accumulated symbol is transmitted equally likely, the BER is given by;

$$P_b(E) \approx {}^1/_2\, P_s(E) \leq {}^1/_2\, \{p(x_A \rightarrow x_B) + p(x_A \rightarrow x_C) + p(x_A \rightarrow x_D)\} \quad \ldots\ldots (\mathrm{C.1})$$

where, $p(x_A \rightarrow x_j), j \in \{B, C, D\}$ represents the average pair-wise error probability (PEP) of confusing x_A with x_j, when x_A is transmitted. Let's consider that the symbol and bit energy are denoted by $\mathrm{E_s}$ and $\mathrm{E_b}$ respectively where, $\mathrm{E_s} = 2\mathrm{E_b}$.

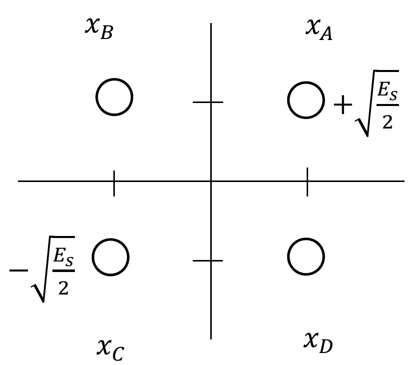

Fig. C.1: Distance between Constellation Points for QPSK Modulation[1]

In Fig. C.1, $d = \sqrt{\frac{E_s}{2}}$; expresses the distance in terms of symbol energy between the adjacent points in a QPSK constellations. If N_0 represents noise energy then, for a MIMO system with N_t transmit antenna and N_r receive antenna, the conditional PEP between two distinct code words can be defined as (2.55).

$$p(x_A \rightarrow x_j | h_1, h_2 \ldots h_l) = Q\left(\sqrt{\frac{\delta}{2N_t}\sum_{j=1}^{N_r}\left\|(x_A - x_j)H_j\right\|^2}\right) \quad \ldots\ldots (C.2)$$

[1]Krishna Sankar, "Symbol Error Rate (SER) for QPSK (4-QAM) Modulation," http://www.dsplog.com/2007/11/06/symbol-error-rate-for-4-qam/ [Online, accessed on: 21 Dec 2018]

where, Q denotes the Q-function

H represents the channel matrix

and the average SNR δ is expressed as,

$$\delta = \frac{E_{sig}}{N_0} = \frac{(d)^2}{N_0} = \frac{\left(\sqrt{\frac{E_s}{2}}\right)^2}{N_0} = \frac{E_s}{2N_0} = \frac{2E_b}{2N_0} = \frac{E_b}{N_0} \qquad as \quad d = \sqrt{\frac{E_s}{2}} \quad \& \quad \mathrm{E_s} = 2\mathrm{E_b}$$

So, the relationship between signal and bit energy can be expressed as;

$$E_{sig} = \mathrm{E_b} \qquad \ldots\ldots\ldots.(C.3)$$

Like (2.45), basing on the QPSK constellation as shown in Fig. C.1, the equation of conditional PEP for a MIMO system with two symbol pair having both *I*- and *Q*- phases in each symbol, can be written in accordance with (C.2) and expressed as;

$$p\left(x_A \to x_j | h_1, h_2\right) = Q\left(\sqrt{\frac{\delta}{2N_t}\sum_{l=1}^{N_r}\left\{\left(x_{AI} - x_{jI}\right)^2 |h_1|^2 + \left(x_{AQ} - x_{jQ}\right)^2 |h_2|^2\right\}}\right)$$

$$p\left(x_A \to x_j | h_1, h_2\right) = Q\left(\sqrt{\frac{E_{sig}}{2N_0N_t}\sum_{l=1}^{N_r}\left\{\left(x_{AI} - x_{jI}\right)^2 |h_1|^2 + \left(x_{AQ} - x_{jQ}\right)^2 |h_2|^2\right\}}\right)$$

Now, for a MISO system with $N_r = 1$, the conditional PEP becomes:

$$p\left(x_A \to x_j | h_1, h_2\right) = Q\left(\sqrt{\frac{E_{sig}}{2N_0N_t}\left\{\left(x_{AI} - x_{jI}\right)^2 |h_1|^2 + \left(x_{AQ} - x_{jQ}\right)^2 |h_2|^2\right\}}\right) \quad \ldots (C.4)$$

In the constellation of QPSK (Fig. C.1), let, a_1 and a_2 be the Euclidean symbol distance between x_A and x_j in both *I*- and *Q*- phase respectively. Therefore, the numerical value of the symbol distances corresponding to $a_1 and\ a_2$ can be expressed as in Table C.1.

Table C.1 QPSK Symbol Distance in Constellation Diagram (Fig. C.1)

Serial	Symbol pair	QPSK symbol distance a_1, a_2	$c_{j1} = \frac{a_1^2}{2}$, $c_{j2} = \frac{a_2^2}{2}$ $(j \in B, C, D)$
1	$(x_A \to x_B)$	*(2, 0)*	*(2, 0)*
2	$(x_A \to x_C)$	*(2, 2)*	*(2, 2)*
3	$(x_A \to x_D)$	*(0, 2)*	*(0, 2)*

In (C.4), putting the value of (C.3), the conditional PEP becomes;

$$p(x_A \to x_j | h_1, h_2) = Q\sqrt{\frac{1}{N_t}\left(\frac{a_{j1}^2|h_1|^2 + a_{j2}^2|h_2|^2}{2}\right)\frac{E_{sig}}{N_0}}$$

$$= Q\sqrt{\frac{1}{N_t}\left(\frac{a_{j1}^2|h_1|^2 + a_{j2}^2|h_2|^2}{2}\right)\frac{E_b}{N_0}} \qquad \therefore\ E_{sig} = E_b$$

$$= Q\sqrt{\frac{1}{N_t}\left(c_{j1}|h_1|^2 + c_{j2}|h_2|^2\right)\frac{E_b}{N_0}} \qquad \text{assuming, } \frac{a_{jl}^2}{2} = c_{jl} \qquad \cdots (C.5)$$

However, similar to (2.49), in Rayleigh fading channel the pdf of instantaneous SNR (γ_{fl}) is given by;

$$f_{\gamma_{fl}}(\gamma_{fl}) = {}^{1}\!/_{\bar{\gamma}_{fl}} \exp\left(-\frac{\gamma_{fl}}{\bar{\gamma}_{fl}}\right) \qquad \ldots\ldots\ldots (C.6)$$

where, the instantaneous SNR per bit for subcarrier l is,

$$\gamma_{fl} = |h_l|^2\frac{\mathrm{E_b}}{\mathrm{N_0}}, \quad l \in 1, 2 \qquad \mathit{and} \qquad \bar{\gamma}_{fl} = \mathrm{E}|\gamma_{fl}| = \mathrm{E}|h_l|^2\frac{\mathrm{E_b}}{\mathrm{N_0}}$$

Putting the above value; $\gamma_{fl} = |\mathrm{h}_l|^2\, {}^{\mathrm{E_b}}\!/_{\mathrm{N_0}}$, the equation (C.5) leads to;

$$p(x_A \to x_j | \gamma_1, \gamma_2) = Q\sqrt{\frac{1}{N_t}\left(c_{j1}\gamma_{f1} + c_{j2}\gamma_{f2}\right)} \qquad \ldots\ldots\ldots (C.7)$$

Similar to (2.67), the equation of cumulative average BER for a QPSK based MB-OFDM UWB MIMO system can be illustrated as;

$$P_b(E) \leq \frac{1}{4\sqrt{\pi}} \times \frac{\Gamma\left(2\mathcal{N}_r + \frac{1}{2}\right)}{\Gamma(2\mathcal{N}_r + 1)} \sum_{j=B}^{D} \left(1 + \frac{c_{j1}\bar{\gamma}_{f1}}{2\mathcal{N}_t}\right)^{-\mathcal{N}_r} \left(1 + \frac{c_{j2}\bar{\gamma}_{f2}}{2\mathcal{N}_t}\right)^{-\mathcal{N}_r}$$
$$\times F_1\left(\frac{1}{2}; \mathcal{N}_r, \mathcal{N}_r; 2\mathcal{N}_r + 1; \frac{1}{1 + \frac{c_{j1}\bar{\gamma}_{f1}}{2\mathcal{N}_t}}, \frac{1}{1 + \frac{c_{j2}\bar{\gamma}_{f2}}{2\mathcal{N}_t}}\right) \quad \dots\dots\dots (C.8)$$

However, like (2.70), the equation for the cumulative average BER of an UWB communication system with QPSK and space diversity can be expressed as;

$$P_b(E) \leq \frac{1}{4\sqrt{\pi}} \times \frac{\left(2\mathcal{N}_r - \frac{1}{2}\right)!}{(2\mathcal{N}_r)!} \left[\left(1 + \frac{2\bar{\gamma}_f}{2\mathcal{N}_t}\right)^{-\mathcal{N}_r} \left(1 + \frac{0\bar{\gamma}_f}{2\mathcal{N}_t}\right)^{-\mathcal{N}_r}\right.$$
$$\times F_1\left(\frac{1}{2}; \mathcal{N}_r, \mathcal{N}_r; 2\mathcal{N}_r + 1; \frac{1}{1 + \frac{2\bar{\gamma}_f}{2\mathcal{N}_t}}, \frac{1}{1 + \frac{0\bar{\gamma}_f}{2\mathcal{N}_t}}\right) + \left(1 + \frac{2\bar{\gamma}_f}{2\mathcal{N}_t}\right)^{-\mathcal{N}_r} \left(1 + \frac{2\bar{\gamma}_f}{2\mathcal{N}_t}\right)^{-\mathcal{N}_r}$$
$$\times F_1\left(\frac{1}{2}; \mathcal{N}_r, \mathcal{N}_r; 2\mathcal{N}_r + 1; \frac{1}{1 + \frac{2\bar{\gamma}_f}{2\mathcal{N}_t}}, \frac{1}{1 + \frac{2\bar{\gamma}_f}{2\mathcal{N}_t}}\right) + \left(1 + \frac{0\bar{\gamma}_f}{2\mathcal{N}_t}\right)^{-\mathcal{N}_r} \left(1 + \frac{2\bar{\gamma}_f}{2\mathcal{N}_t}\right)^{-\mathcal{N}_r}$$
$$\left.\times F_1\left(\frac{1}{2}; \mathcal{N}_r, \mathcal{N}_r; 2\mathcal{N}_r + 1; \frac{1}{1 + \frac{0\bar{\gamma}_f}{2\mathcal{N}_t}}, \frac{1}{1 + \frac{2\bar{\gamma}_f}{2\mathcal{N}_t}}\right)\right] \quad \dots\dots\dots (C.9)$$

$$P_b(E) \leq \frac{1}{4\sqrt{\pi}} \times \frac{\left(2\mathcal{N}_r - \frac{1}{2}\right)!}{(2\mathcal{N}_r)!} \left[\left(1 + \frac{\bar{\gamma}_f}{\mathcal{N}_t}\right)^{-\mathcal{N}_r} \times F_1\left(\frac{1}{2}; \mathcal{N}_r, \mathcal{N}_r; 2\mathcal{N}_r + 1; \frac{1}{1 + \frac{\bar{\gamma}_f}{\mathcal{N}_t}}, 1\right)\right.$$
$$+ \left(1 + \frac{\bar{\gamma}_f}{\mathcal{N}_t}\right)^{-\mathcal{N}_r} \left(1 + \frac{\bar{\gamma}_f}{\mathcal{N}_t}\right)^{-\mathcal{N}_r} \times F_1\left(\frac{1}{2}; \mathcal{N}_r, \mathcal{N}_r; 2\mathcal{N}_r + 1; \frac{1}{1 + \frac{\bar{\gamma}_f}{\mathcal{N}_t}}, \frac{1}{1 + \frac{\bar{\gamma}_f}{\mathcal{N}_t}}\right)$$
$$\left.+ \left(1 + \frac{2\bar{\gamma}_f}{2\mathcal{N}_t}\right)^{-\mathcal{N}_r} \times F_1\left(\frac{1}{2}; \mathcal{N}_r, \mathcal{N}_r; 2\mathcal{N}_r + 1; 1, \frac{1}{1 + \frac{\bar{\gamma}_f}{\mathcal{N}_t}}\right)\right] \quad \dots\dots\dots (C.10)$$